STUDIA
UNIVERSITATIS BABEȘ-BOLYAI

PHYSICA

2

1990

CLUJ-NAPOCA

ANUL XXXV 1990

STUDIA
UNIVERSITATIS BABEŞ-BOLYAI

PHYSICA

2

Redacţia 3400 CLUJ-NAPOCA, str M Kogălniceanu, 1 ● Telefon 11 61 01

SUMAR — CONTENTS

Recenzii — Book Reviews

STUDIA UNIV BABEŞ-BOLYAI, PHYSICA, XXXV, 2, 1990

THE EFFECT OF GERMANIUM DOPPING ON THE PHYSICAL PROPERTIES OF $YBa_2Cu_3O_{7-\delta}$ BASED COMPOUNDS

E. BURZO*, V. POP* and M. OANĂ*

ABSTRACT. The dopping of $YBa_2Cu_3O_{7-\delta}$ compound with germanium ions, leads to a decrease of the superconducting transition temperature, and an increase of the width of transition Above ~ 100 K, the compounds show a temperature independent paramagnetism The magnetic susceptibilities increase when increasing germanium content

1 **Introduction.** In a previous paper [1] we studied the effect of zirconium addition on the physical properties of $YBa_2Cu_3O_{7-\delta}$ superconducting system As a part of an one going investigation of the effect of substitution, we report in this paper some physical properties of $YBa_2Cu_3O_{7-\delta}$ compounds doped with germanium

The transition temperature T_c of $YBa_2Cu_{3-x}M_xO_{7-\delta}$ is strongly suppresed by substitution of Cu by M = Fe, Co, Ni, Zn, Al, etc [2, 3] The Cu ions in $YBa_2Cu_3O_{7-\delta}$ system occupy two different sites one is Cu(1) site on chains and another Cu(2) site in planes [4] The three valent substitutions tend to the chain copper site and increase the overall oxygen content in the chain region, apparently disordering the chains This leads to a phase boundary between orthorhombic and tetragonal-type structures near $x = 0{,}03$ For two valent ions (Zn, Ni) the samples remain orthorhombic for all x values. The superconducting transition temperature decrease nearly linear when increasing x. It is suggested that Zn and Ni ions are randomly distributed between two sites [5, 6] or have a preference for the "plane" site [6] There seems to be little overall change in oxygen content, and very little impact in the chain ordering.

It is also of interest to analyse the effect of dopping $YBa_2Cu_3O_{7-\delta}$ with germanium ions Commonly these ions are in (+4), state, having ionic radius $r_{Ge^{4+}} = 0\,44$ Å In some cases may be also in (+2) valence state with $r_{Ge^{2+}} = 0{,}65$ Å The radius of Cu^{2+} ions is $r_{Cu^{2+}} = 0\,80$ Å Thus, from the point of view of their dimensions the germanium ions may occupy copper sites or/and to be arranged in some interstitial lattice sites.

2 **Experimental.** The samples were prepared by solid state reaction. The mixture of Y_2O_3, GeO_2, CuO and barium carbonate, in required proportions, were homogeneized, finaly grinded and calcinated The calcination has been made in the temperature range (920—950°C), in oxygen atmosphere After calcination, the samples structure was checked by X-rays The formation of perovskite structure was evidenced in all cases The calcinated samples were finely grinded and then compacted at a pressure of 3 t/cm^2 The sintering has been performed in the temperature range (930—960)°C in oxygen atmosphere The sample were then slowly cooled.

---

* *University of Cluj, Department of Physics, 3400 Cluj-Napoca, Romania*

The final X-ray analysis shows the presence of the orthorhombic type structure. The lattice parameters increase slowly with germanium content (figure 1).

Electrical resistivity measurements were made by using a standard four probe technique, in the temperature range 77–300 K.

The magnetic studies were performed with a Faraday-type balance, in the temperature range 77–300 K.

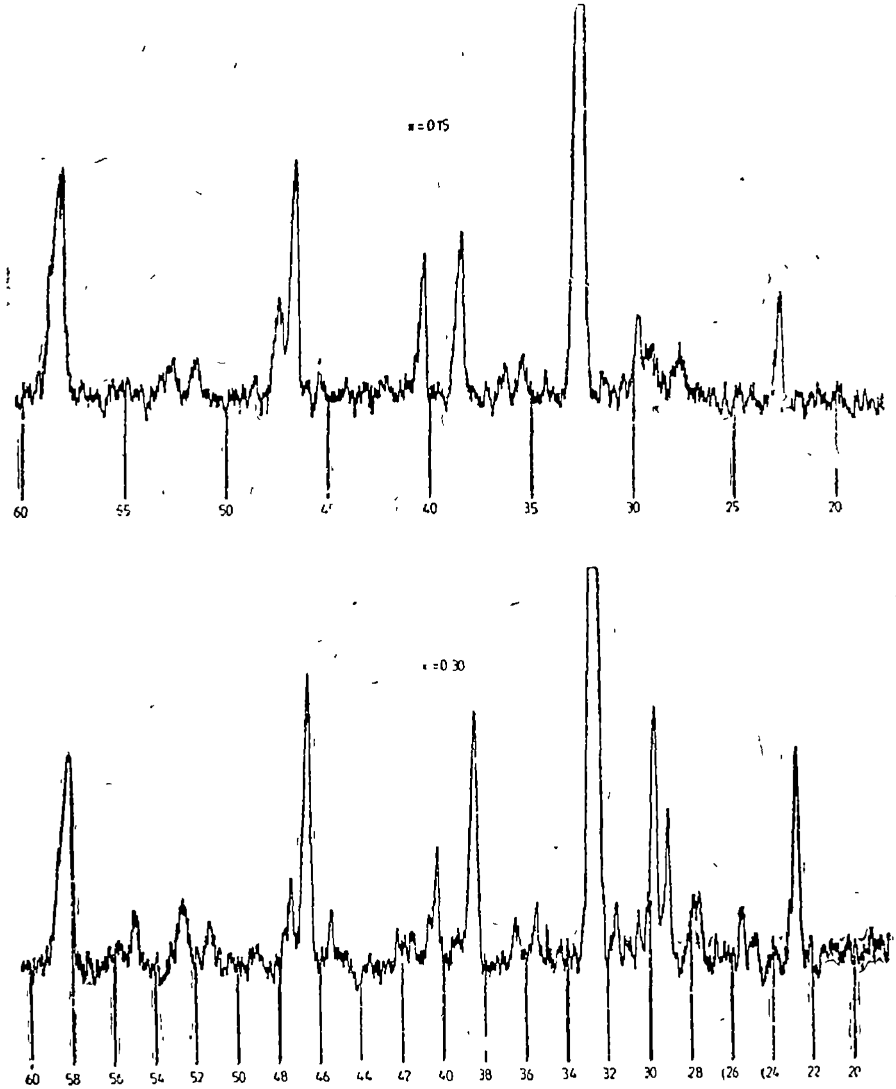

Fig. 1. The X-ray diffraction patterns of $YBa_2Cu_3O_{7-\delta}$ doped with $x = 0.15$ (a) and $x = 0.30$ (b) GeO_2.

3 **Experimental results.** The temperature dependences of the electrical resistivities for $YBa_2Cu_3O_{7-\delta}$ compounds dopped with $x = 0\ 15$ and $x = 0.30$ GeO_2 are plotted in figure 2 The germanium addition decrease somewith the superconducting transition temperatures, T_c, although these still remain higher than 87 K for $x = 0\ 3$ The superconducting transition temperatures seems to be nearly linear dependent on the germanium content (figure 3)

The width of the transition $\Delta T = T_{\text{onset}} - T_{R=0}$ was also analysed. By T_{onset} is denoted the onset temperature of the transition and $T_{R=0}$ is the temperature corresponding to nearly zero resistance As seen in figure 3 the ΔT values increase when germanium content is higher

The temperature dependences of the magnetic susceptibilities, χ, are plotted in figure 4 The sudden changes of χ values around 90 K are connected with the superconducting to normal state transitions Above ~ 100 K, the susceptibilities are not temperature dependent The χ values increase when ioncreasing germanium content, as evidences in inset of the figure

4 **Discussion.** The X-ray analysis of germanium dopped compounds shows the presence of solid solutions at least up to $x = 0\ 3$ No other phases were evidenced, suggesting that germanium ions were incorporated in $YBa_2Cu_3O_{7-\delta}$

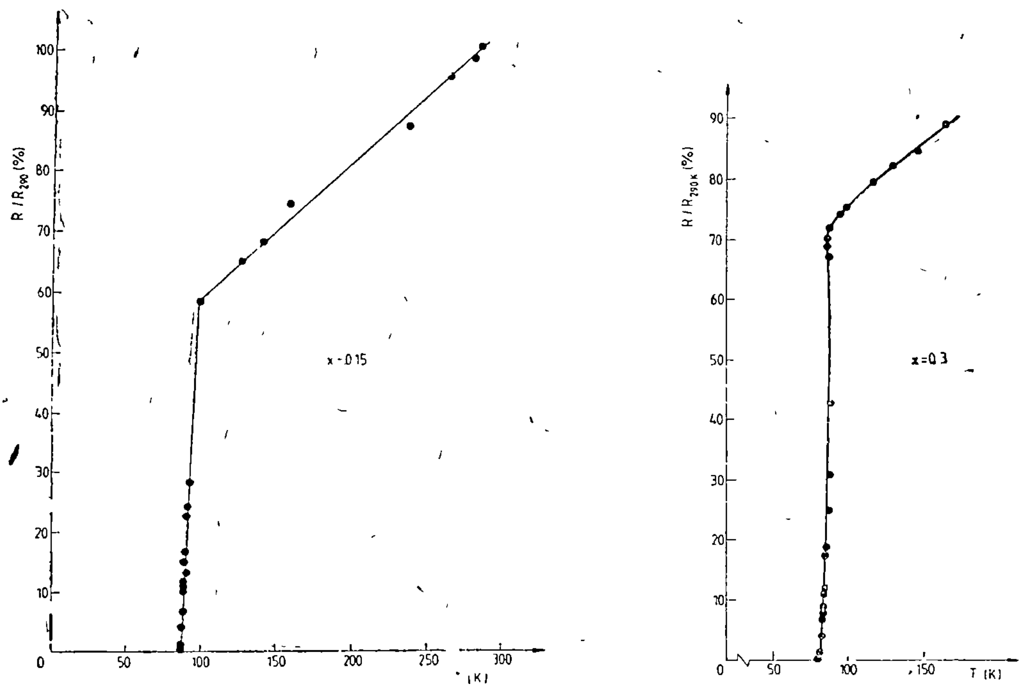

Fig 2 The temperature dependence of the electrical resistivities for samples with $x = 0\ 15$ (a) and $x = 0\ 30$ (b) GeO_2

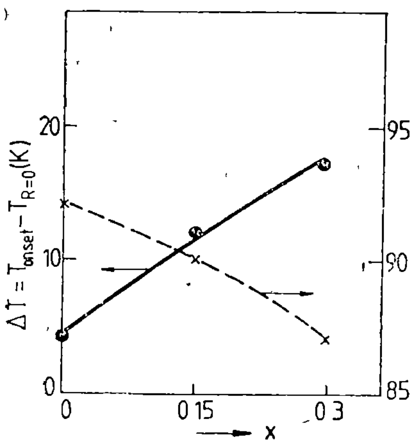

Fig 3 The composition dependence of the superconducting transition temperature and of the width of the transition.

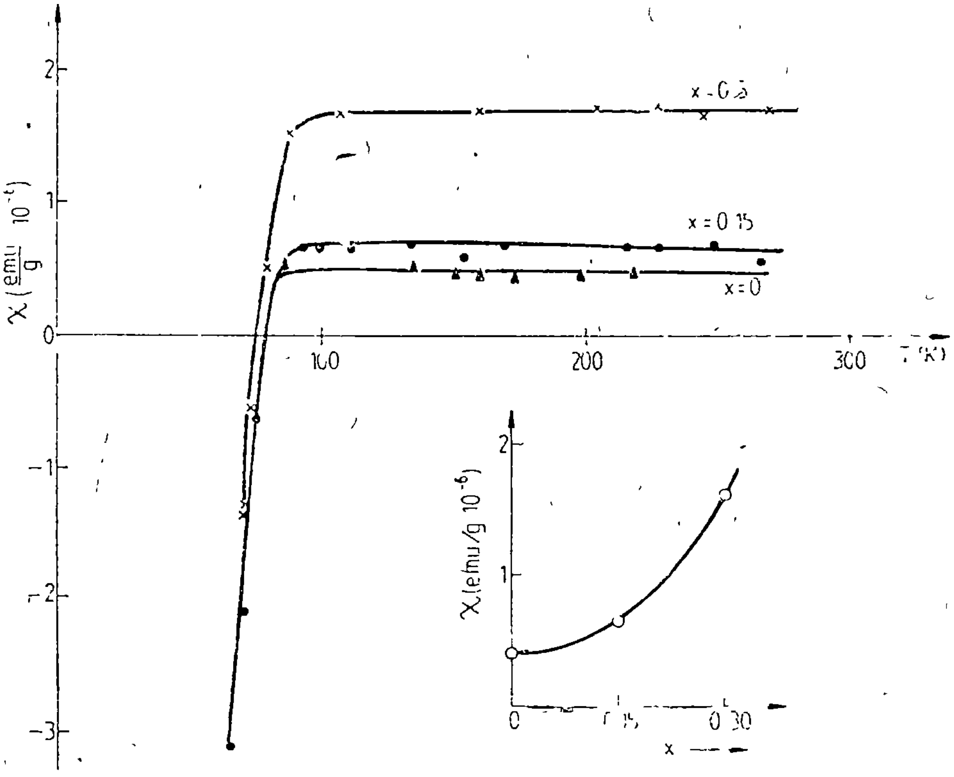

Fig 4 The temperature dependences of the magnetic susceptibilities The composition dependence of the susceptibilities is plotted in the inset

lattice. There are some posibilities for localization of germanium ions These may substitute copper ions, to be situated in interstitial positions or to occupy both mentioned types of site The presence of orthorhombic type structure, even for $x = 0.3$ suggests that germanium ions are not localized in chain sites (Cu(1)).

The germanium ions seem to be not randomly distributed in lattice, as evidenced by the increase of the width of transition, when increasing germanium content There seems to be regions with somewhat slightly different composition ranges The widths of superconducting transitions in our systems are greater than for example in vanadium doped $YBa_2Cu_3O_{6-\delta}$ [7] This may be ascribed to different type of sites occupied by germanium, as suggested by dimensional considerations

The composition dependence of the transition temperatures is not so strong as evidenced in $YBa_2Cu_{1-x}M_xO_{7-\delta}$ compounds with M = Fe, Co, Ni, Zn, Al, etc [2, 3] This is expected only if a limited number of copper sites are affected by substitutions

The magnetic susceptibilities above T_c are not temperature dependent and increase with germanium content The copper ions seem to be in non-magnetic state

REFERENCES

1 V Pop and E Burzo, Mater Sci Forum *62—64*, 205 (1990), E Burzo and V Pop, J Mat Sci (in press)

2 Y Maeno, T Tomita, S Kyogoku, S Awaji, Y Aoki, K Hashino, A Minami and T Fujita, Nature *328*, 512 (1987)

3 S Terada, N Kobayashi, H Iwasaki, A Takigawa, M Kikuchi, Y Siono and S Muto, Physica *165—166 B* 1545 (1990)

4 Y Yu, R L Sabatini, A R Moodenbaugh, Y Zhu, S G Shyu, M Suenaga, K W Dennis and R W McCallun, Physica *169 C*, 205 (1990)

5 R S Howland, T W Geballe, S S Laderman, A Fischer-Colbrie, M Scott, J M Tarascon and P Barboux, Phys, Rev *B39*, 9017 (1989)

6 C Y Yang, A R Moodenbaugh, Y L Wang, Y Xu, S M Heald, D O Welch M. Suenaga, D. A Fischer and J E Penner-Hahu, Phys Rev *B40* (1990)

7 S X Don, A J Bourdillon, Y, X Sun, J. P Zhov, H K Liu, N Savides D Haneman C C Sorreli and K E Easterling J Phys *C21*, L127 (1988).

STUDIA UNIV BABEŞ-BOLYAI, PHYSICA, XXXV, 2, 1990

LANDAU DAMPING SIMULATIONS

SPERANŢA COLDEA*

ABSTRACT. The existence of Landau damping (so called collisionless damping) is discussed, the theory of this basic process in a cold and a warm plasma and the corresponding dispersion relations and growing rates are done Subsequently the imput data and the results obtained by an onedimensional electrostatic simulation code are done and compared with theoretical results Finally the most probable mechanism of Landau damping in a plasma is presented.

1 **Introduction.** The existence of plasma oscillations was first demonstrated some time ago [1] for a homogeneous, infinite, onedimensional plasma system of fixed ions and a cold electrons fluid. The dispersion relation for Langmuir (plasma) oscillations, without an external magnetic field, was given as

$$\varepsilon(\omega, k) = 1 - \frac{\omega_{pe}^2}{\omega^2} = 0 \tag{1.1}$$

where $\omega_{pe}^2 = \frac{ne^2}{m\varepsilon_0}$ is the electron plasma frequency.

The dispersion (ω, k) diagram is a flat line and, consequently, the plasma oscillations have zero group velocity.

Subsequently a plasma of warm electrons and rigid ions was considered [2[and after the analysis was obtained that for small wavelengths ($k\lambda_D \gg 1$) the plasma oscillations obey the following dispersion equation

$$\varepsilon(\omega, k) = 1 - \frac{\omega_{pe}^2}{\omega^2} - 3k^2\frac{v_T^2}{\omega^2} = 0 \tag{1 2}$$

where the thermal velocity is $v_T^2 = \frac{kTe}{m}$, T_e being the electron temperature The plasma oscillations with small wavelengths ($k\omega_{pe}/v_{T} = k\lambda_D \gg 1$) have a small but finite group velocity, smaller than thermal velocity Afterwards the dispersion relation for a hot plasma was obtained and this relation contains the so called kinetic Landau term (a complex contour integral)

$$\varepsilon(\omega, k) = 1 - \frac{\omega_{pe}^2}{2k^2v_T^2} \cdot Z'(\xi e) = 1 + \frac{\omega_{pe}^2}{k^2v_T^2}(1 + \xi e \quad Z(\xi e)) \tag{1 3}$$

where

$$\xi_e = \frac{\omega}{\sqrt{2} \quad k \quad v_T} = \frac{\omega \cdot m^{1/2}}{\sqrt{2} \quad k \cdot k^{1/2} \quad T_e^{1/2}} \tag{1 4}$$

---

* *University of Cluj, Department of Physics, 3400 Cluj-Napoca, Romania*

Analysing this dispersion equation it was concluded that the electrostatic waves of a warm plasma are also damped in the absence of collisions This Landau damping or collisionless damping [3] is a basic phenomenon and one of the most discussed process in plasma physics

Subsequently the physical meaning of Landau damping, by neglecting the collisions in plasma, and the corresponding mathematical treatment will be detailed. The simulation method applied to plasma physics will supply the absence of experimental data and we will describe the Landau damping in a plasma without collisions as a phase mixing of the initial perturbations of the plasma system.

2 **The theory and the physical meaning of Landau damping.** The theoretical study of continuous medium oscillations is based on the Fourier analysis of the movements in space and time, by considering perturbations of the form exp $(ikx - \omega t)$ and obtaining the linear dispersion relation between the frequency w and the wave number k $\omega = \omega(k)$, we use here the linearized Vlasov equation for the distribution function of electron velocities, $f(\vec{x}, \vec{v}, t)$, which describes the dynamics of a plasma

$$\frac{\partial f}{\partial t} + \vec{v} \cdot \frac{\partial f}{\partial x} + \frac{q\vec{E}}{m} \cdot \frac{\partial f_0}{\partial v} = 0 \qquad (2\ 1)$$

So being, the equilibrium distribution function, and the selfconsistent electric field is done by the equation

$$\frac{\partial E}{\partial x} = \frac{q}{\varepsilon_0} \int_{-\infty}^{+\infty} f(v_x) \quad \mathrm{d}v_x \qquad (2\ 2)$$

where

$$f(v_x) = \int_{-\infty}^{\infty} \int_{-\infty}^{\infty} f(v_x, v_y, v_z) \quad \mathrm{d}v_y \mathrm{d}v_z \qquad (2{\cdot}3)$$

Making the assumption that the variations of the distribution function perturbations and of the electric field E have the form exp $i(kr - \omega t)$, it was obtained the following equations

$$f = \frac{q \cdot \vec{E}}{im(\omega - \vec{k} \cdot \vec{v})} \cdot f_0'(v) \qquad (2.4)$$

and

$$ikE = \frac{q}{\varepsilon_0} \int f(v) \mathrm{d}v \qquad (2.5)$$

from which results the dispersion relation for longitudinal electrostatic plasma oscillations.

$$1 + \frac{q^2}{\varepsilon_0 k m} \int_{-\infty}^{+\infty} \frac{f_0(v)}{(\omega - \vec{k} \cdot \vec{v})} = 0 \qquad (2.6)$$

The integral in (2.5) must be clearly defined because of his singularity at $v = \omega/k$ This singularity was neglected by Vlasov himself [4] passing over the collisionless damping which could result, such a singularity not being accepted from the physical point of view [5].

The best modality to analyse the Vlasov equation is to consider it as an initial value problem and to calculate the system response to a determined initial value of the perturbed electrons distribution function [3]

The time evaluation of the perturbations could be studied be using the time Laplace transform (with $Re\, p > 0$), defined as follows:

$$f(k, v, p) = \int_0^\infty e^{-pt} \cdot f(k, v, t)\mathrm{d}t \tag{2.7}$$

and

$$\Phi(k, p) = \int_0^\infty e^{-pt}\Phi(k, t)\mathrm{d}t. \tag{2.8}$$

for the electrostatic potential $\Phi(k, t)$, which is introduced by the relation: $\vec{E} = -\vec{\nabla}\Phi$.

By considering perturbations of the form $\exp(ikx)$, the equations (2.1)—(2.2) are written as

$$\frac{\partial f}{\partial t} + i\vec{k}\vec{v}f - i\,\frac{k \cdot q}{m}\,\Phi\frac{\partial f_0}{\partial v} = 0 \tag{2.9}$$

and

$$k^2\Phi = \frac{q}{\varepsilon_0}\int f\mathrm{d}v \tag{2.10}$$

The inverse Laplace transforms are defined as

$$f(k, v, t) = \frac{1}{2\pi i}\int_{\sigma - i\infty}^{\sigma + i\infty} dp f(k, v, p)e^{pt} \tag{2.11}$$

$$\Phi(k, t) = \frac{1}{2\pi i}\int_{\sigma - i\infty}^{\sigma + i\infty} e^{pt}\Phi(k, p)\mathrm{d}p \tag{2.12}$$

and $\exp(pt) \rightarrow 0$ when $p \rightarrow \infty$, for $t < 0$ For $t > 0$ the pole could be closed by a semicircle in the right half of the $(Re p - Im p)$-plane.

The integral on this contour is zero when his radius $r \rightarrow \infty$, because by definition do not exist singularities included in this contour. Because this integral is zero the integral on the Bromwich contour (defined by σ) must also be zero.

The Laplace transforms of the eq (2.9)—(2.10) are of the form

$$(p + ikv)f(k, v, p) - ik \cdot \frac{q}{m}\,\Phi(k, p)\,\frac{\partial f_0}{\partial v} = g(k, v) \tag{2.13}$$

$$k^2\Phi(k, p) = \frac{q}{\varepsilon_0}\int_{-\infty}^{+\infty} f(k, v, p)\mathrm{d}v \tag{2.14}$$

where $g(k, v) = f(k, v, t = 0)$. Solving the eq (2 13) we obtain

$$f(k, v, p) = \frac{1}{(p + ikv)} \left\{ g(k, v) + ik \frac{q}{m} \Phi(k, p) \cdot f_0'(v) \right\} \tag{2.15}$$

which is replaced in the eq (2.14) with the result

$$\Phi(k, p) = \frac{\dfrac{q}{\varepsilon_0 k^2} \displaystyle\int_{-\infty}^{\infty} \frac{g(k, v)}{p + ikv} \mathrm{d}v}{\left[1 - i \dfrac{q^2}{\varepsilon_0 k m} \displaystyle\int_{-\infty}^{+\infty} \frac{f_0'(v) \mathrm{d}v}{(p + ikv)}\right]} \tag{2.16}$$

and then

$$f(k, v, p) = \frac{g(k, v)}{(p + ikv)} + \frac{ikq}{m} \frac{f_0'(v)}{(p + ikv)} \cdot \frac{\dfrac{q}{\varepsilon_0 k^2} \displaystyle\int_{-\infty}^{+\infty} \frac{g(k, v) \mathrm{d}v}{(p + ikv)}}{\left[1 - \dfrac{iq^2}{k \varepsilon_0 m} \displaystyle\int \frac{f_0'(v) \mathrm{d}v}{(p + ikv)}\right]} \tag{2.17}$$

where p is a complex variable and the integrals are not well defined. In the eq. (2 12) $\Phi(k, p)$ is replaced from eq (2.16) and for $t < 0$, $\Phi(k, t) = 0$, the perturbation being introduced at $t = 0$. The t-integral for $\Phi(k, t)$ is evaluated with the Cauchy theorem (or assomptotically for $t \to \infty$).

Landau has made the assumption that $g(k, v)$ is a whole function (finite for the finite values of v) and the integral

$$\int_{-\infty}^{+\infty} \frac{g(k, v)}{(p + ikv)} \mathrm{d}v \qquad \text{(a)}$$

analytically continued in the left semiplane-p defines a whole function of p. The same argument is also valuable for the integral

$$\int_{-\infty}^{+\infty} \frac{f_0'(v) \mathrm{d}v}{(p + ikv)} \qquad \text{(b)}$$

This consideration permits us to use the singularity, by integrating below it in the complex plane-v when p moves from the right semiplane to the left one, the movement of the pole $v = ip/k$ is made as follows: when $Re(p) > 0$ the integral (a) is well defined because his pole is in the upper semiplane. When p moves with $Re(p) > 0$, the pole $v = ip/k$ crosses the real axis and moves in the lower semiplane ($k > 0$) (see the fig 1).

The initial distribution function $f_0(v)$ is considered to be of the Maxwell-Boltzmann type·

$$f(v) = n_0 \left(\frac{m}{2\pi k T}\right)^{1/2} \cdot \exp\left(-\frac{mv^2}{2kT}\right) \tag{2.18}$$

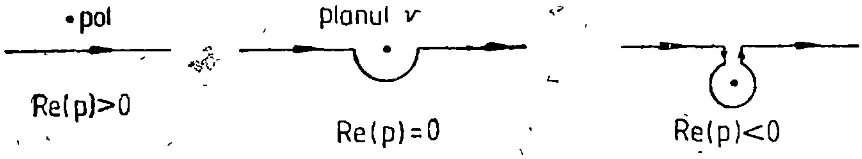

Fig. 1 The complex plane v and the poles for the integrals (2.15)—(2.16)

The potential $\Phi(k, t)$ is a ratio of two whole functions of complex variable p and then it is also a whole function of p

The integration contour becomes deformed in the left semiplane assuring that all the poles of the integrand be at the left of the deformed contour.

The poles come from the zeros of the denominator of the expression (2.16):

$$1 - i\frac{q^2}{k\varepsilon_0 m}\int\limits_C \frac{f_0'(v)\mathrm{d}v}{(p + ikv)} = 0 \tag{2.19}$$

if we note the Landau contour by C It was deduced that for $Re(p) > 0$ does not exist roots of the eq (2.19) when $f_0(v)$ is of the form (2.18), and does not exist in this case growing solutions (instabilities) [3]

Because do not exist poles in the right semiplane, the contour C is deformed like in the fig. 2, where σ is at the left of all $p_n(k)$ (the zeros of eq (2.19))

On this deformed contour (b) the electrostatic potential is evaluated as follows

$$\Phi(k, t) = \sum_n R_n(k)e^{p_n(k)t} + \int\limits_{-\alpha-i\infty}^{-\alpha+i\infty} \Phi(k, p)e^{pt}\mathrm{d}p \tag{2.20}$$

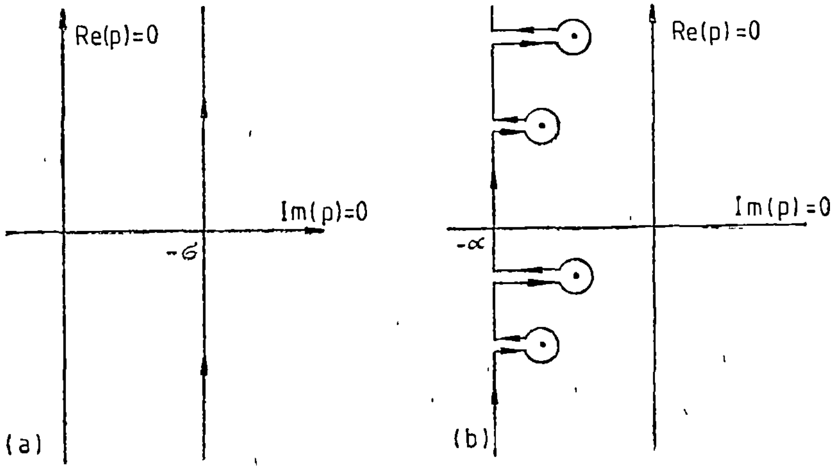

Fig. 2 The deformed contour G (Landau contour) and the poles $p_n(k)$ for the integral (2.19) in the complex plane $Re(p)$, $Im(p)$

when $t \to \infty$ the integral from the right hand of eq. (2 2) is annuled : the contribution of poles $p_n(k)$ is dominant at $t \to \infty$ and in this case we have only a dispersion relation of the form

$$D(p, k) = 0 \tag{2.21}$$

This dispersion equation, which is valuable for many applications, explains the dispersion of the electrostatic plasma oscillations only when, after an enough long time, the contribution done by the integral will be damped. Landau has done a solution of the plasma oscillation modes for the limit of long wave lengths (small wave numbers k) and for times $t \to \infty$ [3] · $Re(p_n) \to 0$ and $Im(p_n)$ remains finite when $k \to 0$ The pole from the complex plane will be under the real axis :

$$p \approx -i\omega + \gamma \tag{2 22}$$

where $|\gamma| \ll \omega$ We use the sign of ω so that the wave propagates in the positive direction of the x-axis, when $k > 0$

The eq (2 19) can be written as

$$1 - \frac{q^2}{\varepsilon_0 k^2 m} \int_C \frac{f_0'(v)\, dv}{\left(v - \frac{ip}{k}\right)} = 0 \tag{2.23}$$

with the contour C illustrated in the fig 3

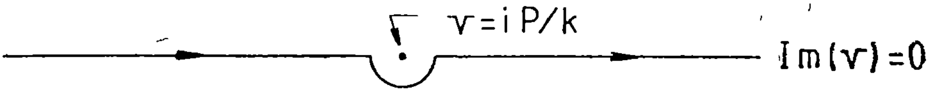

Fig 3 The contour G around a pole $v = ip/k$ of the integrals (2 23)—(2 24)

Then we can deduce that there are two contributions to the integral of eq (2.23), one from the real axis and the other from the integration on the semicircle around the pole

$$\int_C \frac{f_0'(v)\, dv}{\left(v - \frac{ip}{k}\right)} = P\left[\int \frac{f_0'(v)\, dv}{\left(v - i\frac{p}{k}\right)}\right] + i\pi f_0'(v) \tag{2.24}$$

where the first contribution is the principal part of the Vlasov kinetic term and the second imaginary term is small. The principal part P is easy to be evaluated if we use the initial assumption [3] for the real and imaginary parts of the poles p_k(see eq (2 22)) The pole $v = ip/k$ will appear for large values of the velocity

v, where $f_0(v) \to 0$ and we can evaluate the integral on the real axis by expanding the integrand after the powers of k

$$\mathbf{P}\left[\int \frac{\mathrm{d}f_0}{\mathrm{d}v} \cdot \frac{\mathrm{d}v}{\left(v - i\frac{p}{k}\right)}\right] \approx -\frac{k}{ip}\int_{-\infty}^{+\infty} \frac{\mathrm{d}f_0}{\mathrm{d}v}\left(1 - i\frac{kv}{p} + \ldots\right)\mathrm{d}v =$$

$$= -\frac{k^2}{p^2} n_0 = -\frac{k^2}{p^2}\int_{-\infty}^{+\infty} f_0(x, v, t)\mathrm{d}v \tag{2 25}$$

The eq. (2 25) is introduced in the dispersion relation (2 23) with the result

$$1 + \frac{q^2 n_0}{m\varepsilon_0\,(-i\omega + \gamma)^2} - \frac{i\pi q^2}{\varepsilon_0 k^2 m} f_0'\left(v = i\,\frac{(\gamma - i\omega)}{k}\right) = 0 \tag{2.26}$$

equation which could be solved by the method of succesive approximations, considering $p = -i\omega + \gamma$, with $|\gamma| \ll \infty$ The first approximation will be obtained by neglecting γ and the small imaginary part of the equation (2 26) under the form

$$1 - \frac{\omega_{pe}^2}{\omega^2} = 0 \text{ or } \omega = \omega_{pe} \tag{2.27}$$

or $\omega = \omega_{pe} = \left(\dfrac{ne^2}{m\varepsilon_0}\right)^{1/2}$

Including also the term in γ and making the series expansion after this parameters we obtain the expression

$$\gamma = \frac{\omega_{pe}}{2} \cdot \frac{\pi q^2}{k^2 \varepsilon_0 m} \cdot f_0'\left(\frac{\omega_{pe}}{k}\right) \tag{2 28}$$

we have considered here that for a Maxwell distribution function $f_0' < 0$, do not appear growing waves and then the expression (2 28) represents the damping rate of electronic plasma oscillations By substituting $f_0'(\omega_{pe}/k)$ from eq (2 18) we will obtain

$$\gamma = \left(-\frac{\pi}{8}\right)^{1/2} \cdot \frac{\omega_{pe}^3}{k^2} \cdot \frac{\omega_{pe}}{k \cdot v_{Te}^3}\, exp\left(-\frac{\omega_{pe}^2}{2k^2 v_{Te}^2}\right) \tag{2.29}$$

where

$$v_{Te}^2 = \omega_{pe} \cdot \frac{Te}{m} \tag{2.30}$$

we define

$$\lambda_{De} = \frac{v_{Te}}{\omega_{pe}} \tag{2.31}$$

as being the Landau wavelengths and then γ can be written as

$$\gamma = -\omega_{pe}\left(-\frac{\pi}{8}\right)^{1/2} \cdot \frac{1}{k^3 \cdot \lambda_{De}^3} \exp\left(-\frac{1}{2k^2\lambda_{De}^2}\right) \tag{2.32}$$

This result, as the first approximation $\omega = \omega_{pe}$, certifies the presumption initially made that $|\gamma| \ll \omega$.

An other simple approximation of the plasma oscillation damping can be made in the region of small wavelengths $\lambda < \lambda_{De}$ In this case it was considered that for a large k, $\omega/k \ll 1$ The oscillations with $\lambda \ll \lambda_D$ are damped in a fraction of a wavelength and then does exist collective oscillations of the plasma

As a conclusion, the expression (2.32) for γ is the coefficient of so called, "collisionless damping" or Landau damping of the electrostatic oscillations of a plasma This result could not be verified by experiments but different physical interpretations were proposed The most realistic and explicit interpretation [6] was done as follows: the expression (2 32) for γ shows that the oscillations damping is due to a small part of the electrons which move with the wave phase velocity v_f. Those electrons are resonant which can intensively interact with the plasma wave The particles which move with velocities something less than wave phase velocity will be accelerated, will take the wave energy, and the particles with the velocities larger than $v_f = \omega/k$ will transfer energy to the wave In the case of a Maxwellian distribution ($f_0'(\omega/k) < 0$) there are more particles which move slower than the wave, than those which move faster As a result the resonant electrons absorb energy and so the wave is damped

3 The particle simulation of Landau damping process. The use of computer simulation method to study the Landau damping in a plasma is a way to verify the theoretical results and to supply for the absence of experimental data; the results of such a particle simulation of this process confirm the analytical data establish the physical meaning of the collisionless damping, which is not only a consequence of the integration on the complex contour but actually it consists in a phase mixing of the initial perturbations from the plasma.

Using the electrostatic onedimensional model (code) of particle simulation, also used for other plasma processes [7, 8] the following "input" data for Landau damping are introduced in the ES1 programme:

	Nr of spatial cells	Nr of steps	Nr of species	Compens factor	Ateriuation factor	Time step	History of Fourier energy (modes)
Ingen	NG = = 128 256	NT = = 200	NSP = = 2	A1 = 0 5	A2 = 1	DT = 0 1	MPLOT = = 1, 2, 3, 4 End
Species 1	Nr of particles		Plasma frequency		Thermal velocity (quiet star or not)		
	N = 1024 = 2^{10} = 512 = 2^5		WP = 0,383		T1 = 0,0 , = 0,9		l = 2,5 — 4
Specie 2	N = 128		WP = 0 924		T2 = 0,0 , = 0 5 Mode = 1		q/m = 0 01 End

After running this programme, we can see that the MODE-1 presents a damping at $t = 30$ If we take a larger number of electrons $N = 4096$, the physical properties of this damping will be detalied From the diagrams of electrostatic field energy evolution the linear damping rate of the wave amplitude can b deduced and compared with the analytical result which is subsequently done [4], the nonlinear trapping frequency of the electrons by the wave can be also deduced

$$\gamma = \omega_i = \left(-\frac{\pi}{8}\right)^{1/2} \cdot \frac{\omega_{pe}}{k^3 \lambda_{De}^2} \cdot \exp\left(-\frac{1}{2k^2\lambda_{De}^2} - \frac{3}{2}\right) \tag{2.33}$$

for $\frac{\omega}{k} \gg v_T$ and $\lambda_{De} = \frac{\chi_{Te}}{4\pi n_0 e^2}$

If $\omega_r = 0.9$ (from simulation) then $\gamma = \omega_i = -0.058$

$$\gamma = \omega_i = -0.058 \tag{2.34}$$

Other results which are obtained after the computer simulations are the electrostatic plasma wave will be damped with the damping rate

$$\gamma = \omega_i = -0.15 \cdot \omega_{pe} \tag{2.35}$$

a value which is enough closed to that expected from the linear theory [4] but we can see that the wave energy decreases by just an order and then the damping is slow A similar result was obtained by other authors [9] by using a simulation technique which includes a quiet thermal start

If we use the parameters $v_{T1} = 0.5$ (or $v_{T2} = 0$) will be not obtained an exponential decreasing of the wave amplitude as in the first case To reproduce more exactly the Landau damping the following simulation expedients will be used. the electrons will be devided in two groups, as different species of particles — cold and warm electrons, with a Maxwellian distribution of velocities

We choose the values $\omega_{pe}^2 \gg v_f^2$ and $k \cdot v_j \approx \omega_{pi}$ and the phase velocity v_f is placed at the largest slope of the distribution function $f_{0j}(v_j)$, so will exist many particles in the caption region, but the damping rate is $\gamma \ll \omega_{pi}$.

Another expedient permits us to decrease the necessar particle number in the simulation, $N_i \ll N_j$ means that the cold electrons transport a much larger charge than the warm electrons We use for cold electrons $Q/m = 0.01$ with the aim to avoid a nonlinear response and $N_i = NG$, this simulation expedient does not affect the plasma oscillations behaviour at the considered small amplitudes. The imput parameters used in this case of simulation are the following: INGEN DT = 0.1, NT = 1000; NG = 256; NSP = 2; A2 = 10^4; IPHI = = 20; IXVX = 20; MPLOT = 1, 2, 3, 4

The hot electrons are specified by the data.

$N_i = 2^{14}$; $WP = 0.383$; $\bar{v}_{T2} = 0.9$

and the cold electrons by the values:

$N_i = 256$, $QM = 0.01$; $WP = 0.924$; $v_0 = 0{,}0$; $v_{T2} = 0{,}0$; $v_1 = 2{,}5 \cdot 10^{-4}$ (MODEL 1).

There is also the possibility of introducing so called "marker" electrons, the third specie of particles in the simulation code, with the following parameters:

$N_k = 1020$, $NLG = 1020$, $Q/M = -0.1$; $\omega_p = 10^{-10}$; $v_0 = 0.9$, $v_{T2} = 0.8$; 0.9; 1.

The results of these simulations are done in the fig *4a — d* and fig. *4e* which represents the evolution in the phase space (v_x, x) and the electrostatic field energy evolution

The fig. 4a—e represent the time $t = 2, 16, 20, 40$ in the interval $0 \leqslant x \leqslant 2$ and indicate the "markers" at the velocities $v = 0.8, 0.9; 1.0$. Each particle is represented twice, once at (x, v) and second at $(x + L, v)$

In the fig. 4d can be seen the decreasing in the oscillation energy In the fig. 5 the mode-1 energy variation is done, being observed the oscillation damping also as a function of time The growing in wave amplitude, which is observed in

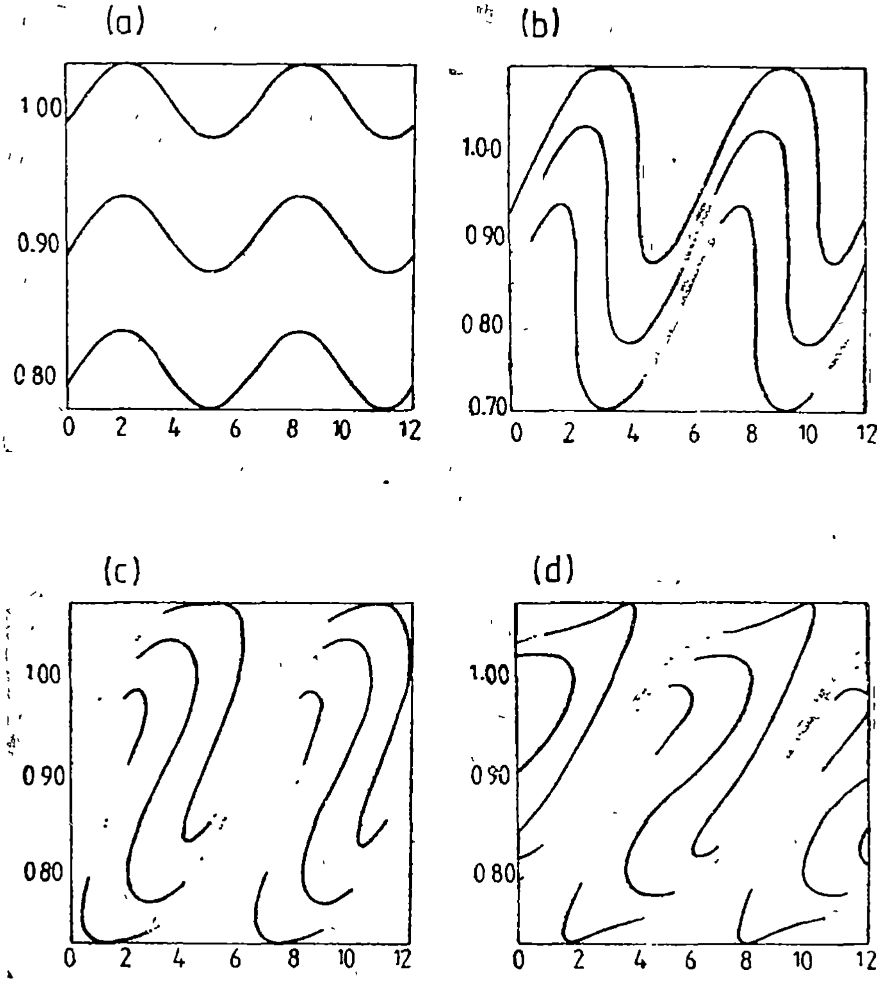

Fig 4 a—d The phase space (v_x, x) evolution of the plasma system at the times $t = 2, 16, 30, 40$

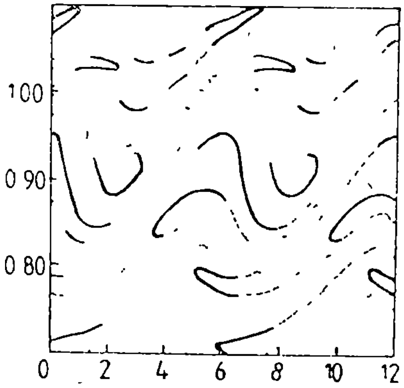

Fig 4e The evolution of the electrostatic field energy and his decreasing

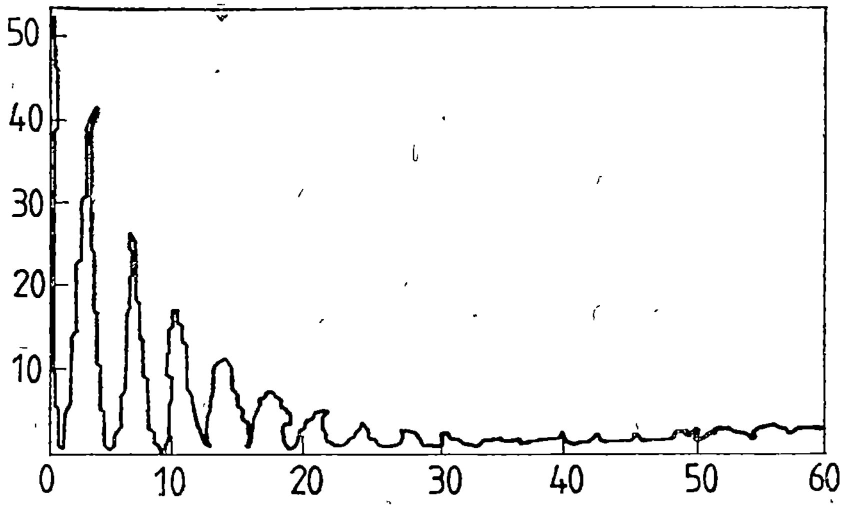

Fig 5 The time evolution of the mode-1 oscillation energy

the fig 3 after the running time $t = 45$, is due to the electrons caption in the wave field Using only the particles with critical velocities $v \gg 0$ 9 the simulation to set—off also the nonlinear process of electron caption in the wave potential and their balance can be seen in the fig 6 for the mode-2 energy.

In the fig 7 it can be seen the damping in time of the wave electrostatic field energy which represents the same evolution compared with that from fig 4f in phase space

These diagrams obtained in phase space (v_i, x) contain information about the integration code of Vlasov equation for $f(x, v, t)$ which represents an other modality of plasma describing

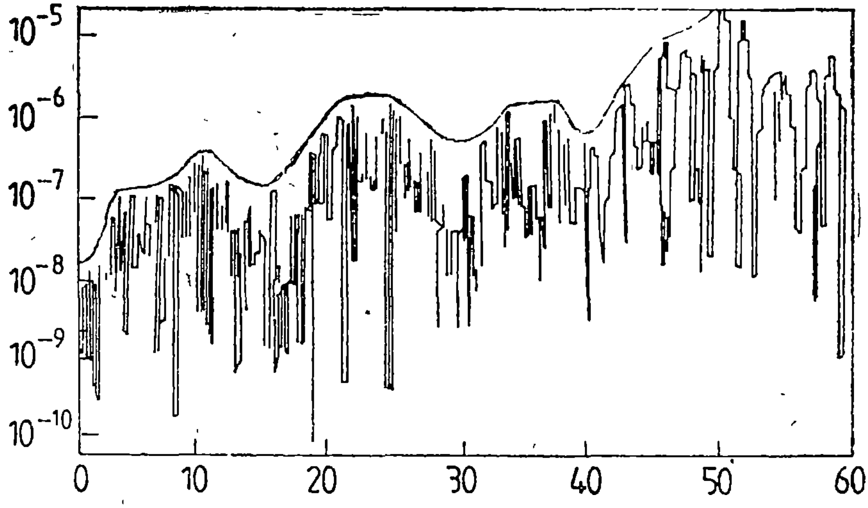

Fig 6' The nonlinear trapping and balance of the electrons in the wave potential

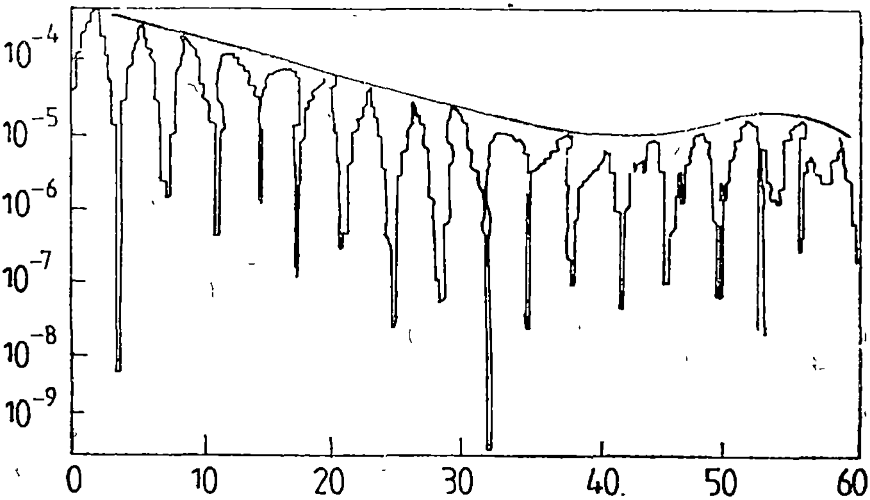

Fig 7 The time damping of the electrostatic field energy of the electrostatic waves

4 **Conclusions.** The Landau damping is a linear phenomenon which is difficult to recover for any significant period of time because in a short time the nonlinear processes of trapping and balance which appear in a plasma impose the end of the damping, usually the nonlinear processes from the real or simulated plasmas consist in the fact that the initial equilibrium is strong distorted or distroyed as the wave amplitude grows very large (the nonlinear stage of the plas-

ma instabilities) In our case of performed simulation we ascribe the nonlinearity which limit the Landau damping to the process of electrons trapping by the waves. From the same reason the linear stage decreases for large perturbations since the trapping period decreases As a conclusion we give a more detailed physical meaning and the most possible mechanism of the Landau damping Considering a Maxwellian distribution of plasma electron velocities there are some electrons which move more rapidly and some of them which move more slowly compared with the phase velocity $v_f = \omega/k$ If we use a system which moves with this velocity v_f the wave potential is a sinusoidal one in x and decreases in time with a damping rate $\omega_i = \gamma$ Neglecting temporary this decreasing it can be observed that the electrons with the velocity in the interval $(v = \omega/k \pm v_{trapp})$ will be trapped by the wave, having an oscillation around v_f, with a frequency ω_{trapp}, we can see that the relations between these parameters are the following

$$\frac{1}{2} m \ v_{trapp}^2 = q\Phi \tag{3 1}$$

and

$$m \cdot \omega_{trapp}^2 = qk^2\Phi \tag{3 2}$$

where Φ is the highest amplitude of the wave component with phase velocity v_f.

If we return in our analysis to a fix reference system we can observ that the resonant electrons with the velocities $v \in \left(\frac{\omega}{k} - v_{trapp}, \frac{\omega}{k}\right)$ are changed with those with velocities $c \in \left(\frac{\omega}{k}, \frac{\omega}{k} + v_{trapp}\right)$, in a time $t \cong \pi/\omega_{trapp}$ If initially there are more slow electrons, with $v \in \left(\frac{\omega}{k} - v_{trapp}, \frac{\omega}{k}\right)$, will appear an amplification of their energies, which is supplied from the plasma wave energy and indicates why the damping rate ω_i is proportional to $(\partial f_0/\partial v) = \frac{\omega}{k}$ and explains the collisionless dissipation which leads to Landau damping in a plasma

REFERENCES

1 L Tonk, I Langmuir, Phys Rev, 1929, **33**, p 195

2 D Bohm, E P Gross, Phys Rev, 1949, **75**, p 1864

3 L D Landau, J Phys (URSS), 1946, **10**, p 25

4 N A Krall, W A Trivelpiece, *Principles of Plasma Physics*, 1973, p 383—389

5 P C Clemmow, J P Dougherty, *Electrodynamics of Particles and Plasmas*, 1969, p 264

6 J Dawson, Phys Fluids, 1961, **4**, p 869

7 S Coldea, C Băleanu, J Karácsony, *Studiul instabilităţii bi-fascicul şi a instabilităţii fascicul-plasmă prin metoda simulării*, în „Transportul fasciculelor încărcate şi a undelor electromagnetice prin plasmă", contract nr 13/1986 cu MEI, faza 1987 şi 1988

8 Ch K Birsdall, B I Langdon, *Plasma Physics via Computer Simulation*, Ed McGrow-Hill, New-York, 1985

9 J Denavit, J M Walsh, Comm Plasma Phys Control Fusion, 1981, **6**, p 209

STUDIA UNIV BABEŞ-BOLYAI, PHYSICA, XXXV, 2, 1990

MAGNETIC PROPERTIES OF Fe—RE—B METALLIC GLASSES

GH. ILONCA* and V. IONCU*

ABSTRACT. Amorphous Fe—RE—B alloys (*RE = Er*, *Ho*) were investigated The temperature dependence of magnetization shows a maximum at low temperature The Curie temperature and the mean magnetic moment of iron and RE decrease with increasing RE content The values for critical exponents δ, β and γ in the immediate neighbourhood of Tc were obtained from magnetic measurements, and these values are in a reasonable agreement with those derived from the theories based on the three-dimensional Heisenberg model

1 **Introduction.** The study of magnetical properties amorphous alloys with the additional of a small amount of a rare earth element to binary iron-boron metallic glasses have shown that these impurities alter magnetic and other physical properties [1—4] The influences of rare earth elements may be explained by taking into account 1) the size effect of rare earth (RE) atoms, this may cause a disturbance of direct exchange between iron atoms thereby decreasing (or increasing) the Curie temperature of the Fe—RE—B amorphous alloys compared with the binary Fe—B [1], 2) the magnetic moment of RE, since, it alters the net magnetization of the alloy, 3) the high chemical affinity between RE and B atoms, which may lower the mobility of boron and makes higher the crystallization temperature by stabilizing the amorphous state, 4) the exchange interactions between the magnetic active atoms

The strongest interaction in crystalline and amorphous *RE—TM* (transition metal) alloys is between the *3d* moments The smallest in strenght is the interaction between the localized *4f* moments [1] The interaction between the *4f* and *3d* moments in all heavy RE—TM alloys gives antiparallel coupling

In this paper we present results of a study the influence of erbium and holmium on the magnetic properties of Fe—B amorphous alloys with respect to the grant magnetic moment of Er^{3+} (9 60 μ_B) and Ho^{3+} (10 6 μ_B) for a free ion

2 **Experimental Techniques.** The $Fe_{82-x}RE_xB_{18}$ (RE = Ho, Er and $0 \leqslant x \leqslant 9$) ternary alloys were prepared from Fe—RE and Fe—B alloys by electric arc melting in inert gas atmosphere The amorphous ribbons, on average about 25 μ *m* thick and 5 mm wide were made by single-roll melt-quenching on a copper-nickel roller in an inert amorphous gas and were judged to be fully amorphous by *X*-ray diffractions All the samples used in this investigation had been previously relaxed in an oil bath at 500 K for 2 *h*

The magnetization and magnetic susceptibility were measured using the standard Faraday technique [5].

3 **Results and Discussion.** In general the temperature dependence of the zero field spontaneous magnetization $\sigma_S(O, T)$ and of zerofield magnetic susceptibility $\chi(O, T)$ are of special interest Both quantities have been derived from mea-

---

* *University of Cluj, Department of Physics, 3400 Cluj-Napoca, Romania*

surements of the magnetization $\sigma(H, T)$ as a function of the magnetic field H and temperature T. According to Krommuller [6], the deviation $\Delta\sigma(H, T)$ from absolute magnetic saturation $\sigma_S(0, 0)$ is composed of three terms

$$\Delta\sigma(H, T) = \Delta\sigma_T(O, T) + \Delta\sigma_P(H, T) + \Delta\sigma_S(H, T) \tag{1}$$

where $\Delta\sigma_T \sim T_{3/2}$ represents the effect of single-particle and spin wave excitations in zero field.

$$\Delta\sigma_P = \chi_P H + \alpha T H^{1/2} \tag{2}$$

results from paramagnetic processes such as Pauli paramagnetism and the spin wave gap $g\mu_B H$ and finally

$$\Delta\sigma_S = C_1 H^{-1/2} + C_2 H^{-1} + C_3 H^2 \tag{23}$$

account for spin inhomogeneities due to stress sources and local structural functions

In Fig 1 we show temperature dependence of mass magnetic polarization σ of Fe—Er—B and Fe—Ho—B in the 77—600 K temperature range where the amorphous alloys are in paramagnetic state

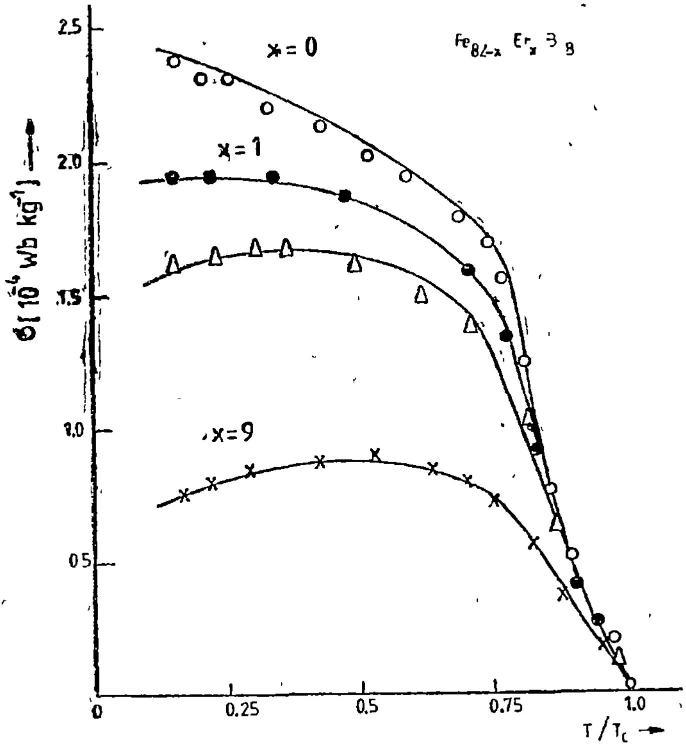

Fig 1 Temperature dependence of magnetic polarization

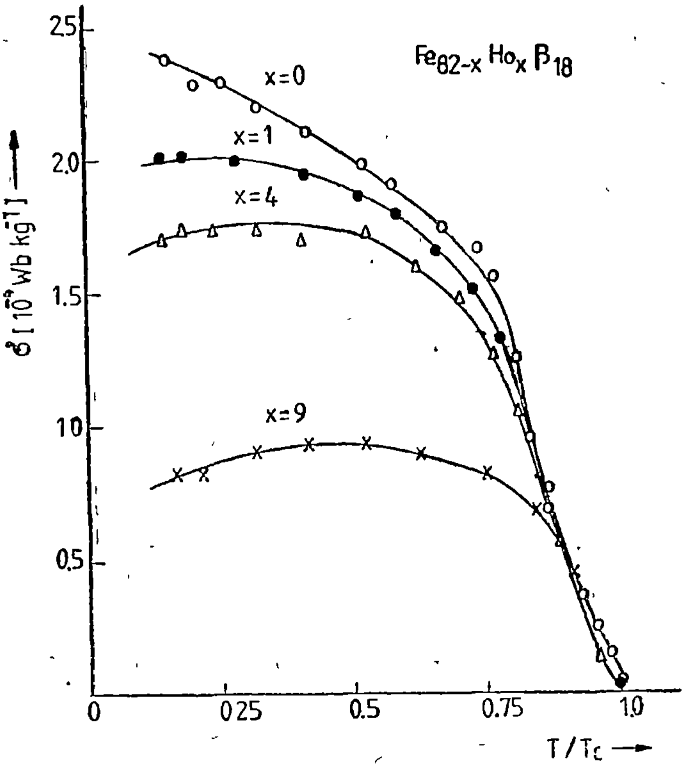

Fig 1b Temperature dependence of magnetic polarization

We used a relative temperature scale for the better comparison

The amorphous Curie temperatures, *Tc*, as a function of RE (RE = Er, Ho) concentration Fig 2 On alloying RE, the Curie temperatures decrease on straight lines This indicates that Er and Ho added to Fe—B weakens the ferromagnetic exchange between iron atoms This decrease of Curie temperature, may be caused by the size-effect of the *Er* and *Ho* atoms due to the distance — dependent exchange interaction or the magnetic moment of iron μ_{Fe}, in the given alloys decreases due to electron transfer from Er, respectively Ho, to the 3*d* band of iron [7] like that of boron to iron [8] On the other hand, Er—Fe of Ho—Fe interaction is more stronger than *Er—Er*, or *Ho—Ho* interaction This RE—Fe interaction (RE = Er, Ho), together with the random single —ion anisotropy of the RE atom, may lead to a misalignment between iron moments

The magnetization data plotted against $1/H$ are shown in Fig 3 The straight lines show that $C_1H^{-1/2}$ and C_3H^2 from eq. (3), (the terms which result from point-like defects or magnetic anisotropy fluctuations on an atomic scale, and isolated quasi-fluctuations) are negligible in comparison with CH^{-1} which is due to quasi-dislocation dipoles

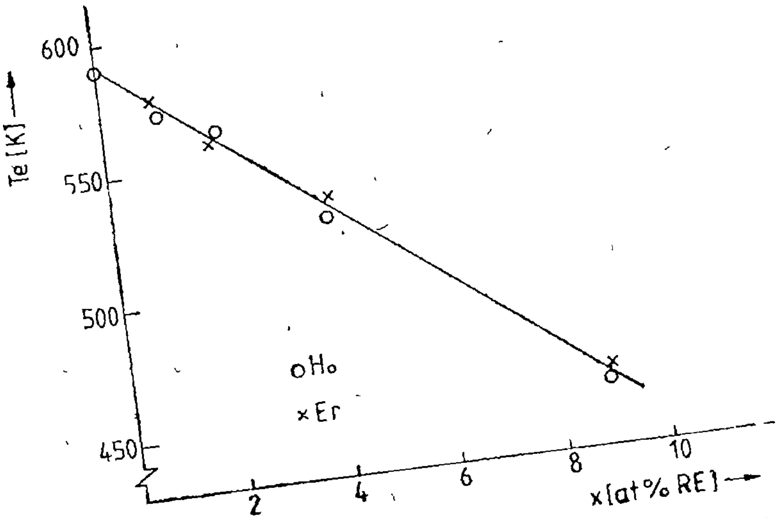

Fig 2. Amorphous Curie temperature versus Er and Ho content

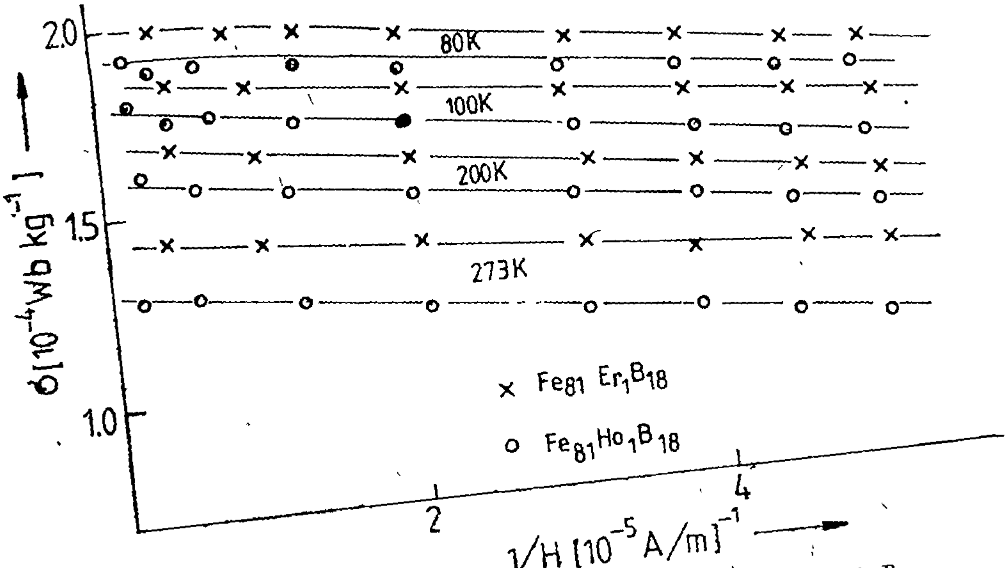

Fig 3 The plots of $\sigma(H, T)$ versus $1/H$ for $Fe_{81}Er_1B_{18}$ and $Fe_{81}Ho_1B_{18}$

The $T^{3/2}$ dependence for many amorphous alloys was verified [9] but from the series of amorphous Fe—RE—B (RE = Re and Ho) alloys only the ninary Fe—B follows this dependence (Fig 4). The σ ($T^{3/2}$) curbe in erbium and holmium-containing alloys has a maximum This maximum is more remarkable in the alloys containing more RE and on increasing the Er, Ho content it is shifted towards higher temperature.

The given results suggest that the magnetic moments of RE (Er and Ho) atoms are oriented antiparallel to iron moments. This is in agreement with the results on many amorphous RE—Fe alloys [10]

From the measured σ (77, 0) values we determined the mean magnetic moment $\bar{\mu}_{Fe+RE}$ which is a function of erbium, respectiv holmium content (Fig. 5) We have calculated μ^{calc}_{Fe+RE} for collinear antiparallel oriented RE and Fe magnetic mament using $\mu_{Ho} = 10\ 3\ \mu_B$, $\mu_{Er} = 9\ 60\ \mu_B$ and $\mu_{Fe} = 2{,}05\ \mu_B$ We have obtaineda good agreement between experimental and calculated values (Fig. 5).

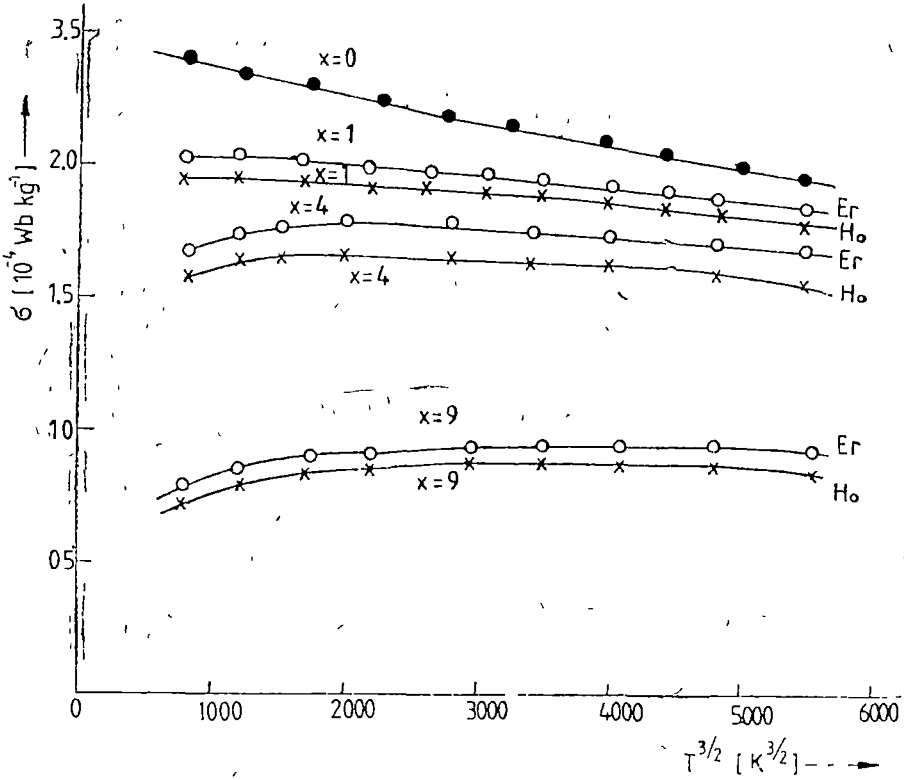

Fig 4 The plots of $\sigma(H, T)$ versus $T^{3/2}$

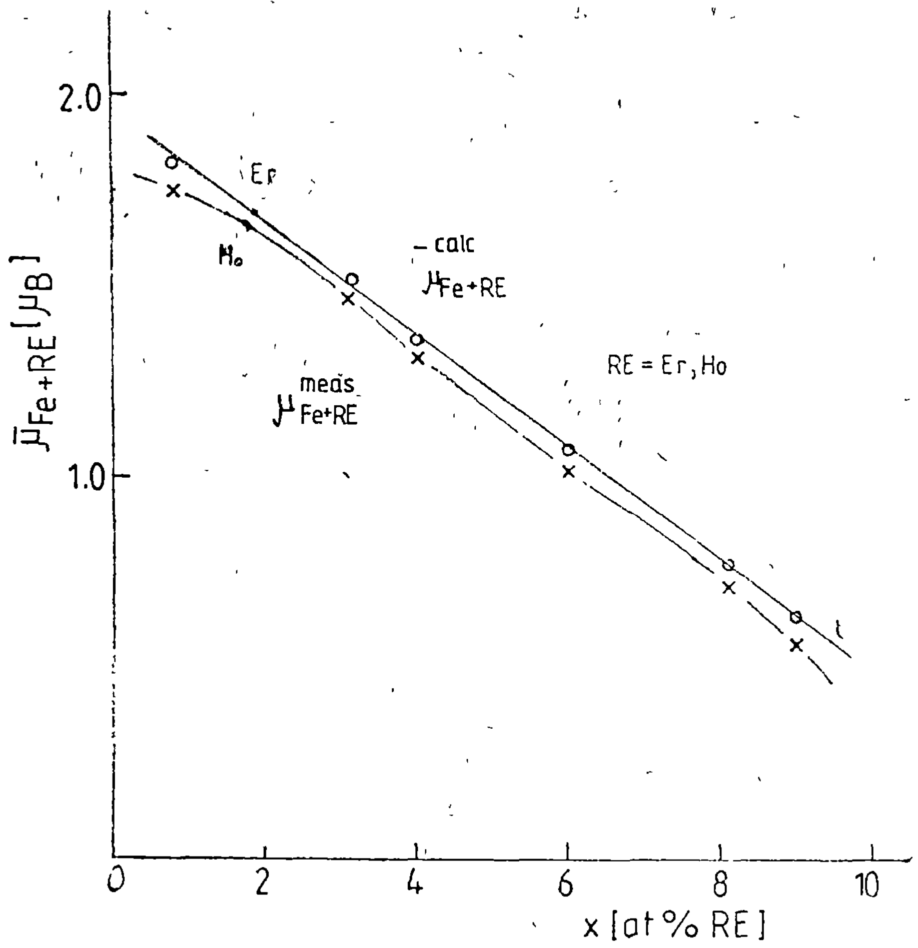

Fig 5 Mean magnetic moments versus Er and Ho content.

The magnetic phase transition is described by

$$\sigma_S = a_0 \left(\frac{T - T_c}{T_a}\right)^{\beta} \quad \text{for } T < T_c \tag{4}$$

$$\chi^{-1} = \frac{b_0}{a_0} \left(\frac{T - T_c}{T_c}\right)^{\gamma} \quad \text{for } T < T_c \tag{5}$$

$$\sigma(H, T) = C_0 H^{1/\delta} \quad \text{for } T = T_c \tag{6}$$

where β, γ and δ are critical exponents and a_0, b_0/a_0 and c_0 are the critical coefficients Since eq (6) is true only at $T = T_c$, we ploted in $\ln \sigma = f(\ln H)$ and we have used an interpolation formula given in ref. [11] A strait line was fitted for each temperature by the least-squares method for 10 experimental points.

The temperature dependence of the slope σ^{*-1} of the straight line fitted for experimental points could be interpolation formula [11] $\sigma^{*}(T) = 4\ 39 - 0.48\ x(T - 592\ 2)$ The value σ^{*} at $T = T_c$ gives the value of the critical exponent. We have obtained the following values for critical exponents $\sigma = 4\ 10 - 5\ 10$; $\beta = 0\ 41 - 0\ 44$ and $\gamma = 1\ 20 - 1\ 50$

4. **Conclusions.** We have investigated the influence of Er and Ho on the temperature dependence of magnetization in Fe—RE—B alloys

The $T^{3/2}$ dependence at low temperature was not verified

The magnetization decreases with decreasing temperature and values of critical exponents δ, β, γ suggest us an antiferromagnetic coupling between the atomic moments of Er, Ho and Fe

The amorphous Fe—RE—B alloys exhibit a well defined magnetic phase transition with critical exponents in a reasonable agreement with those calculated on the base of the Heisenberg model

REFERENCES

1 N Heiman, K Lee, *Proc Int Conf Magn*, Magn Mater **34,** 319 (1976)
2 O Dusa et al, J Magn, *Magn Mater* **41,** 119 (1984)
3 L Potocky, I Kovac, L Novac, E Kisdi-Koszo and A. Lovás, *Proc. of the Fifth Int Conf on Rapidly Quenched Metals*, Ed H Warlimont, 1984, p 1153
4 Gh Ilonca, I Ardelean, and M Oană, *Proc of Conf Advanced in Physics*, Constanța, 1988, p 317
5 C M Hurd, Cryogenics **6,** 264 (1966)
6 H Kronmuller, IEEE, Trans Magn **15,** 1218 (1979)
7 L J Tao et al, Solid State Commun **13,** 1491 (1973)
8 R Hasegawa, R Ray, J Appl Phys, **49,** 4174 (1978)
9 R W Cochrane, G S Cargill, Phys Rev Lett **32,** 476 (1974)
10 A K Bhattacharjee et al, Physica, **91 B,** 179 (1977).
11. A Arrot and J E Noakes, Phys Rev. Lett. **19,** 786 (1967).

STUDIA UNIV BABEŞ-BOLYAI, PHYSICA, XXXV, 2, 1990

DEVICE FOR THERMOSTATTING SMALL ENCLOSURES SYNCHRONIZED WITH THE NETWORK FREQUENCY

V. IONCU*, GH. CRISTEA*

ABSTRACT. An instrument capable of thermostatting small enclosures performing, at the same time, the temperature control within less then ± 0 01 K, and temperature measurement with accuracy better then 0 1 K, is proposed Helium or nitrogen vapour flow is used as thermal agent in the low temperature domaine The varicap diodes or platinum resistors are used as temperature sensors The device is suited for temperature control in NMR and NQR studies, in phase transition and single crystal growth studies as well as for the measuring of the superconducting material parameters.

Introduction. A device for thermostatting the enclosures having the volum smaller then 100 cm^3, which assures its temperature control within less then ±0 01K and temperature measurement with accuracy better then 0.1K is decribed in this paper Unlike the previous devices intended to such purposes which were, generally, orientated towards so called "in phase-control" of the power [1 — 3], we propose a scheme working on the "synchrone-control" principle, also called "switching at passing through zero" In the domain of the low temperatures a helium or nitrogen vapour flow is used as thermal agent The device is suited for temperature control in NMR and NQR studies, in phase transition and single crystal growth studies as well as for superconducting material parameters measurement

The temperature programming circuit. Instead the description of the functioning mode of the apparatus, whose block diagrame is shown in figure 1, as a whole, we present first the role played by each of its blocks.

The temperature programming circuit (Fig 2) is realised by means of the I_{30} operational amplifier The group of the resistive switches K_1 and K_2 allows the rough selection, in steps of 50 K, respectively of 5 K, of the temperature domain which has to be stabilized The P_6 potentiometer assures the fine, i e. continually, adjustment of the temperature within 5 K Practically speaking, the obtaining of the pre-established temperature is equivalent to the restoring the equilibrium of the voltage at the input terminals of the I_{30} operational, so that its output voltage is zero

The 10 mV/K voltage at the inversory input terminals of the I_{30} operational is supplied by the circuit amplifying and linearizing the signal given by the temperature sensor Depending on the magnitude and the sens of the temperature deviation from the pre-established value, a voltage will appear at the I_{30} operational output This voltage automatically commands one of the variants of the analogous digital converter (ADC) of the delta/sigma type [4] This type of con-

---

* University of Cluj, Department of Physics, 3400 Cluj-Napoca, Romania

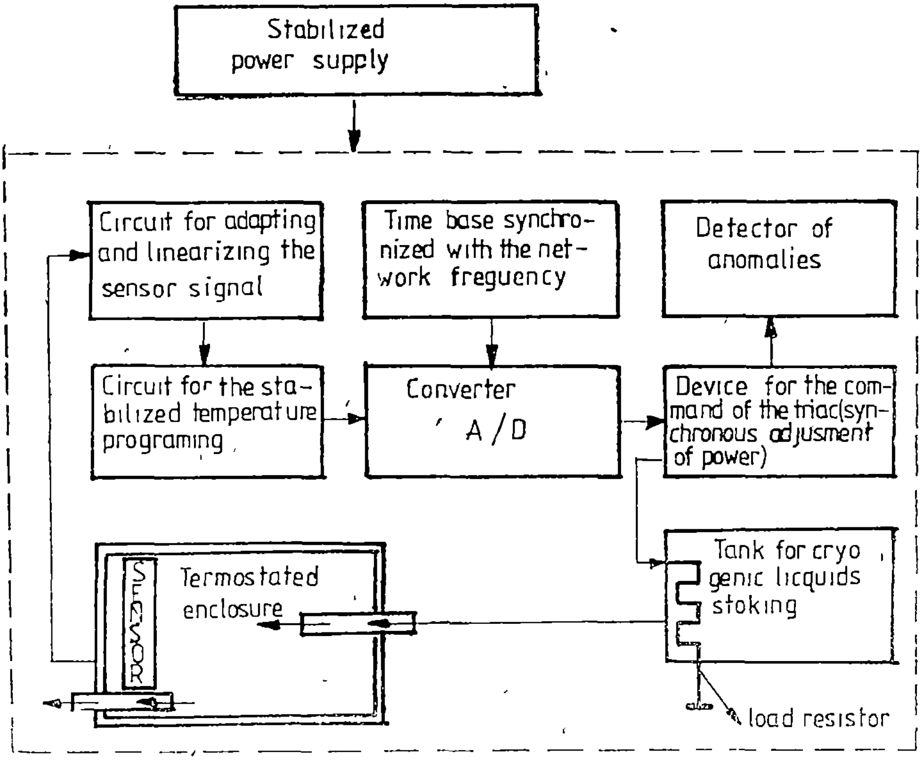

Fig 1 The block-diagram of the thermostatting instrument

verter has been accomodated to accomplish an integral synchrone command of the power in the thermostatting load

The „in phase-control" versus „synchron-control". The applications of the different semiconductor switching devices (thiristors, triacs etc), described previously [1 — 3], to the electric power regulation in leads functioning in alternating current circuits has orientated so far, generally, towards the so called "in phase-control" of power (Fig 3a)
The "in phase-controlled" regulators are simple but a serious difficulty arises, however, concerning the suppression of the perturbating radiofrequency spectrum, which appears as a result of the initial profile of the harmonical evolution of the impulses The spectrum suffers changes according to the degree of the adjustment, the nature of the load and so on. The avoiding of radio interferences is particularly difficult, especially when high power is controlled

When the feeding voltage is not harmonical (but squre) and the power is a linear function of phase difference (Fig. 3b), another question must be resolved This is the necessity of linearization of the adjustment characteristic In the case of sinusoidal evolution of the signal, the power does not change in a linear manner. However, available power may be estimated by calculating the integral of the

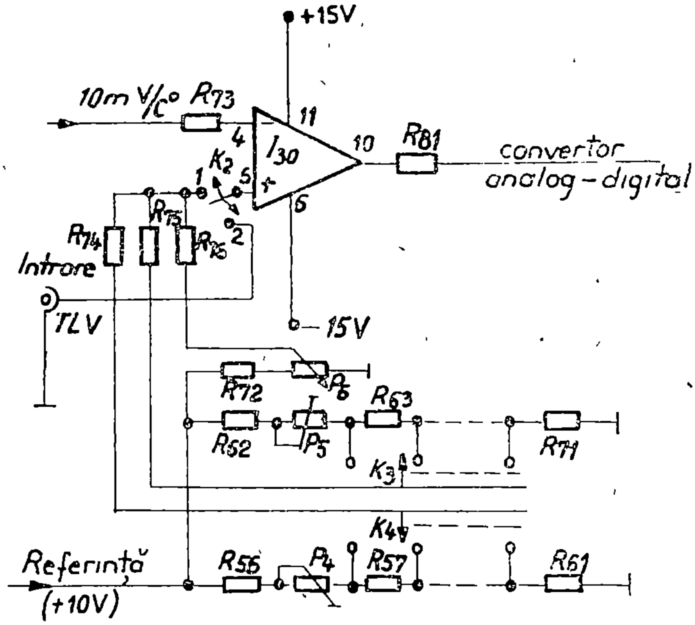

Fig 2 The circuit for temperature programming

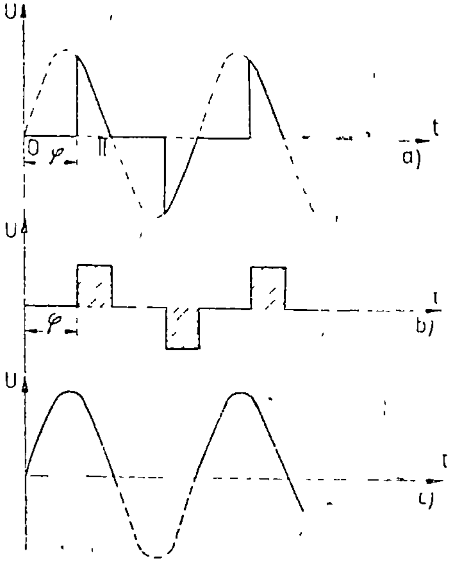

Fig 3 The modalities for the command of switches a) voltage evolution for „in phase — command, b) linear voltage evolution for "in phase-command" , c) load voltage evolution for synchronous — command"

signal over a whole period of time, using the sampling side of the voltage. The analogical character of the "in phase-control" manifests itself even in the limitation of the temperature and/or of the long lasting stability of the circuits (the phase-circuit, the semiconductor components etc)

In many cases, especially in controling of the thermal processes, finds itself an application so called "synchronous-driving" which, though yields a perturbating radio spectrum too, is much smaller [5, 6] The functioning principle of the analogical-digital (*A*/*D*) converter with synchronous-driving is autlined in figure 3 Unlike the "in phase-control" command, here not every halfwave of the network voltage is commanded The voltage (current) evolution remaine harmonical but it changes periodically, together with the switchings, so that to the controller arrives the needed number of halfwaves The figure 3 justifies also the name of "switching at passing through zero" given to this kind of control.

Owing to the reduced level of the voltage (and current) impulses (u_t, $i_z = 0$), which occure in the switching moment, the distortion spectrum is practically negligible as compared with that appearing in the case of "in phase-control". Concerning the power, the most simple are the regulators with synchronous command, which are very much similar to the classical ones, having two alternatives, of on-off type

The order of magnitude of the thermal sources and environment time constants is much higher then the period of the network voltage Therefore, in order to obtain the pre-established temperature it is not decisive the sampling of every halfwave Depending on the requirements of the regulating stage, only the ratio between the number of the active halfwaves and the number of the blocked halfwaves is decisive for transfering power towards the load, in a well determined instant of time To illustrate intuitively, the physical phenomenon taking place we present in figure 4 a succession of sinusoidal voltage patterns

The comparation between the "in phase-control" and the "synchronous-control" of the heating source is possible with the help of figure 4 The analysis of this figure logically leads to the conclusion that heating source can be controlled not only in two positions but also in steps, by changing the ratio of the number of the active halfwaves on the load to the number of blocked halfwaves Therefore, the impulses succession, which releases the switch, must be matched to the requirements of the analogous nature of the control This means that a linear dependence between the input cantities (voltage in our case) and the amount of energy transfered to the load should be assured A synchronized version of the analogous-digital converter (of delta-sigma type) has been used by us for the control of the impulses succession

The analogous-digital converter. In figure 5 we present the diagramme of the analogous-digital converter constructed by us, in order to control synchronously the block driving the triac The alternating voltage of the network, having the frequency of 50*Hz*, is used for control only after it has been shaped in a rectangular one, of 100 *Hz*, which is synchronous with the passings through zero The voltage shaping is done in the monolitic circuit I_6 of the phase blocker and in the circuits $I_6 + I_9$ of frequency devider (Fig 6) The access of the impulses ($\sim$0 5 *ms* width) to the optocouplings O_1 and O_2, to drive the triacs, is commanded by the analogous-digital converter The information is transmited from data

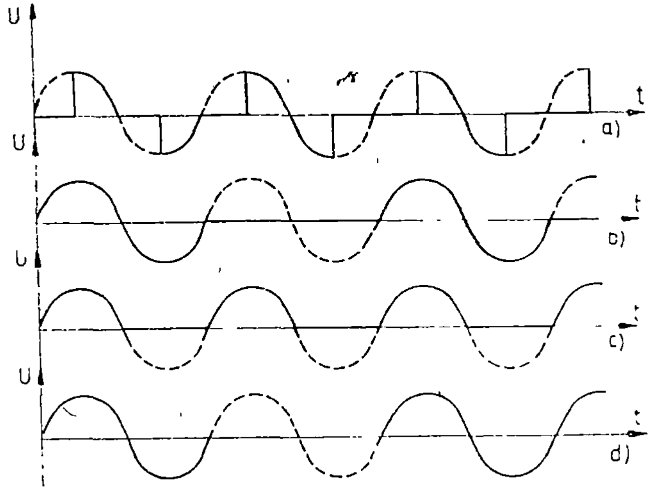

Fig 4 The time diagrams comparation a) the "in' phase-command", b) synchronous-command with whole period blocked, c) synchronous-command with blocked half periods of a single signe, d) "synchronous-command" by integrated cycles

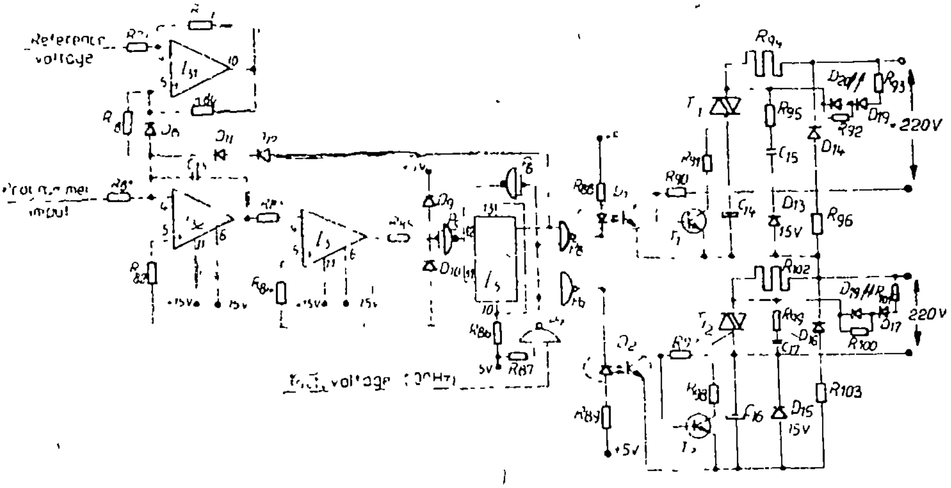

Fig 5 Utilization of analogous-digital converter for the load power command by means of the triac

input D to the output Q (or $\overline{Q}$) by means of the active front of the tact impulses delivered by the bi-stable D ($1/2\ I_6$), determining in this way the state of the I_{33} comparator input

As it has been previously pointed out, the comparator switches at the instant when the "tooth" from the integrator's output passes through zero level.

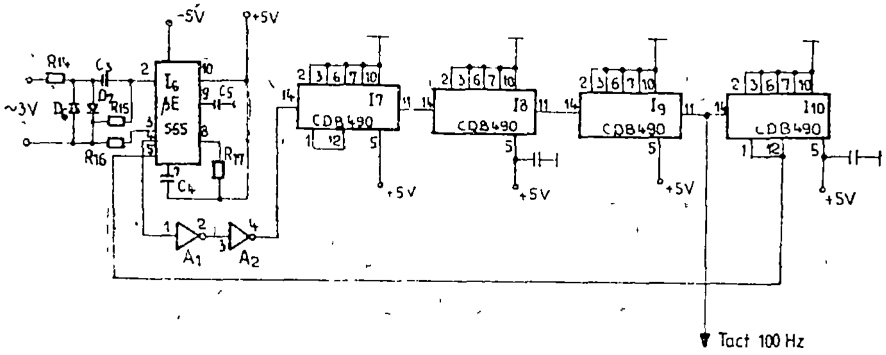

Fig 6 The time base and phase blocking circuit

The logical level at the output of bi-stable D changes as soon as the comparator switches over.

Tipping the output of Q (or $\bar{Q}$) and releasing or blocking, simultaneously, the gate P_8 (P_{13}) is always synchronous with the positive front of the next tact impuls Depending on the connection manner of the gates to the tipping circuit Q (or $\bar{Q}$) they are always active (or blocked) for a single time interval t_a (or t_b) of the integrator period. The working mode of this unit can be properly understood by simple inspecting the time diagram in Figure 7 For this sort of command both positive and negative halfwaves are used

In order to perform a high quality synchronous regulator it was necessary to select an integrator having a large time constant, when we have built the analogous-digital converter For exemple, to distinguish the order of units (in percentage) it is necessary that the repetition period of the converter to be approximatively equal to 100 × 10 $ms = 1$ s The convertion slope can be modified by choosing the proper value for R_{81} resistor The length of the integrator's period changes according to the value of the controlled voltage Because the ratio t_a/t_b (t_b/t_a) is used for the control (Fig 7), generally speaking, this is not a deficiency On the contrary, since the temperature dependence projects itself identically both in the limited interval $t_a(t_b)$ of the convertion period and in the entire time interval

The optoelectronic coupling block. The coupling which we have in mind is between the power group and the detector of anomalies Both from practical and security reasons are adequate to connect the controller with the power switch by means of a transformer or by an electrooptic coupling device, avoiding in this manner the galvanic contact between controller and network The electrooptic controllers are ideal for optimum control, as they assure a good separation of control block from network

The control of a high power circuit, by means of low power signals, energized directly from the alternating current network, may be obtained in version proposed by us The d c voltage of -15 V, feeding the T_1 (T_2) transistor, is obtained with the $C_{14}(C_{16})$, $D_{13}(D_{15})$, $D_{14}(D_{16})$ and R_{96} (R_{103}) group For the logical level

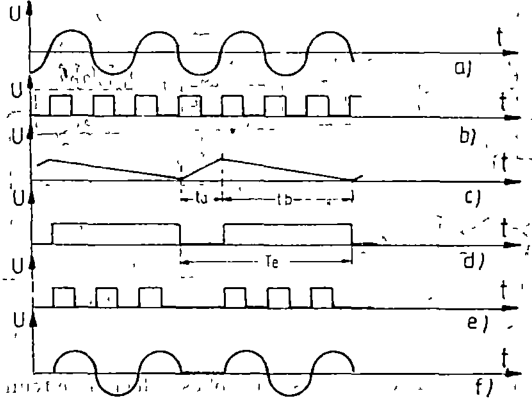

Fig. 7 The time diagrams for integral-synchronous control of the power, a) the network voltage voltage evolution, b) the signal evolution at the output II of the I devider (Fig. 6), c) the signal evolutionat integrator output for a determined value of the command voltage from programmer, d) the signal evolution at the Q output of the tipping bistable circuit $(2/2I_5)$; e) the impulses succesion at the output of the P_8 gate (Fig 5), f) the voltage (current) on the resistive load

L at the $P_8(P_9)$ exit, a sufficient illumination is created by electroluminiscent diod, so that the phototransistor in optocoupler works. In such conditions the $T_1(T_2)$ transistor opens, and a current of about 10 mA passes through the controlling gate of the triac. As a result the triac opens too and introduces a new charge in circuit. When logical level at the $P_8(P_9)$ gate exit is changed to H, the triac becomes blocked. The $R_{95}(R_{99})$ resistor and $C_{15}(C_{17})$ capacitor eliminates the possibility of noise appearance and improves the working confidence in the case when the load has inductive features, too.

In short, the detector of anomalies is a signalling device It is built using the D_{19}, D_{20}, R_{92}, R_{93} and D_{17}, D_{18}, R_{100}, R_{101} groups Its role is to signalize the interruption of the load, ceasing in consequence, the thermostatting of the working enclosure.

Conclusions. The thermostatting instrument realised allows the extension of measurement possibilities of the NQR spectrometer, to which it is attashed, in a large domain of temperature and, at the same time, improves the accuracy of phase transition temperature measurement. By moving the switch K_2 (Fig. 2) from position 1 into position 2, the thermostabilizer may be commanded with an external voltage, and programmed for the thermal treatments of materials or for single crystal growings The main purpose of the instrument is to assist us in measuring the parameters of the new high temperature superconducting materials and in performing accurate NQR measurements as function of temperature

REFERENCES

1. T L. Martin, P Perinmarèchal, *Electron Microel Industr* **1**, 68 (1970).
2. R Roublet, *Electron. Microel. Industr* **4**, 228 (1970)
3. A S Baclaghin, J I Smeliov, PTE, **5**, 156 (1983).
4. M Seifort, *Electronik*, **27**, nr. 6, 255 (1977)
5. E L Zuch, *Electronics* **48**, nr. 5, 91 (1975).
6. V F. Kudriasov, A N Sacs, *PTE*, **4**, 72 (1974)

STUDIA UNIV BABEŞ-BOLYAI, PHYSICA, XXXV, 2, 1990

MINISUPERSPACE TWISTOR QUANTUM COSMOLOGY

S. VĂCARU*

ABSTRACT. — The twistor wave function of the Universe is introduced Using twistor methods a finite-normed solution of the Weeler-De Witt equation for a homogeneous minisuperspace model is constructed

1 **Introduction.** The Penrose's twistor programme [1] intends to give a new approach for describing physical phenomena and laws by methods of algebraic and complex analytic geometry In recent years, twistor formalism have been applied with success in various areas: linear and non-linear field equations of the Yang-Mills, Einstein, supergravity and string theories [2—4]

We would like to explore the possibility of a twistor interpretation of the wave function of the Universe [5]. Namely, we'll consider the generation by twistor holomorfic functions of the general solution of the Wheeler-De Witt (WD) equation in a simple minisuperspace model

2 **The basic minisuperspace formalism.** In order to illustrate the twistor approach to the quantum mechanisc of the Universe we consider [5, 6] a minisuperspace model consising of a homogeneous massive scalar field $\Phi(t)$ minimally coupled to a Friedman-Robertson-Walker space-time metric (FRW_{Φ} model)

$$ds^2 = \frac{2}{3} G\pi^{-1}[-N^2(t)dt^2 + a^2(t)d\Omega^2_{(3)}],$$

where $N(t)$ is the lapse function and $d\Omega^2_{(3)}$ is the metric on a unit three-sphere With the cosmological constant set equal to zero, $a(t)$ and $\Phi(t)$ to be fixed on the boundaries at t_1 and t_2 the action is

$$S = \frac{1}{2}\int_{t_1}^{t_2} dt \frac{N}{a}\left[-\left(\frac{a}{N}\frac{da}{dt}\right)^2 + a^2 + \left(\frac{a^2}{N}\frac{d\Phi}{dt}\right)^2 - m^2 a^4 \Phi^2\right]. \tag{1}$$

We note [6] that the Klein-Gordon (KG) equation

$$(\check{\Box} - m^{-2})\Psi = 0$$

for a particle of squared mass m^{-2} in the auxiliary metric

$$d\check{s}^2 = m^2 M^2(\alpha, \Phi) dS^2_{(0)}, \tag{3}$$

where

$$a = m^{-1}e^{\alpha}, \quad M^2(\alpha, \Phi) = m^{-4}(e^{4\alpha} - \Phi^2 e^{6\alpha}), \ dS^2_{(0)} = d\alpha^2 - d\Phi^2 \tag{4}$$

---

* *Academy of Sciences of Republic Moldova, Institute of Applied Physics Chişinău, Rep Moldova*

is proportional to WD equation for FRW_Φ model with action (1) (the Hawking's measure-dependent parameter ρ is set equal to one). Equation (2) is conformally equivalent to the KG equation with the variable masse squared term $M(\alpha, \Phi)$

$$(\square - M^2(\alpha, \Phi))\Psi = 0 \tag{5}$$

if one performs the conformal translation to the flat metric

$$d\check{s}^2 \rightarrow dS^2_{(0)} = \Omega^2(\alpha, \Phi)d\check{s}^2,$$

where

$$\Omega^2(\alpha, \Phi) = m^{-2}M^{-2}(\alpha, \Phi),\ \check{\square} = \square = \frac{\partial_2}{\partial\alpha^2} - \frac{\partial^2}{\partial\Phi^2},\ \Psi = \Omega^{-1}\check{\Psi}$$

We' ll consider only nonsingular $\Omega(\alpha, \Phi)$ factors

It should be emphasized that there is a wide class of quantum cosmological models (see for exemple the cosmology based on the $R + \varepsilon R^2$ Lagrangian [7], a semiclassical approximation for the entire Universe [8], or the quantum field theory of the Universe [9]) when the WD equation (equ) is equivalent to the KG equ with a variable squared mass and one can consider analogically more general models than (1) if a conformal transformation to a constant mass KG equ may be found

In the following section we apply twistors to describe mass field Ψ, equivalently, the wave function of the Universe, in order to generate the general solution of the minisuperspace WD equ by means of a contour integral in twistor space

3 **The twistor description of the Wheeler-De Witt equation.** a) Twistor configuration space of FRW_Φ-models. Let us parametrize points on the flat configuration two-space $M^2_{(0)}$, provided by the metric (4), by coordinates $\tau^b = (\alpha, \Phi)$, where b = 0,1, or by spinor coordinates $\tau^b = \tau^{BB'} = \frac{1}{\sqrt{2}}\begin{pmatrix} \tau^0 + \tau^1 & 0 \\ 0 & \tau_0 - \tau' \end{pmatrix} = \frac{1}{\sqrt{2}}\begin{pmatrix} \alpha + \Phi & 0 \\ 0 & \alpha - \Phi \end{pmatrix}$, where A,A = 0,1.

Twistors as elements of the minisuperspace FRW_Φ configuration twistor space ${}_c\pi$ can be represented by pairs of spinors $Z^\alpha = (\omega^A(\tau), \pi_{A'}) = (\omega^A_{(0)} - i\tau^{AA'}\pi_{A'}, \pi_{A'})$ where $\omega^A(\tau) = \omega^A_{(0)} - i\tau^{AA'}\pi_{A'}$ is the solution of the twistor equ $\nabla^A_{A'}\omega^B(\tau) + \nabla^B_{A'}\omega^A(\tau) = 0$, $\nabla_\alpha = \partial/\partial^\alpha_\tau$ and $\alpha = 0, 1, 2, 3$ For simplicity we denote $Z = Z^\alpha = (\omega^A, \pi_{A'}) = (i\tau^{AA'}\pi_{A'}, \pi_{A'})$ and use dual twistors $W = W_\alpha = (\lambda_A, i\tau^{AA'}\lambda_A)$ which are elements of the dual twistor configuration space ${}_c\pi^*$

Now we would mention that under conformal rescaling $ds^2_{(0)} \rightarrow d\check{S}^2 = \Omega^{-2}(\alpha, \Phi)dS^2_{(0)}$ components of "new" twistors $\check{Z}^\alpha$, $\check{W}_\alpha$ are expressed through the components of initial twistors Z^α, W_α by formulas $Z^\alpha \rightarrow \check{Z}^\alpha = (\check{\omega}^A, \check{\pi}_{A'})$, $W_\alpha \rightarrow \hat{W}_\alpha = (\hat{\lambda}_A, \hat{\mu}^{A'})$, where

$$\check{\omega}^A = \omega^A,\ \check{\pi}_{A'} = \pi_{A'} + i\gamma_{AA'}\omega^A,\ \check{\lambda}_A = \lambda_A - i\gamma_{AA'}\mu^{A'},\ \check{\mu}^A = \mu^A \tag{6}$$

and $\gamma_{AA'} = \Omega\Delta_{AA'}\Omega^{-1}$. We'll also consider projective spaces $P_c\pi$, $P_c\pi^*$.

b) Twistor functions and massive fields We recall [4, 5] that the solution in a flat space of non-massive spin $S = \frac{1}{2} n$ $(n = 0, 1, 2, \ldots)$ field equation in terms of arbitrary holomorfic on the same domain D of dual twistor space ${}_c\pi^*$ function $f(W)$, homogeneous of degree $(-n-2)$ is

$$\varphi_{PQ\ldots S}(q^a) = (2\pi i)^{-1} \oint \lambda_P \lambda_Q \ldots \lambda_S f(\lambda_A, -iq^{AA'}\lambda_A) D\lambda,$$

where $D\lambda = \varepsilon^{AB}\lambda_A d\lambda_B$ This formula may be generalized for massive fields. For conformally transformed configuration minisuperspace twistors (6), we consider a function

$$f(\check{W}_\alpha, \check{Z}^\alpha) = F(\check{\lambda}_A, -i\tau^{AA'}\check{\lambda}_{A'}; i\tau^{AA'}\check{\mu}_{A'}, \check{\mu}_{A'})$$

holomorfic on two twistors $\check{W}_\alpha$ and $\check{Z}^\alpha$ and homogeneous of degree $(-p-2)$ and $(-q-2)$ correspondingly,

$$\alpha_{P\ldots SG'\ldots K'}(\tau^a) = (2\pi i)^{-2} \oint \underbrace{\lambda_P \ldots \lambda_S}_{p} \underbrace{\mu_{G'} \ldots \mu_{K'}}_{q} \tag{7}$$

$$F(\check{\lambda}_{A'}, -i\tau^{AA'}\check{\lambda}_A; i\tau^{AA'}\check{\mu}_{A'}, \check{\mu}_A) D\check{\lambda} \wedge D\check{\mu}.$$

We introduce spinors

$$\beta_{P\ \ \ STH'\ \ \ K'} = \nabla^{\sigma}_{\tau}\,\alpha_{P\ \ \ SG'H'\ldots K'} \tag{8}$$

which is symmetric on indexes $P\ldots ST$ and

$$\gamma_{Q\ \ \ SG'\ \ \ K'L'} = \nabla^{P}_{L}\,\alpha_{PQ\ \ \ SG'\ \ \ K'} \tag{9}$$

which is symmetric on indexes $G\ldots KL$ Using the twistor version of the Dalambertian

$$\Box = -2\left(I_{\alpha\beta}\check{Z}^\alpha \frac{\partial}{\partial \check{W}_\beta}\right)\left(I^{\rho\sigma}\check{W}_\rho \frac{\partial}{\partial \check{Z}^\sigma}\right) = -2I_{\alpha\beta}\check{Z}^\alpha I^{\rho\sigma}\check{W}_\rho \frac{\partial^2}{\partial \check{W}_\beta \partial \check{Z}^\sigma} \tag{10}$$

and quantum mechanical changes $\partial/\partial Z^\alpha \leftrightarrow \bar{Z}_{\bar{\alpha}}$, $\partial/\partial W_\beta \leftrightarrow \bar{W}^\beta$; $\Box \to -\mu^2$ we have

$$\mu^2 = 2|I_{\alpha\beta}\check{Z}^\alpha \bar{\check{W}}^\beta|^2, \tag{11}$$

where $I_{\alpha\beta}$ is the "infinity twistor".

If $f(\check{W}_\alpha, \check{Z}^\alpha)$ is an eigen state with an eigen value μ^2 of the operator (10), the generated according to (7) field $\alpha\ldots$ satisfies the KG eq $(\Box + \mu^2)\alpha\ldots = 0$. From this eq. together with (7) it follows that $\alpha\ldots$ (in pair with $\beta\ldots$ from (8) or, if we need with $\gamma\ldots$ from (9)) describe an unreducible, free, of high spin $\left(= \frac{1}{2}(p+q)\right)$ Dirac field of mass μ (supposed to be positive).

Finally, we should mention that contour integral (7) generates solutions of KG equ. (2) $\check{\Psi}(\alpha, \Phi)$ if we set $p = q = 0$ and $\mu^2 = m^{-2}$ Multipling by conformal factor $\Omega^{-1}(\alpha, \Phi)$ we'll find solutions of WD equ. (5).

c) Twistor quantization of the Universe. We mean by twistor quantization of the Universe the set of rules according to which variables of classical twistor geometry are systematically replaced by certain operators, out of which one constructs quantum mechanics of the Universe.

When the twistor quantization rules $\bar{Z}_\alpha \; f \rightarrow -h \frac{\partial f}{\partial Z^\alpha} = \bar{Z}_\alpha f$, $\hat{Z}^\alpha \; f \rightarrow Z^\alpha f = \hat{Z}^\alpha f$ where f is a holomorphic function in Z^α, and $W_\alpha \; f^{II} \rightarrow W_\alpha f^{II} = \hat{W}_\alpha f^{II}$; $\bar{W}_\alpha \; f^{II} \rightarrow h \frac{\partial f^{II}}{\partial W_\alpha} = \hat{W}^\alpha f^{II}$, where f^{II} is a holomorphic function in W_α, are brought into effect, we find the commutation relation $[\hat{Z}^\alpha, \hat{Z}_\beta] = \delta^\alpha_\beta$ and $[\hat{W}^\alpha, W_\beta] = \delta^\alpha_\beta$ which implies that the helicity operator $\hat{S} = \frac{1}{4}(Z^\alpha \bar{Z}_\alpha + \bar{Z}_\alpha Z^\alpha)$, or $\hat{S} = \frac{1}{4}(\bar{W}^\alpha W_\alpha + W_\alpha \bar{W}^\alpha)$ should be given by $\hat{S} \cdot f \rightarrow -\frac{1}{2} \hbar \left(Z^\alpha \frac{\partial}{\partial Z^\alpha} + 2\right) f$ in ${}_c\pi$ representation, or $\hat{S} \; f^{II} \rightarrow \frac{1}{2} \hbar \left(W_\alpha \frac{\partial}{\partial W_\alpha} + 2\right) f^{II}$ in ${}_c\pi^+$ representation

If we take $f(Z^\alpha)$ degree of homogenity to be $(-q-2)$, and $f(W_\alpha)$ degree of homogenity to be $(-p-2)$ the eigen values of the helicity operator is $\frac{1}{2} \hbar q$ or, correspondingly, $-\frac{1}{2} hp$

We define the holomorfic on twistors (6) function $f(\check{W}_\alpha, \check{Z}^\alpha) = F(\tau^a, \lambda_A, \pi_{A'})$, which is contained in the integral (7), as the twistor wave function of the Universe This function may be considered as the integral transformation describing the translation to usual wave function of the Universe on a superspace. More exact definition of this twistor wave function is possible on the language of shaves and cohomologies because, it is an element of cohomology group, of shaves on projective twistor space [2—3].

It would be emphasized that the twistor wave function of the Universe $f(W_\alpha, Z^\alpha)$ generates in the space-time, after differentation on twistor variables, spinor-tensor wave fields, as we have seen according to formulas (7)—(9) This way, in minisuperspace approximation, the Universe may be described alternatively by spinor-tensor variable squared mass wave fields

4 **Twistor mass eigenstates of the Universe.** Our starting point of this section is the classic paper [2] in which a twistor version of the KG equ was first given Penrose's equ for mass eigenfunctions is

$$-2I_{\alpha\beta}\check{Z}^\alpha \check{X}^\beta I^{\lambda\mu} \frac{\partial}{\partial \check{X}^\lambda} \frac{\partial}{\partial \check{Z}^\mu} F(\check{X}^\alpha, \check{Z}^\alpha) = \mu^2 F(\check{X}^\alpha, \check{Z}^\alpha) \quad (12)$$

If $F(\check{Z}^{\alpha}, \check{X}^{\alpha})$ of degree (—2, —2) homogenity satisfies (12) it is easely verified that

$$\Phi(\tau_a) = (2\pi\imath)^{-2}\oint F\{(\imath\tau^{AA'}\check{Z}_{A'}, \check{Z}_{A'}), (\imath\tau^{AA'}\check{X}_{A'}, \check{X}_{A'})\}\check{Z}_{A'}\mathrm{d}\check{Z}^{A'}\lambda\check{X}_{A'}\mathrm{d}\check{X}^{A'} \qquad (13)$$

satisfies KG equ. if $\mu^2 = m^{-2}$ and $\Phi(2^{\alpha}) = \check{\Psi}(\tau_a)$

We are interested by a general solution of the WD equ in a form amenable to twistor-diagrammatic formulation A P Hodges in his work [10] had given detailed calculations and diagram representation of the contour integrals for solutions of type (12) equ

To generate an elementary solution for KG equ. (3) with $\mu^2 = m^{-2}$, i.e. a Hankel solution, we write down

$$F(\check{X}^{\alpha}, \check{Z}^{\alpha}) = (2\pi i)^{-1}\int ds^2 \left(\frac{1}{2}\mu\right)^S \pi \ell^{i\pi S}(\sin\pi S)^{-1}(2\pi i)^{-12}\times$$
$$\times\int d^4\check{W}\wedge d^4\check{Y}\, f(\check{W}_{\alpha}, \check{Y}_{\alpha})(\underbrace{\check{W}\check{Z}}\overbrace{\check{X}\check{Z}})^{-1-s}\begin{pmatrix}\check{W} & \check{Y}\\ \downarrow & \downarrow\\ \check{X} & \check{Z}\end{pmatrix}^{s-1}\{\Gamma(1-S)\}^2, \qquad (14)$$

$$\text{where } f(\check{W}_{\alpha}, Y_{\alpha}) = \begin{pmatrix}\check{W} & \check{W} & \check{Y} & \check{Y}\\ \downarrow & \downarrow & \downarrow & \downarrow\\ A & \check{B} & E & F\end{pmatrix}, \quad \check{W}-\check{A} = (2\pi i)^{-1}(\underbrace{\check{W}\check{A}})^{-1} = (4\pi i)^{-1}\check{W}_{\alpha}I^{\alpha\beta}\check{A}_{\beta}$$

If we introduce the notation $\check{W}\overset{S}{—}\check{Y}$ for $(2\pi\imath^{-1})(\underbrace{\check{W}\check{Y}})^{-1-s}$ we can represent (14) as

$$F(\check{X}^{\alpha}, \check{Z}^{\alpha}) = (2\pi i)^{-4}\int_{\underline{L}} dS\left(\frac{1}{2}\mu\right)^S \left\{\pi\ell^{i\pi S}(\sin\pi S)^{-1}\right\}\cdot \qquad (15)$$

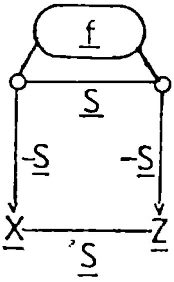

Here L is a contour from —∞ to ∞ that loops round all the poles of $\Gamma(-1-s)$ We emphasize that formulas (14), (15) differ from those, presented in [10] for Minkowski space, because $\check{X}, \check{Y}, \check{Z}, \check{W}$ are twistors in the conformally flat space with auxiliary metric (3) which are related with twistors in the flat space with metric (4) by formulas (6)

Using a contour Γ_4 with the propetry for integrals

$$(2\pi i)^{-4}\oint_{\Gamma_4}\{c_1+\ln(x_Aa^A-k_1)\}\{c_2+\ln(\omega^Ac_A-k_2)\}\,(x_A\omega^A-k)^{-2}d^2\omega\lambda d^2x=$$

$$=c_1+c_2+ln(ka^Ac_A),$$

where c_A, k_1, k_2, k are constants, the generation of finite-normed eigenstates can be represented as

$$F(\check X^\alpha,\check Z^\alpha)=$$

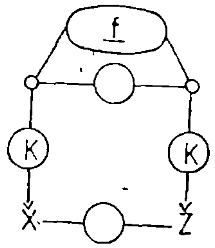

$$\check W-\textcircled{K}-\check Z \qquad U(\check W_\alpha,\check Z^\alpha)=\sum_{-\infty}^{\infty}\check W-\textcircled{K}^{h}-\check Z= \tag{16}$$

$$=(2\pi i)^{-1}\sum_{-\infty}^{\infty}\frac{\partial}{\partial s}\Big/_{s=n}(\check W_\alpha\check Z^\alpha-k)^{-1-s}\{\Gamma(-s)\}^{-1}=(2\pi i)^{-1}\Big\{E(\check W_\alpha\check Z^\alpha-k)+$$
$$+\sum_{n=0}^{\infty}(-1)^n\,n\,(W_\alpha Z^\alpha-k)^{-n-1}\Big\}$$

In (16) $E(y)$ is the Euler function and $U(\widehat W_\alpha,\widehat Z^\alpha)$ satisfies the relation $\frac{\partial U}{(\check Z,^\alpha W_\alpha)}=$ $=\check W_\alpha U(\check Z^\alpha,\check W_\alpha)$ where although $U(\check Z^\alpha,\check W_\alpha)$ is not finitely defined, the result of (16) is nevertheless finite, when contour Γ_4 is used. Indexes ν, $\tilde\nu$ in (16) are introduced due to property of the mass pole $\left(\overline{\check X\check Z}\,\underline{\check X\check Y}-\frac{1}{2}\mu^2\right)^{-1}=(\overline{\check X\check Z}-\nu)^{-1}$ $(\overline{\check X\check Y}-\tilde\nu)^{-1}$ where $\nu\tilde\nu=\frac{1}{2}\mu^2$.

To conclude this section, we note that the Hilbert space of the Universe for FRW models is determined by mass eigenstate finite-normed solutions of the WD equ. (equivalently of the KG equ. with a variable squared mass (5)), which are multiplied by conformal factor $\Omega^{-1}(\alpha,\Phi)$ mass eigenstate finite-normed solutions of KG equ. (3) according to integral transformations (14) from the twistor wave function $F(\check X^\alpha,\check Z^\alpha)$ (16).

5. Discussion. We have analysed the twistor interpretation of a particular tor FRW_Φ minisuperspace model Using twistor diagram methods a contour integral representation for the finite-normed general solution of the WD equ. is obtained. This result is important to construct Hilbert spaces in the recently developing "second" and "third" quantisation of the Universe [11, 7] Of course, a pure twistor interpretation of the quantum cosmology whould be interesting and promising.

One might ask to what extend our results are generalisable since our tor model is quite simple The answer about the possibility of a twistor interpretation of the WD equ. in a superspace of dimension $n = 3, 4, \ldots$ is afirmative. In [3] the twistor theory for spaces $n > 4$ is presented. Therefore, one may expect that twistor approach will be effective too for superspaces of higher than two dimensions. Perhaps, when the theory is invariant under rescalling transformations, one needs to introduce local superspace twistor connections (see [12], $n = 4$). The Yang-Mills equ. for twistor superspace connection whould describe a supplimentary twistor dynamics for the Universe.

The author highly appreciates the warm hospitality extended to him at the Cluj-Napoca University. This paper summarises the results of the talk given at the Romanian National Conference on Physics was held there (24—27 Octobre 1990)

REFERENCES

1 R Penrose, Reports on Math Phys, **12** (1977) 65
2 R. Penrose and M MacCallum, Phys Rep **6** (1972) 241
3 R Penrose and W. Rindler, *Spinors and space-time*, Vol 2 (Cambridge U P, Cambridge, 1986).
4. Yu I Manin, *Kalibrovochnie Polea i Komplexnaea Geometrya*, Nauka, Moskow, 1984, in Russian.
5 J. B Hartle and S W. Hawking, Phys Rev **28 D** (1983) 2960.
6 D N Page, Class Quant Grav, **1** (1984) 417
7 M B Mijic, M S Morris and Wai-Mo Suen, Phys Rev **39 D** 1496, (1989)
8. A Vilenkin, Phys Rev **39 D** (1989) 1116
9. A Hosoy and M Morikava, Phys Rev **39 D** (1989) 1123
10 A P Hodoes, Proc. R Soc London, **397 A** (1985) 375
11 J J Halliwell and R C Myers, Phys Rev **40 D** (1989) 4011
12 S A Merkulov, Commun Math Phys **93** (1984) 93

STUDIA UNIV BABEŞ-BOLYAI, PHYSICA, XXXV, 2, 1990

ON THE SPECIFIC HEAT OF SUPERCONDUCTORS

I. GROSU*

ABSTRACT. — The specific heat ratio $\frac{\Delta C}{C_{en}}$ was calculated for large class of superconductors We found that for large values $\frac{2\pi T_c}{\omega_D}$ the specific heat ratio falls below BCS result

Introduction. In this paper we consider an electron-phonon superconductor described by the Eliashberg equations For the electron-phonon spectral density $\alpha^2(\Omega) \cdot F(\Omega)$ we consider first a simple δ-function model and then a two-δ-function model. The specific heat ratio $\frac{\Delta C}{C_{eN}}$ is quatitatively estimated.

Theory. a) *The free-energy difference* between the normal and superconducting states is given by the relation [1]
(for weak coupling superconductors)

$$\Delta F = -N(0) \cdot T \cdot \sum_m \frac{\left[\sqrt{\omega_m^2 + \Delta^2} - |\omega_m|\right]^2}{\sqrt{\omega_m^2 + \Delta^2}} \tag{1}$$

where $\omega_m = \pi T(2m+1)$, $m = \ldots, -1, 0, +1, \ldots$
$K_B = 1$
$N(0)$—the density of electron states at Fermi surface.
T—temperature

The Eliashberg equations, written on imaginary frequency axis are [2]

$$\omega_n Z_s(n) = \omega_n + \pi T \sum_{m=-\infty}^{\infty} \lambda(n-m) \frac{\omega_m}{[\omega_m^2 + \Delta^2(m)]^{1/2}} \tag{2}$$

$$\Delta(n) \cdot Z_s(n) = \pi T \sum_{m=-\infty}^{\infty} [\lambda(n-m) - \mu^*] \frac{\Delta(m)}{[\omega_m^2 + \Delta^2(m)]^{1/2}} \tag{3}$$

where $\Delta(n)$ are the gaps and $Z_S(n)$ are the renormalization factors.

$$\lambda(n-m) = \int_0^{\infty} \frac{2\Omega \cdot \alpha^2(\Omega) \cdot F(\Omega) \cdot d\Omega}{\Omega^2 + [2\pi T(n-m)]^2} \tag{4}$$

where $\alpha^2(\Omega)F(\Omega)$ is the electron-phonon spectral density.

According to [2], the specific heat jump at T_c is

$$\Delta C = -N(0) \cdot \frac{1+\lambda}{\lambda - \mu^*} \cdot T_c \cdot \frac{[F'(T_c)]^2}{G(T_c)} \tag{5}$$

---

* University of Cluj, Department of Physics, 3400 Cluj-Napoca, Romania

where.

$$F(T) = \frac{\lambda - \mu^*}{1 + \lambda}\left[\Psi\left(\frac{\omega_D}{2\pi T} + 1\right) - \Psi\left(\frac{1}{2}\right)\right] \approx \frac{\lambda - \mu^*}{1 + \lambda} \cdot ln\left(\frac{1{,}134\,\omega_D}{T}\right) \tag{6}$$

$\Psi(x)$ — is the digamma function.
and

$$G(T) = -\frac{7}{8} \cdot \frac{\lambda - \mu^*}{1 + \lambda} \cdot \frac{\zeta(3)}{(\pi T)^2} \tag{7}$$

$\zeta(n)$ — is the Riemann zeta function.
Using (6), (7) and (5) we get (at $T = T_c$)

$$\frac{\Delta C}{C_{eN}} \simeq 1{,}43$$

which is well known BCS result, where

$$C_{eN} = \gamma T_c \tag{8}$$

and $\gamma = \frac{2}{3}\pi^2 N(o)$ is the Sommerfeld constant.

b) *For intermediate coupling* superconductors the specific heat ratio is:

$$\frac{\Delta C}{C_{eN}} \simeq -\frac{N(o)}{\gamma} \cdot \frac{(1 + \lambda)^2}{\lambda - \mu^*} \cdot \frac{[F'(T_c)]^2}{G(T_c)} \tag{9}$$

For Bi—O superconductors which are not in the strong coupling limit (experimental results are consistent with weak-to-intermediate coupling [3]) (9) gives

$$\frac{\Delta C}{C_{eN}} \sim 2 \quad \text{for} \quad \lambda \sim 0{,}5$$

c) *For strong-coupling* superconductors [2], [4], with a simple δ-function model for the electron-phonon spectral density $\alpha^2(\Omega)F(\Omega)$

$$\alpha^2(\Omega)F(\Omega) = \frac{\lambda\Omega_0}{2} \cdot \delta(\Omega - \Omega_0) \tag{10}$$

the specific heat ratio is

$$\frac{\Delta C}{C_{eN}} \simeq 1{,}43(1 + \lambda) \cdot \left\{1 + \frac{\pi^2}{3} \quad \frac{\lambda}{\lambda - \mu^*} \cdot \left(\frac{T_c}{\Omega_0}\right)^2 \cdot \left[6 \cdot ln\left(\frac{1{,}134\,\Omega_0}{T_c}\right) - 11\right]\right\}^2 \tag{11}$$

For realistic values $\lambda \sim 1{,}5$, $\mu^* \sim 0{,}155$, $T_c \sim 18$ K, $\Omega_0 \sim 93$ K (case of Nb_3Sn), $\frac{\Delta C}{C_{eN}} \sim 3$

For large Ω_0 (Ω_0 less then ω_D), and only in this case, the specific heat ratio is given by.

$$\frac{\Delta C}{C_{eN}} \simeq 1{,}43(1 + \lambda) \frac{\left\{1 + \frac{\pi^2}{3} \quad \frac{\lambda}{\lambda - \mu^*} \quad \left(\frac{T_c}{\Omega_0}\right)^2 \quad \left[6 \ln\left(\frac{1{,}134\Omega_0}{T_c}\right) - 11\right]^2\right.}{1 - \frac{12\pi^2}{7\,\zeta(3)} \quad \frac{\lambda}{\lambda - \mu^*}\left(\frac{T_c}{\Omega_0}\right)^2 \cdot \left\{\ln\left(\frac{1{,}134\Omega_0}{T_c}\right) + \frac{1}{3}\left[\frac{7}{4}\,\zeta\,(3) - 1\right]\right\}} \tag{12}$$

For : $\lambda \sim 1$, $\mu^* \sim 0{,}3$, $T_c \sim 35$ K, $\Omega_0 \sim 300$ K ; $\frac{\Delta C}{C_{eN}} \sim 14$. If : $\Omega_0 \sim \omega_D \gg T_c$ we have the following approximate formula :

$$\frac{\Delta C}{C_{eN}} \simeq 1{,}43(1+\lambda) \cdot \left\{1 + \pi^2 \frac{\lambda}{\lambda - \mu^*} \cdot \left(\frac{T_c}{\Omega_0}\right)^2 \cdot \left[5{,}43 \ln\left(\frac{1{,}134\,\Omega_0}{T_c}\right) - 6{,}81\right]\right\} \quad (13)$$

Because there are considerable differences in $\alpha^2(\Omega)F(\Omega)$ from one system to another we adopt for the electron-phonon spectral density the two-δ-function model :

$$\alpha^2(\Omega)F(\Omega) = \frac{\lambda}{4}\,\Omega_0 \cdot \delta(\Omega - \Omega_0) + \frac{\lambda}{4}\,n\Omega_0 \cdot \delta(\Omega - n\Omega_0) \quad (14)$$

and :

$$\frac{\Delta C}{C_{eN}} \simeq 1{,}43(1+\lambda)\,\frac{\left\{1 + \frac{\pi^2}{2} \cdot \frac{\lambda}{\lambda - \mu^*} \cdot \left(\frac{T_c}{\Omega_0}\right)^2 \cdot \left[2\left(1 + \frac{1}{n^2}\right) ln\left(\frac{1{,}134\,\Omega_0}{T_c}\right) + 2\frac{ln\,n}{n^2} - \frac{11}{3}\left(1 + \frac{1}{n^2}\right)\right]\right\}^2}{1 - \frac{2\pi^2}{7\zeta(3)}\,\frac{\lambda}{\lambda - \mu^*}\left(\frac{T_c}{\Omega_0}\right)^2\left[3\left(1 + \frac{1}{n^2}\right) \cdot ln\left(\frac{1{,}134\,\Omega_0}{T_c}\right) + 3\frac{ln\,n}{n^2} + 1{,}1\left(1 + \frac{1}{n^2}\right)\right]} \quad (15)$$

For $\lambda \sim 1{,}55$, $\mu^* \sim 0{,}131$, $\Omega_0 \sim 99$ K, $T_c \sim 7{,}2\ K$, $n \sim 0{,}53$ (case of Pb) $\frac{\Delta C}{C_{eN}} \sim 2$

d) *Superconductors with large* $\frac{2\pi T_c}{\omega_D}$

For this kind of supercoductors the specific heat ratio is :

$$\frac{\Delta C}{C_{eN}} \approx \frac{3}{7\pi^2\zeta(3)} \cdot (1+\lambda) \cdot \left(\frac{\omega_D}{T_c}\right)^2 \cdot \left\{\left(\frac{\omega_D}{2\pi T_c} + 1\right)^{-2} + \left(\frac{\omega_D}{2\pi T_c} + 2\right)^{-2} + \left(\frac{\omega_D}{2\pi T_c} + 3\right)^{-2} + \left(\frac{\omega_D}{2\pi T_c} + 4\right)^{-2}\right\}^2 \quad (16)$$

For $\omega_D \sim 500\ K$, $T_c \sim 45\ K$, $\lambda \sim 1$, $\left(\frac{2\pi T_c}{\omega_D} \sim 0{,}56\right)$ and : $\frac{\Delta C}{C_{eN}} \sim 0{,}7$

From (16), $\frac{\Delta C}{C_{eN}}$ decreases slowly as $\frac{2\pi T_c}{\omega_D}$ is increased (for λ fixed).

Conclusions : Our estimations for the specific heat ratio $\frac{\Delta C}{C_{eN}}$ are in qualitative agreement with the experimental data. If the characteristic phonon energy is less than ω_D, values of order $\frac{\Delta C}{C_{eN}} \sim 10$ are possible, but in this situation lattice stability problems can occur. For superconductors with $\frac{2\pi T_c}{\omega_D} \sim 1$, the specific heat jump $\frac{\Delta C}{C_{eN}}$ falls below BCS result, in qualitative agreement with [5].

REFERENCES

1 G Eilenberger, in 8 *Ferienkurs über Supraleitung,* in der KFA Jülich vom 14 bis 25 Marz 1977, p VII—1 — p VII—23

2 F. Marsiglio, J P Carbotte, Phys Rev B, **33**, 6141, (1986)

3 B Batlogg, R J Cava, L F Schneemeyer G P Espinosa, IBM Journal of Research and Development, **33,** 208, (1989)

4. F. Marsiglio, J P Carbotte, E Schachinger, J Low Temp Phys, **65,** 305, (1986)

5 F Marsiglio, R Akis, J P Carbotte, Phys Rev B **36,** 5245, (1987)

STUDIA UNIV. BABEŞ-BOLYAI, PHYSICA, XXXV, 2, 1990

RAMAN STUDY OF MOLECULAR RELAXATIONS FOR ETHYL IODIDE

T. ILIESCU*, S. AŞTILEAN*, I. BRATU**, D. CHIRIAC**

ABSTRACT. — Informations about molecular dynamics for ethyliodide in pure liquid and in different solvents are obtained by the reorientational and vibrational correlation functions for Raman C—I stretching vibration These relaxation mechanisms are strongly solvent and concentration dependent

I. Introduction. It is known [1] that informations about molecular relaxations are obtained from the study of the vibrational band profiles.

Raman spectroscopy offers a simple possibility to separate vibrational and reorientational contributions to the vibrational profiles by using the technique of measuring the I_{vv} and I_{vh} components. This procedure is correct only when both relaxation types are statistically uncorrelated.

It is possible to obtain isotropic (I_{iso}) and anisotropic (I_{aniso}) profiles for Raman lines as follows [2]

$$I_{iso}(\omega) = I_{vv}(\omega) - \frac{4}{3} I_{vh}(\omega) \tag{1}$$

$$I_{aniso}(\omega) = I_{vh}(\omega) \tag{2}$$

The time evolution of these relaxations can be observed by using the correlation functions technique (C F.) Vibrational C F. $G_v(t)$ and reorientational CF $G_{2R}(t)$ are given by [1]

$$G_v(t) = \int_{-\infty}^{\infty} I_{iso}(\omega)\exp(i\omega t)d\omega \tag{3}$$

and

$$G_{2R}(t) = \int_{-\infty}^{\infty} I_{aniso}(\omega)exp(i\omega t)d\omega \Big/ \int_{-\infty}^{\infty} I_{iso}(\omega)exp(i\omega t)d\omega \tag{4}$$

The aim of this paper is related to the study of vibrational and reorientational relaxations for C_2H_5I in pure liquid and in carbon disulphide, —*n* pentane and cyclohexane solutions from the analysis of band profile for the $C-I$ stretching vibration ($\sim$500 cm^{-1}, $\rho = 0.11$)

II. Experimental. The Raman spectrum was excited with the 488 *nm* (0.17 *W*) line of the Ar^+ laser of *ILA* 120—1 type The scattered light at 90° was analysed with a double monochro-

---

* *University of Cluj-Napoca, Department of Physics, 3400 Cluj-Napoca, Romania*
** *Institute of Isotopic and Molecular Technology, P. O. Box 700, R—3400 Cluj-Napoca 5, Romania*

mator of GDM 1000 type, I_{vv} and I_{vh} being obtained by the rotation with 90° of the polaroid situated in the collection optics The gypsum depolarized edge situated in the front of the monochromator slit rejects the selective reflexion of the light with different polarization states in the spectral aparatus Ethyl iodide was prepared by us and solvents (of „Merck-Uvasol" type) were used without further purification

The spectra were obtained with the following experimental parameters the registration speed 0,06 $cm^{-1}s^{-1}$, and the slit width 1 2—2 5 cm The spectra were normally digitized at 0 4 cm^{-1} step Only the high frequency side of the band was used in order to eliminate the asymmetry in the low frequency side due to the hot bands

The experimental CF $G_v(t)$ and $G_{2R}(t)$ were obtained by deconvolution (Fourier method) by taking into account the triangular slit function, determined with a corresponding line of the helium.

The measurements were done at the following temperatures 286, 303, 313 and 323 K

III. Results and discussions. Fig 1 presents the *CF* in the form of ln $G_v(t)$ and ln $G_{2R}(t)$ at a concentration $c = 0{,}94$ M in cyclohexane at 286 K. As $G_v(t)$ decays slower than $G_{2R}(t)$, vibrational relaxation mechanisms have a smaller contribution to the band profile than the rotational relaxation The same ratio of these contributions is maintained at 303, 313, 323 K For small concentrations in cyclohexane ($c = 0$ 77 *M*) the situation is the same for all temperatures. In pure liquid and for high concentrations ($c = 8.25$ *M*) in cyclohexane at different temperatures an inversion of the contributions to the band profile was observed, rotational *CF* decays more slowly, than vibrational *CF*, prooving an increase of the vibrational relaxation contribution in the band profile (fig. 2)

The same ratio of the vibrational and rotational relaxation is observed also in other solvents like carbon disulphide and *n*-pentane

All solvents used are inert (without dipolar moment) We believe that the small rotational contribution at high concentrations is due to a strong dipole-

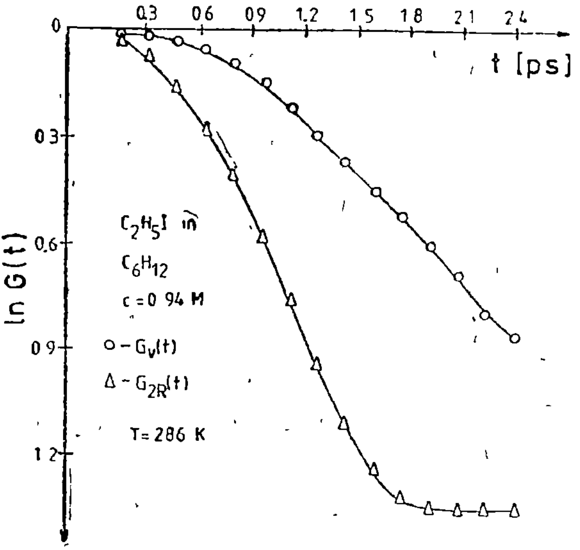

Fig. 1 $G_v(t)$ and $G_{2R}(t)$ for $C-I$ stretching vibration of ethyliodide in cyclohexane at low concentrations.

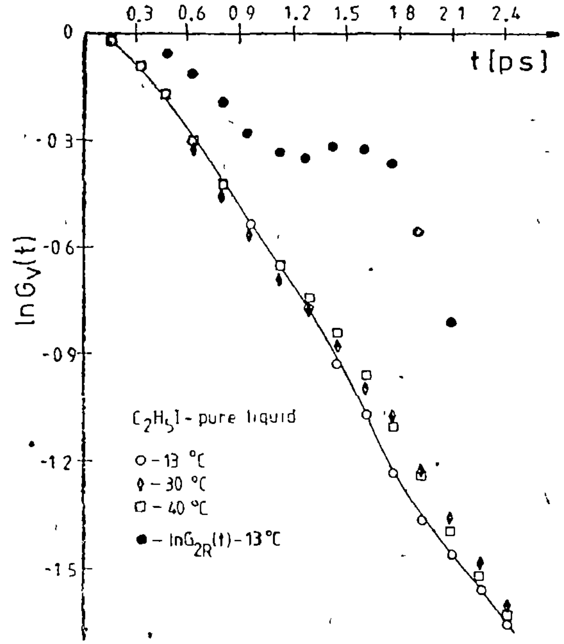

Fig 2 $G_v(t)$ and $G_{2R}(t)$ for $C—I$ stretching vibration of etyliodide in pure liquid and in cyclohexane at high concentrations for different temperatures.

-dipole interaction between ethyl-iodide molecules, which decreases as the dilution is increased.

The vibrational *CF* being of the shape

$$G_v(t) = exp(-t/\tau_v) \qquad (5)$$

permits the evaluation of the vibrational relaxation time τ_v. The values of τ_v are represented as a function of temperature for pure liquid and different concentrations in various solvents at $T = 280\ K$ (fig. 3). τ_v for pure liquid is practically unchanged with the increasing temperature whereas in the solutions increases with the decreasing dilution in different ways in the used solvents, the most powerful increasing being observed for n-pentane solutions. Small change of τ_v with temperature in pure liquid is another proof of the major vibrational contribution to the band profile, knowing that a temperature change strongly influences only the rotational relaxation [1]. By taking into account the relationship

$$\tau_v = (\pi c \Gamma_{1/2})^{-1} \qquad (6)$$

in which $\Gamma_{1/2}$ is the halfwidth of the isotropic line, it results a decrease in the halfwidth of the line with the dilution increasing In fig 4 the $G_{2R}(t)$ *CF* at $T = 286$ K for different dilutions in cyclohexane are presented. The time decreasing of $G_{2R}(t)$ is well described by the relationship

$$FG_{2R}(t) = \exp(-t/\tau_r) \qquad (7)$$

where τ_r is the reorientational time

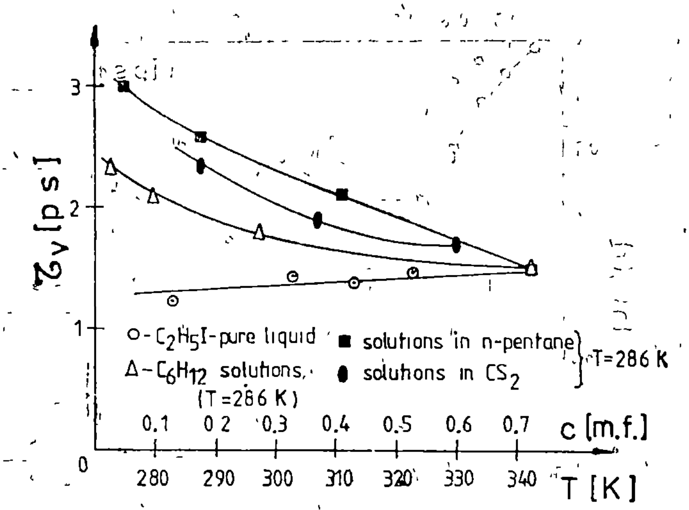

Fig. 3. The temperature dependence of τ_v for pure liquid and different solutions of ethyliodide.

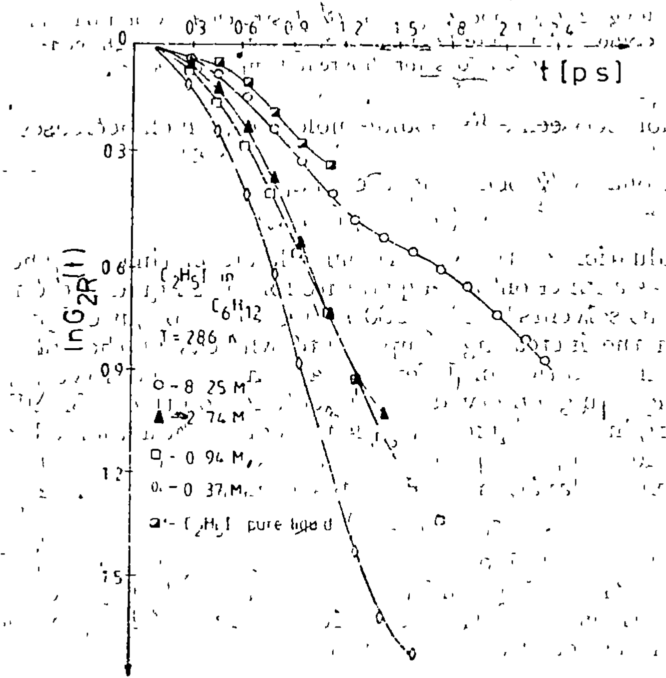

Fig. 4. $G_{2R}(t)$ for different dilutions in cyclohexane

$G_{2R}(t)$ decreases more rapidly as the dilution increases. Thus the restriction in the reorientation of the C_2H_5I molecules decreases, in diluted cyclohexane solutions by the reduction of the dipolar interactions between C_2H_5I molecules in these solutions

The nonlinear behaviour of the ln $G_{2R}(t)$ can be explained by the statistical nonindependence of both relaxation mechanisms, opposite to the hypothesis on which $G_v(t)$ and $G_{2R}(t)$ are obtained At high concentrations this deviation is higher, showing a stronger rotation-vibration interaction

Conclusions. The study of the $C—I$ profile for ethyliodide gives us the informations on the relaxation mechanisms responsible for the band profile and are depending on dilution and the used solvent.

By a corresponding selection of the non-polar solvents it is possible to stress on the importance of the dipole-dipole interactions in the restriction of the reorientation for ethyliodide molecules

REFERENCES

1 T. Iliescu, I Bratu, O Cozar, Studii Cerc Fiz **40,** 777 (1988)
2 F J Bartoli, T A Litovitz, J Chem Phys **56,** 404 (1972)

STUDIA UNIV BABEŞ-BOLYAI, PHYSICA, XXXV, 2, 1990

THE SELECTIVE *IRMPD* DISSOCIATION OF CF_2HCl MOLECULE AT HIGH FLUENCES

IOAN DEAC*, VIOREL COSMA*

ABSTRACT. — The ^{13}C separation parameters were measured as a function of substrate pressure at three different CO_2 — laser lines situated in the P branch of 9 4 μm band The measurements were carried out in a strongly focused beam and with normal shape laser pulse The results give a picture of the kinetic behaviour of vibrationally excited CF_2HCl molecules produced in the presence of strong infrared fields

Introduction. The advent of laser as a source of well-colimated high intensity radiation of narrow spectral band which has stimulated the discovery of many new schemes of laser isotope separations (LIS) [1, 2] One of the particular method of LIS is infrared multiphoton dissociation (IRMPD). The best advantage of laser isotope separation by IRMPD is larger single-step selectivity which can be achieved in the separation of medium-weight elements From a number of isotope from ^2H to ^{235}U, ^{13}C separation has been most extensively investigated by IRMPD [4]—[24].

Natural carbon consist of two stable isotopes: 98 9% ^{12}C and 1 1% ^{13}C. A number of parametrical studies have been published on ^{13}C enrichment by CO_2 — laser induced IRMPD of flurocarbons, whereby molecules are high vibrationally excited through optical pumping of their C — F stretching of vibrational modes. Enriched products were obtained via IRMDP of CF_3X (X = Cl, Br, I) [4—10], CCl_2F_2 [11, 12] and $CHClF_2$ [13—24] under selected experimental conditions.

Several groups [15, 18, 20, 22, 24] are trying to find a workable photochemical separation for large scale enrichment of ^{13}C by IRMPD of the above mentioned flurocarbons and it appears that the most favorable case studied so far is the IRMPD of CF_2HCl [15].

We wish to report in this paper a parametric study of *IRMPD* of CF_2HCl at high fluences in the irradiation zone We studied the separation process with special emphasis of two important parameters · laser wavelenght and substrate pressure. IRMPD of CF_2HCl was investigated using the laser lines situated in the red edge of the ν_3 ($^{13}CF_2HCl$) band.

Experimental setup and method. A CO_2-*TEA* laser built by us was used in the experiments described below [19, 20] The laser was operated at a repetition rate of 1 Hz using a mixture of CO_2 N_2 He = 1 1 6 gas as laser medium In this conditions, generated laser pulse has an ordinary shape (100 nsec FWHM power peak followed by 1 μ sec tail whith contains twice as much energy as the peak) Laser tuning on the line of 9 4 μm band was performed using a diffraction grating blazed for 10 6 μm (100 gr/mm)

As shown in Fig 1 a 1 m radius concave mirror focused the initial 2×2 5 cm^2 laser beam into the reaction cell, giving a cross section of about 7 mm^2 in the beam waist

The laser photolysis was carried out in a cylindrical cell consisting of two crossed tubes of 25 mm i d each The long tube (50 cm) was used for the irradiation and the short one (15 cm) for IR spectroscopy analysis Four NaCl windows enclose a total cell volume of 0 3 l

---

* *Institute of Isotopic and Molecular Technology, 3400 Cluj-Napoca, POB 700 — Romania*

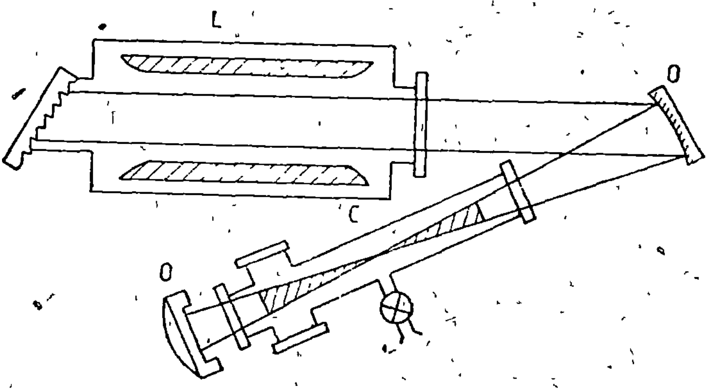

Fig 1 Schematic of the experimental setup · (L) laser, (C) dissociation cell, (O) concave mirror, (D) energy meter

Upon excitation by a CO$_2$ laser radiation CF$_2$HCl molecules dissociates into CF$_2$ and HCl fragments Two CF$_2$ radicals recombine to yield the C$_2$F$_4$ dissociation product Since the CO$_2$ laser was tuned to the lines of P branch of the 9 4 μm band ^{13}C bearing molecules selectivity decompose and residual CF$_2$HCl gas shows a ^{13}C deplention as compared to natural carbon [13].

The isotopic concentration both in the residual gas CF$_2$HCl (C_g) and in the dissociation product (C_p) were measured with a mass-spectrometer (MS) VARIAN-MAT-311 We determined the isotopic ratio $^{13}C/^{12}C$ in C$_2$F$_4$ from the intensity of the signals at $m/e = 81,82$ and 83 (corresponding to $^{12}C_2F_3^+$ $^{12}C^{13}CF_3^+$ and $^{13}C_2F_3^+$ respectively) The same ratio in CF$_2$HCl was calculated from the intensities of signals at $m/e = 51$ and 52 ($^{12}CF_2H^+$ and $^{13}CF_2H^+$, respectively).

The relative yield of product P/L defined as the amount P of C$_2$F$_4$ produced by IRMPD divided by the amount L of CF$_2$HCl present initially, was measured both by MS an GC methods Calibration of the MS and GC response was achieved with aliquots of C$_2$F$_4$ diluted in CF$_2$HCl in the same range of concentration as obtained in the IRMPD experiments. We used industrial grade CF$_2$HCl with its two main isotopic species present in natural abundance ratio with no added gas.

Results and discussions. We have been studying the dependence of the separation parameters (C_p, C_g, P/L) on substrate pressure at three different laser lines, situated in 9P branch. 9P(12), 9P(26) and 9P(30) The wavelength of these lines (1053 9 cm^{-1}, 1041.27 cm^{-1} and 1037 4 cm^{-1}) respectively are near the maximum of the a sorbtion band of $^{13}CF_2HCl$ molecules (~ 1076 cm^{-1}) [13], in the red edge.

Each sample of CF$_2$HCl was irradiated with 1500 laser pulses. Laser pulse energy for each of three lines was fixed at 2 J. In this conditions, laser fluence in the beam waist was about 30 J/cm^2 Fig. 2 shows our results obtained for 9P(12) line.

As one can observe there are three different domains for the separation parameters behaviour. In the first domain situated at pressure below 0,6 Torr has been emphasized a collisionless dissociation regim. This assertion is supported by the fact that C_p is kept constant (~ 10 5%) when the pressure increases The slowly decrease of C_g is probably due to the diminution of the "bottle-neck effect" with the pressure increase In this region, P/L increases on the account of the more efficient extraction of ^{13}C from residual gas

In the second domain situated between 0 6 Torr and 3 Torr, the isotopic selectivity rapidly decreases. This fact suggests that $V-V$ energy transfer plays

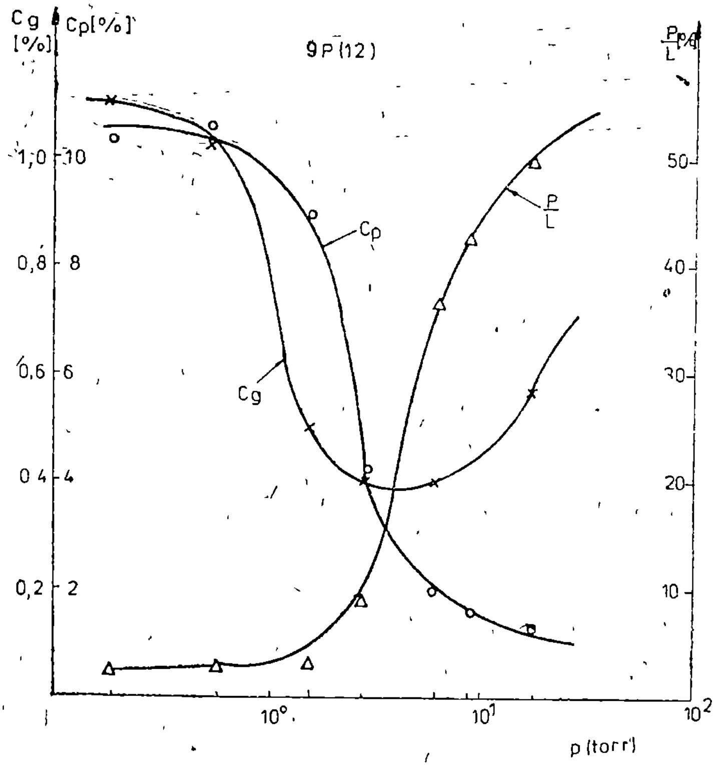

Fig 2 Variation of separation parameters $C_p(0)$ $C_g(X)$ and P/L (Δ) with pressure at 9P (12) laser line

an important role in dissociation mechanism Simultaneously the relative yield (P/L) begins to strongly increase in agreement with a common decrease of C_p and C_g.

The third domain (above 3 Torr) is characterized by the occurence of thermal decomposition of the residual gas. In this case isotopic selectivity drops rapidly to unitary value, while P/L strongly increases, and C_g reaches the natural abundance value.

As it is known, the dramatic drops of the process selectivity at high pressure of CF_2HCl may be caused by $V-V$ energy transfer from the excited $^{13}CF_2HCl$ to $^{12}CF_2HCl$ [15] so that a certain number of $^{12}CF_2HCl$ molecules decompose via collisional excitation in subsequent process At sufficiently high gas pressures these processes lead to the thermalisation and non-selective bulk dissociation. The fact that this phenomenon appears at lower pressures than observed in other works [16], is due the relative high fluence used in our experiment

In fig 3 the results obtained for 9P(26) line are shown. The three specific domains can be observed again Their characteristic pressure region is shifted to higher values, especially due to the laser line taking off the resonant absorbtion

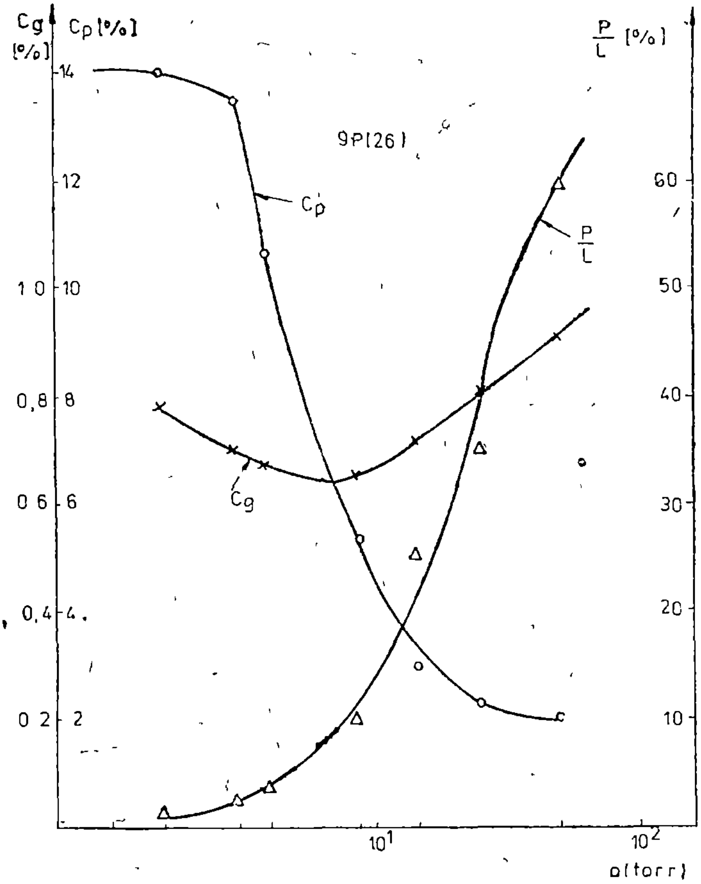

Fig 3 Variation of separation parameters $C_p(0)$, $C_g(X)$, and P/L (Δ) with pressure at 9P (26) laser line

of $^{13}CF_2HCl$ In this case the isotopic selectivity in collisional regime is higher than for the 9P(12) line Also, the extraction grade ($1/C_p$) has a maximum value lower than in the same case (9P(12))

The trends observed in the C_p and $1/C_p$ behaviour in passing from the 9P(12) to 9P(26) laser lines are conserved also when using 9P(30) line (Fig 4).

In particular the same C_g minimum is observed in this case, but it is less pronounced and has a higher absolute value Also the drop of the process selectivity is present for higher pressures and has a better value in the collisionless regime

Conclusions. We reported in this paper the IRMPD characteristics of the CF_2HCl gas phase molecules at high fluences and with normal laser pulses as function of substrate pressure and three different CO_2 laser lines Three specific do-

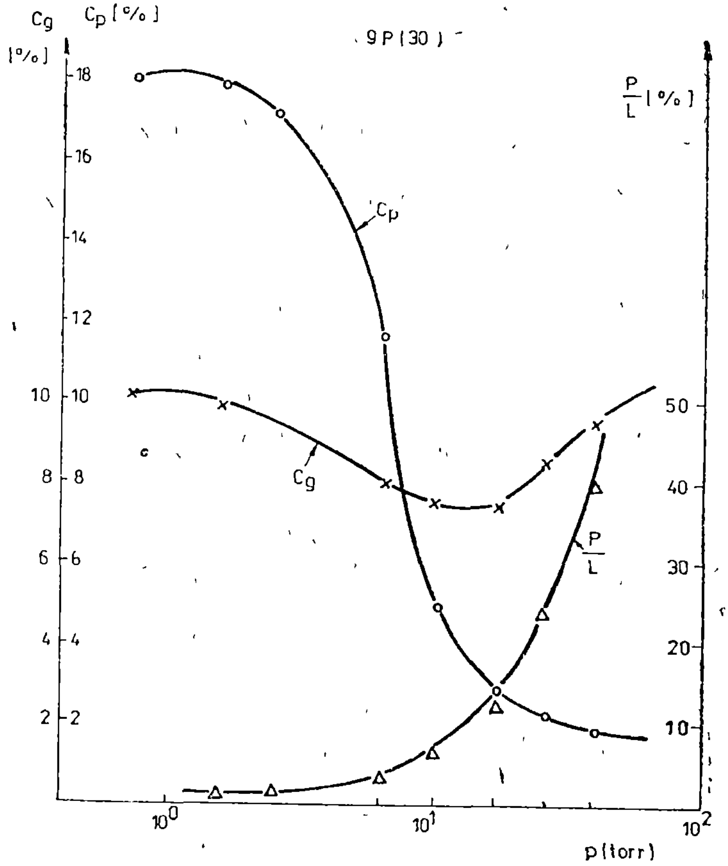

Fig 4. Variation of separation parameters $C_p(0)$, $C_g(X)$ and P/L (Δ) with pressure at $9P$ (30) laser line

mains were found in the pressure range of 0.8—30 *Torr*: a collisionless regime of dissociation at low pressures, a second domain in which up-pumping by infrared radiation competes with collisional decomposition processes, and for high pressure values a third dominated by thermal decomposition phenomenon The pressure limits of this domain and the values of the separation parameters in each one are dependent on the laser wavelength.

The general feature of the process, when the laser frequency get nearer to the absorbtion band of the $^{13}CF_2HCl$ molecule, is the increase of the relative yield of the product and extraction grade of ^{13}C from residual gas and the decrease of the process selectivity in dissociation products For our data this means to move from $9P(30)$ (Fig. 3) to $9P(26)$ (Fig 2) and finally to $9P(12)$ (Fig 1) laser lines. For all these laser lines there is a pressure threshold for which the thermal decomposition sets in.

The above data represent a part of a more elaborated parametric study concerning the CF_2HCl *IRMPD* in laser fields They are important for any tentative of scale-up of ^{13}C separation process.

REFERENCES

1. C D Cantrell, S M Freund, J L. Lyman, in *Laser Handbook*, vol **3**, ed M L. Stitch (North Holland, Amsterdam, 1979), pp. 485—576

2 V S Letokhov, C. B Moore, *Chemical and Biochemical Applications of Lasers* vol **3**, ed C B. Moore (Academic Press, New York, 1977).

3. E. P Veliknov, V Yu Baranov, V. S Letokhov, E A Ryabov, A. N Starostin, *Power Pulsed CO_2 Lasers and their Applications for Isotope Separation* (Nauka, Moscow, 1983)

4. S Bittenson, P. L. Huston, J Chem Phys **67**, 4819, 1977.

5 M Druin, M. Gauthier, R Pilson, P A Hackett, C. Willis, Chem Phys. Letters, **60**, 16, 1978

6. T Watanabe, T Oyama, O Hayashi, Y. Ishikawa, T Ishii, S Aria Nippon Kagaki Kaishi, 1517, 1984

7. G I. Abdushelishvili, O N Avatkov, V. N. Bagratashvili, V. Yu Baronov, A B Bakhtadze, E P Velikhov, V M Vetzke, L G Gverdtsiteli, V S D Olzhikov, V G Esadze, S A. Kazakov, Yu R Kolomiiskii, V. S. Letokbov, S V Pigul'skii, V D. Pis'mennyi, E A Ryabov, G. I Theshelashvili, Soviet J Quantum Electron. **12**, 459, 1982

8 H Kojima, T Fukumi, S Nakojima, Y Maruyama, K Kosasa, Chem Phys. Letters, **95**, 614, 1983

9. W Fuss, W E Smith, Ber Bunseges Physik Chem, **83**, 1148, 1979

10. M Chauthier, O Croix, M Luce, S Tistchenko, Note CEA-N-2348, 1983

11 D S King, J C Stepenson, J Am Chem Soc, **100**, 7151, 1978

12. J J Chou, E R Grant, J Chem Phys, **74**, 5679, 1981.

13 M Gauthier, C G Cureton, P A Hackett, C Willis, Appl Phys B**28**, 43, 1982

14 M Gauthier, A Outhouse, Y Ishikawa, K O. Kutschke, P. A. Hackett, Appl Phys B**35**, 173, 1984

15. A Outhouse, P Lawvrence, M Gauthier, P A Hackett, Appl Phys, B**36**, 63, 1985

16 H Kojima, K Uchida, Y Takagi, Appl Phys, B**41**, 43—48, 1986

17 S Arai, K Sugita, P Ma, Y Ishikawa, H Kaetsu, S. Isomura, Chem. Phys. Lett, **151**, 516, 1988.

18 S Arai, K Sugita, P. Ma, Y Ishikawa, H Kaetsu, S Isomura, Apply, Phys, B**48**, 427, 1989

19 I Deac, V Cosma, D Silipaş, L Mureşan, St Cerc Fiz, **40** (5—7), 473, 1988.

20 I Deac, V Cosma, D Silipaş, L Mureşan, V Toşa, Appl Phys, B**51**, 211. 1990.

21. I Deac, V Cosma, V Toşa, L Mureşan, D Silipaş, *Procedings of the Second Int. Conf, Trends in Quantum Electronics*, Bucharest, Romania, 1985

22 P H Ma, G Sugita, S Arai, Appl Phys, B**49**, 503, 1989

23 P H Ma, K Sugita, S Arai, Appl Phys, B**50** (5),385, 1989.

24 K Chiba, Y Fujioka, T Murata, N Hamada, T Sakai, K Sugawara, H Tokee, *Intern Symp Isotope Separation and Chemical Exchange Uranium Enrichment*, Oct 29—Nov 1, 1990, Tokyo, Japan

STUDIA UNIV BABEŞ-BOLYAI, PHYSICA, XXXV, 2, 1990

OPTOACOUSTIC LASER SPECTRA AND DETECTION OF ISOTOPIC LABELLED ORGANIC COMPOUNDS

I. BRATU[*], ADRIANA BARBU[*], ŞT. KREIBIK[*]

ABSTRACT. — Optoacoustic laser spectra in the 9–11 μm spectral range for some deuterated organic vapours present remarcable isotopic effects By a proper selection of the laser lines it is possible to identify these labelled compounds and also to detect their traces in air at a sub*ppm* level

1 **Introduction.** The optoacoustic (OA) spectroscopy in the CO_2 laser range is one of the most important branch of the molecular spectroscopy. It is possible to investigate the isotopic effects which appear in these spectra by replacing some nuclei from different molecular compounds with isotopic nuclei.

Many molecular compounds labelled with ^{13}C, ^{18}O, ^{15}N, D, ^{11}B have numerous applications in medicine, biology, agrochemistry, geochemistry, geology and even in optoelectronics (optical fibers, electrooptic modulators). Related with their use in these domains is necessary to perform:

— measurements in isotopic mixtures around natural concentration,

— exact determination of the isotopic content and its small variations

Some important results for H_2S and HDS, $^{15}NH_3$ and $^{14}NH_3$, $^{10}BCl_3$ and $^{11}BCl_3$ are given in [1]. In order to solve these problems it is necessary to know the contrast in absorption of isotopic homologoues in the OA laser spectra — the isotopic effects. The OA laser spectra in the 9–11 μm spectral range for a series of deuterium labelled compounds are presented aromatic hydrocarbons (benzene-d_6, o-xylene-d_{10}), alcohols (methanol-d_1, ethanol-d_1), halogenated hydrocarbons (chloroform-d, dichlormethane-d_2). These *OA* laser spectra are recorded in order to identify the wavelengths (corresponding to certain laser line) at which the contrast in absorption (U_H/U_D) is maximum (U_H and U_D are the *OA* signal for protonated and deuterated compounds, respectively)

At the same time, the detection limit in air for some labelled compounds formarly presented is established.

2 **The Experimental Setup.** In order to record the OA laser spectra is used the following setup (fig 1) [2] consisting on

— CO_2 CW frequency stabilised laser,
— mechanical chopper with frequency range between 4 and 4000 *Hz*,
— powermeter, LM2 Carl Zeiss Jena,
— OA brass cell with 100 mm length and volume of $7.07 \cdot 10^4$ mm^3, endowed with a condenser microphone and two NaCl windows, used in nonresonant regime,
— lock-in nanovoltmeter of 232B Unipan.

---

[*] *Institute of Isotopic and Molecular Technology, 3400 Cluj-Napoca, POB 700 — Romania*

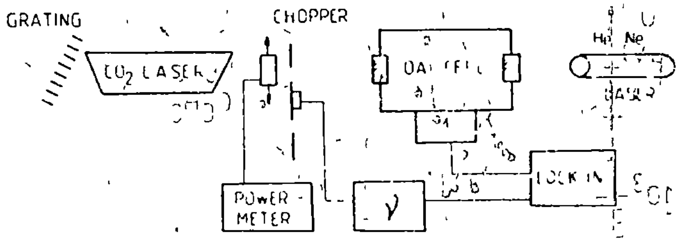

Fig 1 The experimental setup

3 Sample Preparation and the Selections of the Work Parameters.

The labelling with deuterium of the above mentioned compounds was performed as follows

— by homogeneous isotopic exchange (for CD_2Cl_2 97 at.% D, C_2H_5OD 97 a t% D, CH_3OD 97 at % *D*, ND_3 5 at % D);
— by chemical synthesis ($CDCl_3$ 97 at % D)
— by heterogeneous isotopic exchange (C_6D_6 97 at.%D, o-$C_6D_4(CD_3)_2$ 97 at %D.

In all situations the deuterium source was D_2O

The following gas mixture was introduced in the OA cell vapours of the organic liquid obtained by vacuum evaporation and buffer gas (ex. air) at atmospheric pressure In order to obtain a high responsivity of this setup, the modulation frequency was selected to be 12.5 *Hz* (knowing the fact that in a non-resonant regime the *OA* signal decreases with the increasing of the modulation frequency) For each laser line the emission power was fixed at the same value (0.2 *W*) in order to avoid the saturation effects and to obtain as many laser lines as possible.

4 Experimental Results and Discussions. 4 1 *Benzene*. The absorption spectra for isotopic homologues of benzene (the microphonic signal *U* in arbitrary units of wavelength of the laser beam) is presented in fig 2

The isotopic effect is well established especially in the frequency range of the 9*P* emission branch of the CO_2 laser. The values of these frequencies, as well as the ratios of the *OA* signals (the spectral contrast in absorption) obtained for both isotopic homologues are presented in table I

For 9*P*32 laser line the ratio U_H/U_D is maximum (16 1) The OA signal for C_6H_6 is at least one order of magnitude greater than that for C_6D_6 for the wavelengths noted with (*).

4 2. *Orto-xylene* In this case the *OA* spectra for isotopic homologues are presented in fig 3

In agreement with these spectra the ratio of the OA signals for both isotopic homologues is maximum for 9*R*20 laser line. Table II presents these ratios for several laser lines

4 3 *Dichlormethane and chloroform.* Both compounds, especially dichlormethane present strong isotopic effects in the 10 *μm* branch of the CO_2 laser. This fact is illustrated in fig 4 for both isotopic homologues of the dichlormethane and chloroform. Table III presents the values of the *OA* signal ratios for dichlormethane.

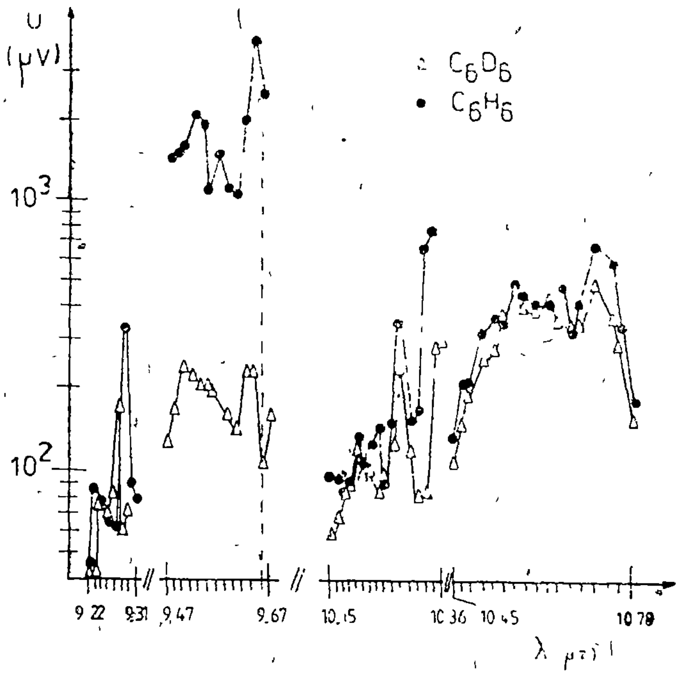

Fig 2 The OA laser spectra for isotopic homologues of benzene

Table I

The ratios of the OA signals for isotopic homologues of benzene at different laser wavelengths.

Branch	λ/μm	$U_{C_6H_6}/U_{C_6D_6}$
9*R*	9 24	2 1
	9 28	0.4
	9 29	5 5
9*P*	9.65*	16 1
	9 64*	16 0
	9 62*	8 4
	9 60	7 5
	9 58	7 3
	9 57	7 5
	9 55	5 1
	9 53*	8 6
	9 52*	9 1
	9 50	6 5
	9 49*	8 9
	9 47*	11 1

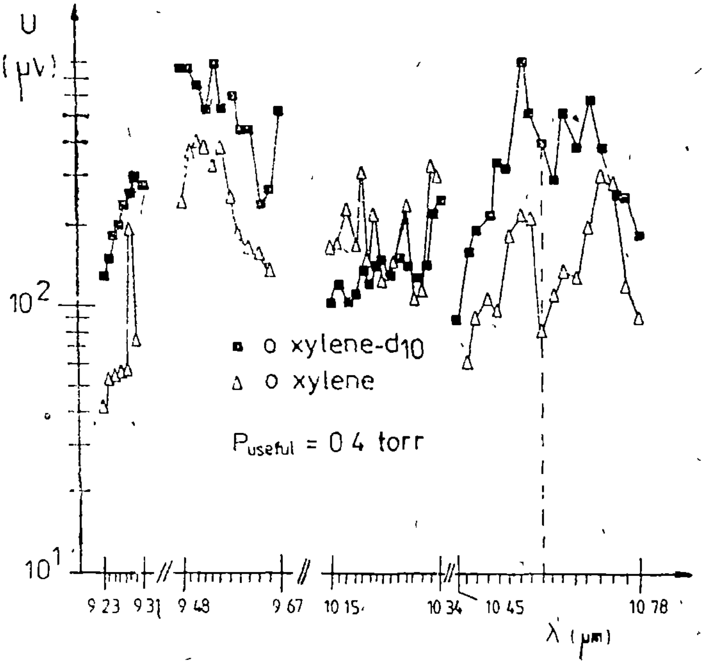

Fig 3 The OA laser spectra for isotopic homologues of o-xylene.

Table II

The ratios of the *OA* signals for isotopic homologues of o-xylene at different laser wavelengths

λ/μm/	U_D/U_H	λ/μm/	U_D/U_H
10 529	3 5	9 303	4 2
10.568	3 8	9 280	4 2
10.609	4 9	9 269	4 3
10 650	3 1	9 258	3 3
10 693	3 0	9 237	3 1

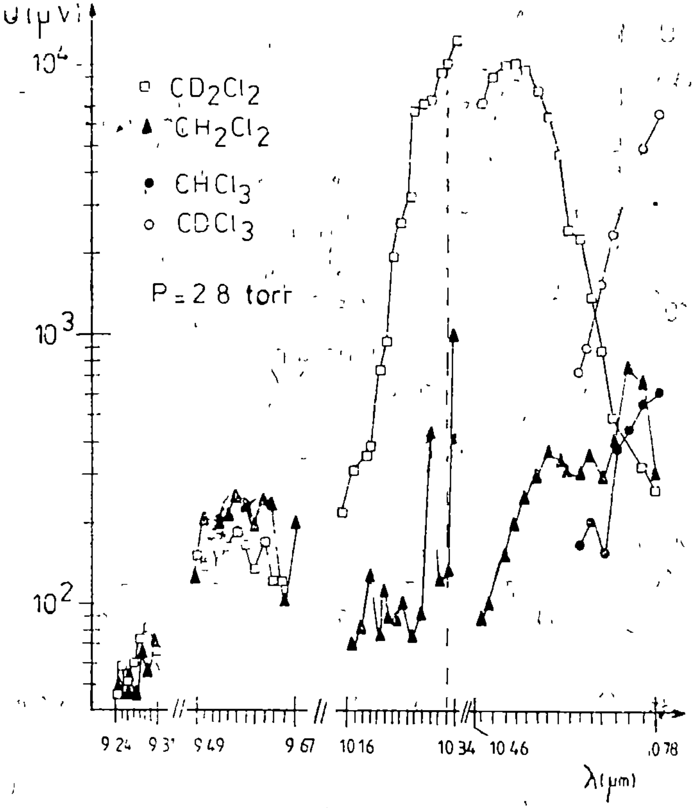

Fig 4 The OA laser spectra for isotopic homologues of dichlormethane and chloroform.

Table III

The ratios of the *OA* signals for isotopic homologues of dichlormethane at different laser wavelengths

$\lambda/\mu m/$	U_D/U_H
10 22	28
10.23	10
10 24	32
10 26	25
10 27	52
10.29	137
10 30	76
10 32	291
10 33	227
10 34	167
10 47	80
10 51	63
10 53	49
10 55	37
10 57	26
10 59	17
10 61	13

A very good contrast in absorption (about 300) is observed at the 10.32 μm wavelength. For the isotopic homologues of chloroform this ratio has a value of approximatively 10 both for 10.69 μm and 10.78 μm

4.4 *Methanol and ethanol* For these alcohols the isotopic effects are weaker than for the previous compounds, especially for ethanol The OA spectra for methanol-d_1 is presented in fig. 5 and the values of the OA signal ratios can be found in the table IV. The laser lines 10*R*18 and 10*R*12 can be used for the identification and quantitative analysis of the isotopic mixtures of methanol In the

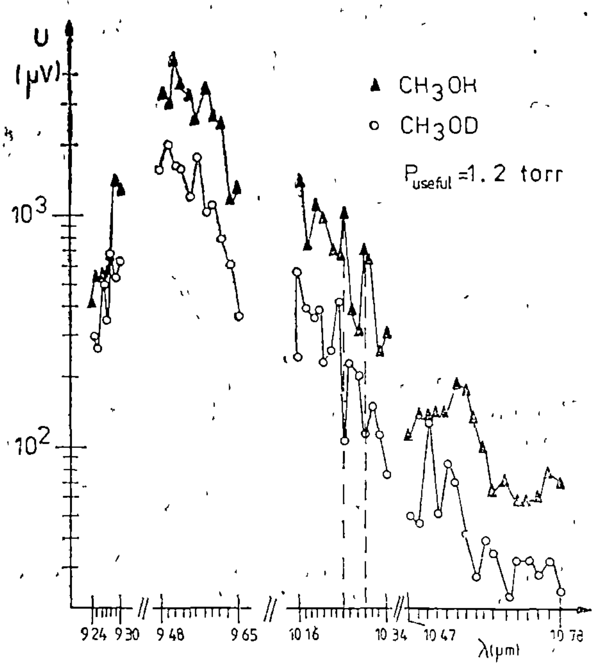

Fig 5 The OA laser spectra for isotopic homologues of methylic alcohol

Table IV

The ratios of the *OA* signals for isotopic homologues of methanol at different laser wavelengths

λ/μm/	U_H/U_D	λ/μm/	U_H/U_D
9.59	3.5	10.26	9.7
9.62	3.2	10.30	6.3
9.65	3.6	10.34	4.3
10.17	5.8	10.59	4.3
10.19	3.8	10.61	4.8
10.22	4.1		

case of ethanol-d_1 the isotopic effect is small only for three wavelengths (10 72 *μm*, 10 32 *μm* and 10'33 *μm*) the ratios of the OA signals is approximately 1 7

4 5 *Ammonia.* Fig. 6 presents OA spectra for NH_3 and ND_3 5 at % *D* /3/.

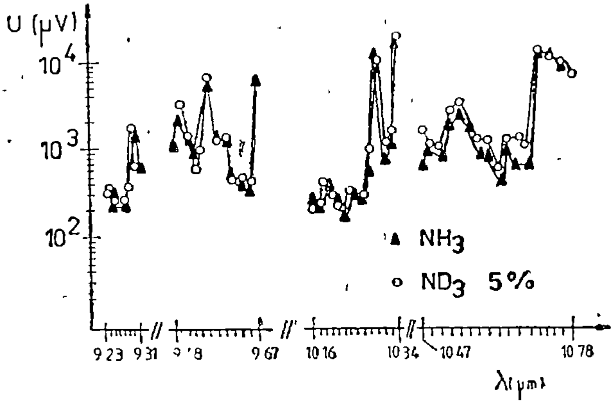

Fig 6 The OA laser spectra for isotopic homologues of ammonia

Very good isotopic contrasts (about two orders of magnitude) can be obtained both in 9*R* and 10*R* branches of the CO_2 laser. Table V presents the recommended wavelengths which can be used for the analysis of the isotopic content of the studied compounds

Table V

The recommended wavelengths and the corresponding ratios of the *OA* signals for the investigated isotopic homologues

Compound	λ/μm/	U_H/U_D	Compound	λ/μm/	U_D/U_H
benzene	9 65	16 1	chloroform	10 78	10 6
	9 64	16 0		10 69	9 9
	9 47	11.1		10 76	8 9
o-Xylene	10 61	4 9	dichlormethane	10 32	291
	9 27	4 3		10 33	227
	9 30	4 2		10 34	167
	9 28	4 2			
methanol	10 26	9 7	ammonia	9 29	40 7
	10 30	6 3		10 29	27 7
	10 61	4 8		10 33	13 4

5 **Vapour Trace Detection.** In order to find the detection limit (vapour trace detection in air), the initial mixtures of several torrs from each compound diluted in air at atmospheric pressure were halved successively The OA signals measured each time for selected laser lines, were represented versus partial pressure of the molecular compounds in order to find the limit of detection The

initial mixtures are diluted successively until OA signal to noise ratio is not lower than 10 The corresponding results for the studied compounds are presented in figs. 7,8.

6. **Conclusions.** The OA laser spectra for deuterated molecular compounds can be used both for qualitative (isotopic effects) and quantitative analysis by a proper selection of the laser lines The aim is to obtain the maximum ratios of the OA signals for the isotopic homologues.

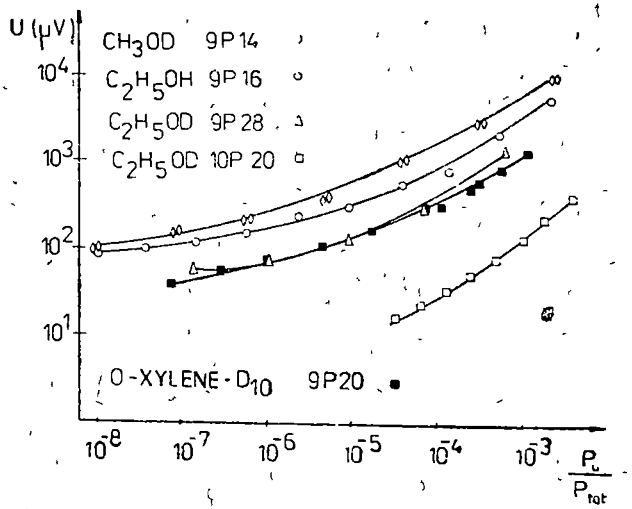

Fig 7 Trace detection limits of the deuterium labelled alcohols

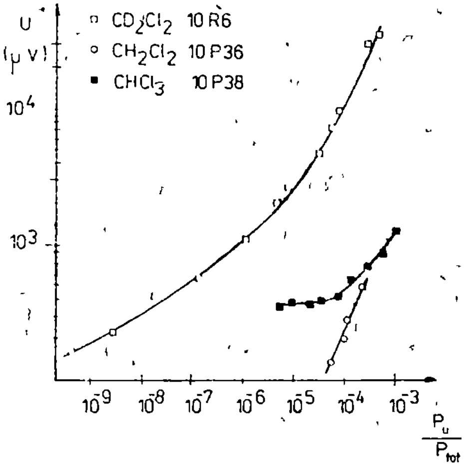

Fig 8 Trace detection limits of some deuterium labelled haloforms

Through the identification of the laser lines where the absorption cross sections are high, trace vapour detection limits in air for these compounds are established

REFERENCES

1. V P. Jarov, V S Letokhov, *Lazernaja optoakusticeskaya Spektroskopija*, Nauka, Moscow 1984
2. I Bratu, Adriana Barbu, *Trends in Quantum Electronics*, TQE'88, 27 aug —3 sept. 1988, Bucharest
3. I Bratu, Adriana Barbu, *CAER* 2-nd *Symposium on Stable Isotopes*, Tbilisi 27—30 nov 1989

STUDIA UNIV BABEŞ-BOLYAI, PHYSICA, XXXV, 2, 1990

MINITORCH FOR INDUCTIVELY COUPLED PLASMA USED IN ATOMIC EMISSION SPECTROSCOPY

S. D. ANGHEL*

ABSTRACT. — In this work is shown the modality for achievement of a minitorch for inductively coupled plasma used in atomic emission spectroscopy It is characterized by an argon consumption and a radiofrequency power absorbed into the plasma with 30% approximately lower than in the case of the conventional three concentric quartz tubes torch presented in the work [1], under conditions in which analytical capabilities are unchanged

1 **Introduction.** In the last years the modern analytical methods by emission spectroscopy have wittnessed a remarcable progress thanks to the rapid development of the electronics and computation systems, on the one hand, and thanks to use of news spectral sources among that inductively coupled plasma, on the other hand Thus has been found atomic emission spectroscopy using inductively coupled plasma (ICP-AES) Greenfield [2] and Fassel [3] have been optimized the geometrical parameters of the torch and developed the ICP-AES system, the follow commercial apparatus using these achievements. For to improve this class of spectrometers one has taken into consideration modernization of the measuring and computation systems, projecting of more stable and adaptable radiofrequency generators, achievement of the improved systems for introduction of the sample into the plasma and not in the last time, manufacturing of new types of torches with lower argon consumption (therefore with lower consumption of radiofrequence power) without sacrifying analytical capabilities of this method.

The total argon consumption (15—20 l/min) from the conventional torches amounts the running costs of the radiofrequency generators for ICP, what is the main disadvantage of ICP-AES method The accomplished researches [4—10] have imphasized a lot of possiblities to reduce the running costs of this A first possibility, but deserted of practical reasons, is the recirculation of argon. A second possibility is to use a less expensive gas, such as nitrogen, but the temperature and consequently the analytical properties of plasmas generated with molecular gases are inferior compared to an argon plasma, since the dissociation of these gases absorbs too much radiofrequency power A third alternative maintains argon as a sustaining gas, but operates to reduce the total gas requirements of the torch Three approaches can be distinguished for this last purpose reducing of the physical dimensions of the three torch tubes, external cooling of the torch (with water for example), using of the uncooled torches but made of other thermoresitant materials (silica, ceramic)

Starting from these considerations, the author has proposed himself to make a low argon consumption torch, at a radiofrequency power lower than that pre-

---

* IAUC — University of Cluj, Department of Chemistry, 3400 Cluj-Napoca, Romania

sented in the work [1], and what is constituent part of the ICP spectrometer made in IAUC—Cluj-Napoca University.

2 **Considerations on inductively plasma torch.** In an ICP spectrometer the conventional torch consists of three concentric quartz tubes system. It is introduced in a coil connected at a radiofrequency generator (12—50 *MHz*), able to supply a great enough useful power (1—2 *kW*) for ignite and maintain an argon discharge at atmospheric pressure (Fig. 1)

Through the space between outer tubes is introduced the cooling gas whose flow rate is of 18—20 *l/min* and through the space between inner tubes is introduced the gas adjusting the vertical position of the plasma with 1—2 *l/min* flow rate The central tube is used for introduction of the sample into the plasma, pneumatic pulverized from liquid solutions with 1,5—2 *l/min* gas flow rate Due to the torroidal shape of the plasma the core is relatively cool, which facilitates introduction of the sample The linear velocity of the carrier gas is a compromise between a minimal value necessary to penetrate the plasma and a maximal value that allows sufficient residence time in the plasma.

Several researches on high-efficiency torches show that plasma can be sustained on an argon flow rate down to 4 *l/min* Below this flow rate the plasma becomes unstable and eventually extinguishes. In the work [9] has been studied physical appearance of the ICP sustained in an air cooled torch After the plasma has been ignited at an argon flow rate of 12 l/min this was slowly diminished to 0,5 *l/min*, watching the physical appearance of the discharge At 12 *l/min* the plasma has a very long tail, obviously due to the torch extension. When the gas flow rate is diminished, the tail decreases in length with the gas flow rate. At about 4 *l/min*, the plasma becomes somewhat unstable but it is not extinguished. When the flow rate is 2 *l/min*, the plasma becomes suddenly very white and is stable again, having a spherical shape rather than the conventional tail-flame shape. At this flow rate the plasma touches the wall of the torch, which is then glowing softly inside, a large hole with a diamater of 5 mm being present in the center of the plasma When the gas flow is reduced further, the plasma shrinks somewhat in size, until a gap of 1—1,5 mm exists between the plasma and the torch, the torch wall stops glowing and the hole in the plasma becomes smaller At flows less than 1 *l/min*, the hole becomes just a darker spot and a gap of 2 mm exists between the torch and the plasma Below 0,5 *l/min*, the plasma shrinks somewhat further in size, but the brightness remains the same and the hole disap-

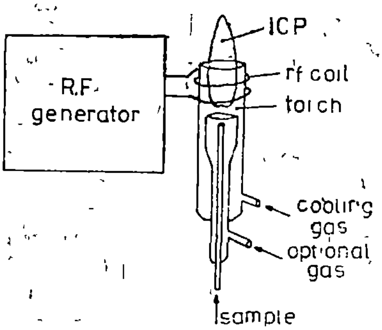

Fig 1 Generation of inductively coupled plasma

peares when the gas flow is turned off, the plasma gradually turns purple due to oxygen diffusion and extinguishes.

3 Presentation of the minitorch and experimental results. As a result of the accomplished researches for realization of a low argon consumption torch, the author has been chosen a constructive solution shown in Fig. 2.

The novelty of this torch is the ceramic piece of sinterized alumina (Al_2O_3), thermoresistent of 2000°C approximately. Also it can be observed that is used only a single dimension of quartz tube, that can be easyly replaced when it is damaged.

The decrease of the geometrical dimensions of the torch and the optimisation of the ratio between inner diameter of the quartz tube and the outer diameter of the ceramic piece have many important effects. On the one hand the argon flow rate for cooling and sustaining of the plasma has been decreased from 20 *l/min* to 13,2 *l/min*, that is 34% On the other hand the radiofrequency power absorbed into the plasma has been decreased with 37,4%, from 1656 *W* in the case of the conventional torch, to 1037 *W* in the case of the low argon consumption torch Though the energy transfered to the plasma presents an important diminution, nevertheless temperature is not decreased. By an approximate calculation results that, thanks to reduction of the torch dimensions the volume of the plasma has been diminished with 44%, that is the energy density into the plasma is greater with 12,5% approximately in the case of the minitorch, which means an increase of the plasma temperature This supposition has been verified by

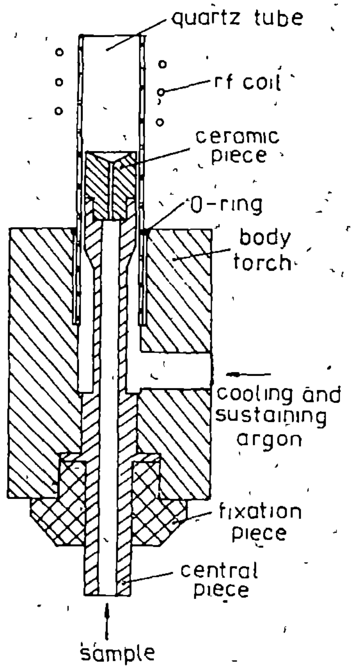

Fig 2 Minitorch construction

measuring the intensity of the spectral line with wavelength of 403,307 *nm* of manganese using the conventional torch and the low argon consumption torch, in the same exerimental conditions, ascertaining that the intensity in the second case is greater.

For to confirm the ability for using as a great performance spectral source of the inductively coupled plasma obtained with the aid of this torch, the analytical results obtained in the case of mercury analysed at 194,227 *nm* wavelength are presented In Fig 3 is presented the calibration curve obtained for concentration range between 3,4 and 100 *ppb* (μg/l) and in Fig. 4 is shown the spectral range between 193,952 and 194,576 *nm* of a solution containing 3,4 *ppb* concentration of mercury Starting from the accepted condition in literature, according to which the intensity of a spectral line, for to be measurable, must be three times bigger than deviation of the spectral background in its close proximity, one can estimate that the detection limit in the case of this element is below 1 ppb, what is at the level of the best results obtained with this analytical method

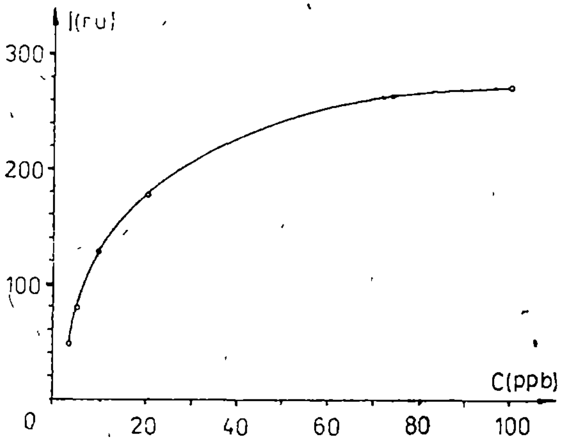

Fig 3 Calibration curve for mercury line of 194,227 *nm*

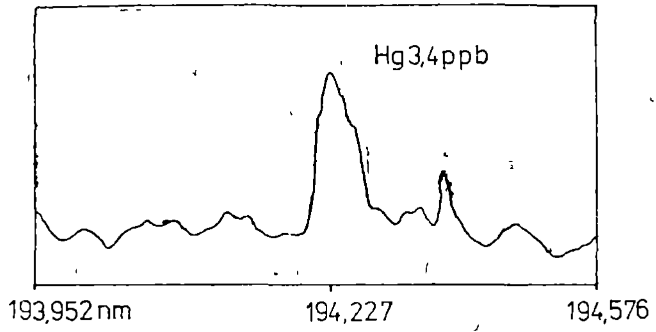

Fig 4 Mercury line of 194,227 *nm* in concentration of 3,4 *ppb*

4 **Conclusions.** Taking into consideration the above mentioned results one can assert that the minitorch manufactured and experimented by the author has more advantages in comparison with the conventional three concentric quartz tubes torch low argon consumption, greater density of energy into the plasma, reduced gauge; being the only deteriorable piece, the quartz tube can be easyly replaced, this technology is not necessaryly a pretentious one Also one foresees the possibility of using ceramic materials for manufacturing other pieces of low argon consumption torch

Acknowledgement. The author acknowledges with thanks the help of Mr E Darvasi for obtaining of experimental results

REFERENCES

1 S D Anghel, A Popescu, F Racz, E Tătaru and E Cordoş, Rev Chim, **40,** 344 (1989)

2 S Greenfield, I L Jones and C T Berry, Analyst, **89,** 713 (1969)

3 R A Wendt and V A Fassel, Anal Chem, **37,** 920 (1965)

4 C. D Allemand and R M. Barnes, Appl Spectrosc, **31,** 434 (1977)

5. R Razaaiyaan, G M Hieftje, H Anderson, H Kaiser and B Meddings, Appl Spectrosc **36,** 627 (1982)

6 G R Kornblum, W van der Waa and L de Galan, Anal. Chem, **51,** 3278 (1979)

7. H Kawaguchi, T Ito, S. Rubi and A Mizuike, Anal Chem, **52,** 2440 (1980).

8 H Kawaguchi, T Tanaka, S Miura, J Xu and A Mizuike, Spectrochim Acta, **38B,** 1319 (1983)

9 P S C van der Plas, *Realization of Low Flow Torches for Inductively Coupled Plasm Spectrometry*, Dr thesis, Technical University, Delft, Netherland (1987)

10 L de Galan and P S C van der Plas, Fresenius, Z, Anal Chem, **324,** 472 (1986)

STUDIA UNIV BABEŞ-BOLYAI, PHYSICA, XXXV, 2, 1990

STATIC SUSCEPTIBILITY AND MAGNETIZATION MEASUREMENTS IN THE HIGH-T_c SUPERCONDUCTOR SYSTEM $Y_{1-x}Gd_xBa_2Cu_3O_{7-\delta}$

AL. NICULA*, A. V. POP*, AL. DARABONT**, I. COSMA***

ABSTRACT. — Static susceptibility and magnetization measurements were performed in the normal state of the $Y_{1-x}Gd_xBa_2Cu_3O_{7-\delta}$. The dependence of Curie constant C and Curie paramagnetic temperature θ versus x indicates the Curie—Weiss behaviour and possible exchange interactions. The normal state magnetization Mn(H) evidenced the paramagnetic behaviour.

Introduction. Since the discovery of the oxide superconductors $YBa_2Cu_3O_{7-\delta}$ [1], many researchers have been devoted to various experimental investigations probing the nature of the superconductivity. The Y can be replaced by many rare-earth elements while maintaining the same crystal structure and achieving approximately the same superconducting transition temperature T_c, independent of whether or not they are magnetic. Magnetic susceptibility in the normal state is one of the fundamental quantities which characterize the framework of superconducting systems [3, 4]. An analysis of the normal state magnetic susceptibility of the present metallic oxides is still somewhat uncertain. One of the difficulties consists in estimating the effect of reduced-dimensional short range order of fluctuating cooper magnetic moments. However, the partial substitution of a rare earth element for Y in $YBa_2Cu_3O_{7-\delta}$ has not led to the enhancement of superconductivity, but more often has caused its degradation. Our EPR measurements in the $Y_{1-x}Gd_xBa_2Cu_3O_{7-\delta}$ system [2] indicates at room temperature the overlapping over the characteristic Gd^{3+} line of a signal typical for Cu^{2+} resonance. In fact several groups have reported EPR results which differ considerably [6, 7], function of sample preparation. A reliable explanation is not attainable from *EPR* results alone.

In this context the magnetic properties are studied here through magnetization and static susceptibility on $Y_{1-x}Gd_xBa_2Cu_3O_{7-\delta}$ ($x = 1, 5, 10, 15, 25\%$) function of magnetic fields and temperature.

Experimental procedure. The samples were prepared by the solid phase reaction method and the thermal history is described in [2].

The normal-state susceptibility $\varkappa_n(T)$ and the magnetization $M(H)$ were measured by a magnetic Faraday balance. The presence of a superconducting phase with $T_c > 77$ K was established by testing the Meissner Ochsenfeld effect on the samples cooled under liquid nitrogen temperature. The magnetic susceptibility was measured from 90 K up to 300 K in the applied field of 0.99 T for samples by $x = 5\%$, 10%, 15% and 0.53 T for $x = 25\%$.

Results and discussion. The normal-state susceptibility $\chi_n(T)$ and the inverse of the static susceptibility $1/\chi_n(T)$ is shown for the samples of $Y_{1-x}Gd_xBa_2Cu_3O_{7-\delta}$ in Fig. 1 ($x = 5\%$, 10%, 15%).

---

* University of Cluj, Department of Physics, 3400 Cluj-Napoca
** Institute of Isotopic and Molecular Technology, P O Box 700, 3400 Cluj-Napoca
*** Politechnical Institute of Cluj-Napoca, Department of Physics, C 3400 Cluj-Napoca, Romania

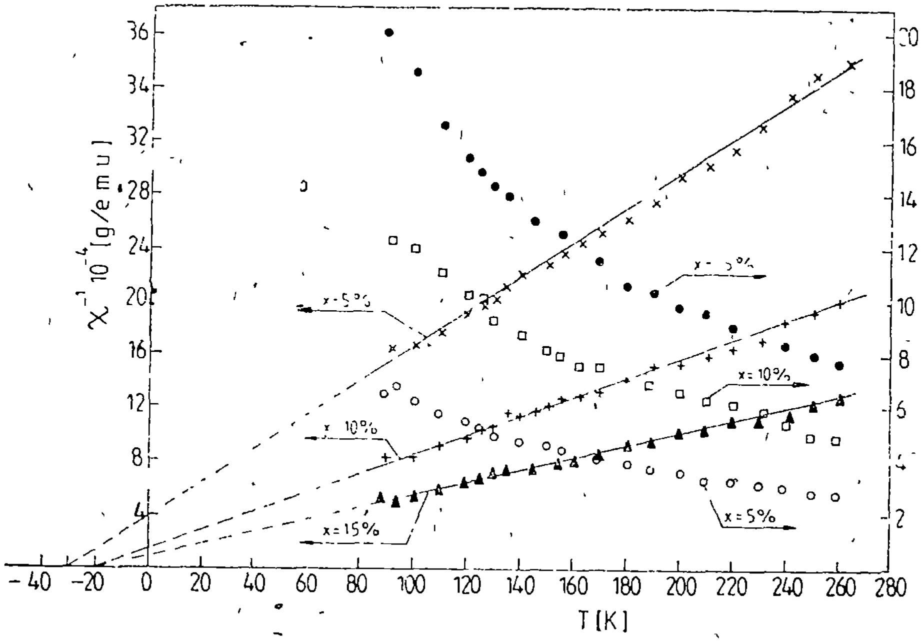

Fig 1 The temperature dependence of magnetic susceptibility $\varkappa_n(T)$ and reciprocal susceptibility under the field of 0 99 T for samples by $x = 5,\ 10,\ 15\%$ *Gd*

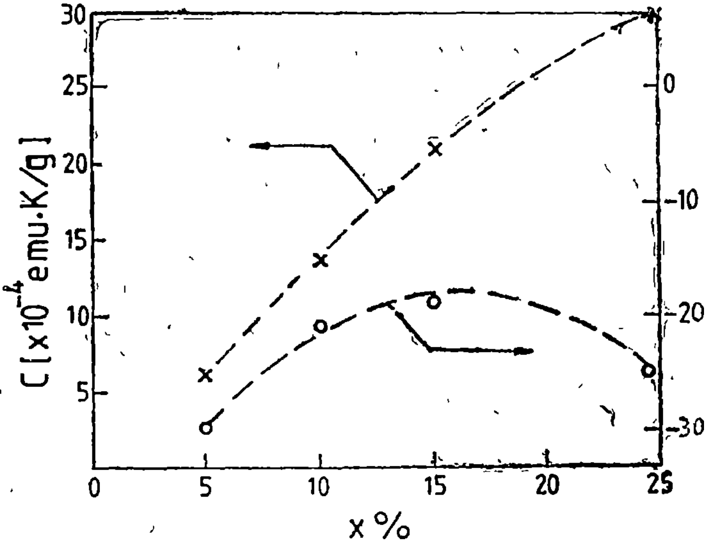

Fig. 2 Curie constant $C(x)$ and Curie paramagnetic temperature $\theta(x)$ function of the *Gd* concentration x in $Y_{1-x}Gd_xBa_2Cu_3O_{7-\delta}$

It is reasonable to assume that $\chi_n(T)$ is described by the law $\chi_n(T) = \chi_0 + C/(T - \theta_p)$. Here χ_0 is the constant background, θ_p is the Curie temperature and C is the Curie constant

The least squares fit to the data using this formula yields the value of C and θ_p shown in Fig 2 For $x \in (0 - 15\%)$ the Curie constant increased linearly The magnetic susceptibility is estimated by substracting the values of diamagnetic contribution ($-3{,}66 \cdot 10^{-7}$ *emu/g*) for the ion cores in $YBa_2Cu_3O_{7-\delta}$ As can be seen in Fig 2, an increase in the Gd concentration x raises C, corresponding to the enhancement of the Curie-Weiss behaviour in $\chi_n(T)$
The deviation from $\mu_{eff/Gd} \simeq 8\,\mu_B$ which caracterize the Gd^{3+} ions in the single phase orthorhombic structure, can be explained assuming the presence of insulating phases $(Y_{1-x}Gd_x)Ba_2CuO_5$ with supplimentary C_1 due to the effective moment of Cu^{2+} ions ($\mu_{eff} \simeq 1{,}7\,\mu_B$), and the presence of Cu^{2+} in the chains.

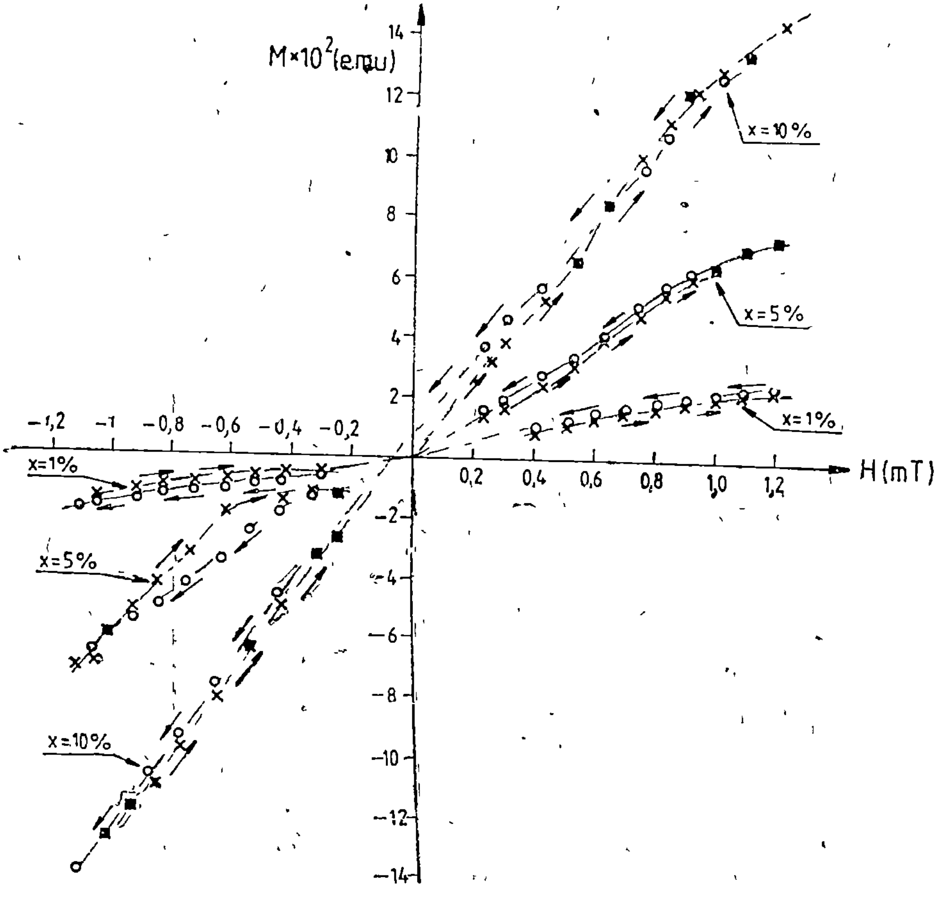

Fig 3 Normal-state magnetization as a function of the magnetic field at T = 92 K for samples by 5, 10, 15% *Gd*

The assumption of insulating phases is related with the existence of similar negative Curie temperatures evidenced by some autohrs [6, 7] in Y_2BaCuO_5 and Gd_2BaCuO_5 "green" phases The dependence of the paramagnetic Curie temperature θ_p function of x contain an exchange interaction effect
The normal state magnetization Mn(H) measured by a Faraday balance at T = = 92 K, is shown for several samples of $(y_{1-x}Gd_x)-Ba_2Cu_3O_{7-\delta}$ in Fig 3 The curves Mn(H) provide an experimental evidence for the paramagnetic nature of samples for T > T_c

Conclusions. The static susceptibility and magnetizations measurements evidenced the Curie-Weiss behaviour in the normal state of superconducting system $Y_{1-x}Gd_xBa_2Cu_3O_y$ The dependence $C(x)$ can be explained assuming the presence of insulating phase with supplimentary C_1 due te the Cu^{2+}. An exchange interaction's effect contain the dependence of $\theta_p(x)$

REFERENCES

1 M K Wu, J. R Ashburn, C J Torng, P. H. Hor, R L Meng, L Gao, Z. J. Huang, Y Q Wang and C W Chu, Phys Rev Lett, **58,** 908 (1987)

2. Al Nicula, A V Pop, L V Giurgiu, Al Darabont, Studia, Physica **32,** Nr 2, (101) (1989)

3 K Sezikawa, Y Takano, T Inaba, Physica C **162, 164** (1989)

4 K Kanoda, T Takahashi, T Kawagoe, T Mizoguchi, M Hasumi, S Kagoshima, Physica C, **153, 155** (1988)

5 Al Nicula, A V Pop, L V Giurgiu, Al Darabont, Conference on Radio and Microwave Spectroscopy, RAMIS 89, Poland

6. K Kanoda, T Takahashi, T Kawagoe, T Mizoguchi, S Kagoshima, M Hasumi, Journal of Applied Physics, vol **26,** 12 (1987)

7. F Mehran, S E. Barnes, E A Giess, T R McGuire, Solid State Communications, vol **67,** nr 1, 66—59, (1988)

STUDIA UNIV BABEŞ-BOLYAI, PHYSICA, XXXV, 2, 1990

SPECIFIC PROBLEMS RELATED TO THE CORRELATION BETWEEN THE LOWER AND THE UPPER IONOSPHERE

SZŐCS GÉZA* and SZŐCS HUBA**

ABSTRACT. — The objective of this research was to study the interaction between the ionospheric layers Correlation coefficient between Wolf's number and the average of critical frequencies was computed for the *E* and *F* layers Using method of multiple correlation the existence and characteristics of this interaction has been attempted

The condition of the ionosphere-layers is influenced primarly by external effects, viz solar activity and cosmic radiation Simultaneously terrestial effects such as geomagnetic activity also influence this condition. The actual problem is the interaction between the lower and upper layers of the ionosphere

In order to study the interaction between the layers of the ionosphere the following method has been applied ·

1. Using the data available for the periods from 1959 to 1977 and from 1984 to 1986, the critical frecvency f_0E_1 for layer E_1 was computed each month for the ordinary wave. Thus 3 654 data for the critical frequency was determined ;

2. The correlation coefficient between the monthly-hourly averages of the critical frequency and the pertaining monthly Wolf's number was determined (174 data) for each month (see table),

Table 1

Correlation Coefficients

Time month	04	05	06	07	08	09	10	11	12	13	14	15	16	17	18
I				0,47	0,58	0,72	0,77	0,85	0,72	0,87	0,69	0,74			
II				0,31	0,76	0,68	0,87	0,83	0,87	0,90	0,84	0,78	0,77		
III			0,46	0,83	0,74	0,93	0,83	0,86	0,87	0,80	0,88	0,85	0,70	0,64	
V	0,96	0,62	0,71	0,77	0,74	0,70	0,74	0,78	0,73	0,75	0,93	0,76	0,69	0,80	0,89
V	0,59	0,65	0,93	0,87	0,88	0,90	0,93	0,89	0,89	0,91	0,84	0,85	0,91	0,52	0,66
VI	0,96	0,62	0,71	0,77	0,74	0,70	0,74	0,78	0,73	0,75	0,93	0,76	0,69	0,60	0,89
VII	0,35	0,83	0,90	0,86	0,83	0,92	0,90	0,93	0,85	0,87	0,91	0,86	0,89	0,83	0,73
VIII		0,88	0,86	0,94	0,87	0,90	0,95	0,95	0,92	0,93	0,82	0,92	0,87	0,78	
IX		0,40	0,84	0,84	0,85	0,90	0,85	0,84	0,90	0,85	0,86	0,76	0,78	0,81	
X.			0,41	0,67	0,76	0,82	0,81	0,87	0,87	0,84	0,73	0,44			
XI					0,58	0,64	0,80	0,83	0,77	0,85	0,73				
XII				/0,64/	0,69	0,74	0,85	0,80	0,68	0,77	0,58				

---

* *Eszterhazy Karoly Pedagogical College, Eger, Hungary*
** *Kando Kalman Tehnical College, Székesfehervar, Hungary*

3 Correlation coefficients for F layers were determined similarly (f_0F_2);

4 Multiple correlation for coefficients of layers E and F was determined differently. Final correlation coefficients are summarized in Table 1, while graphical representation of data is shown in Fig 1,

5 The average value of correlation coefficients was computed; the result is $r = 0.600$,

The result of the above procedure can be summarized as follows

1 The graph of correlation coefficients contains four maximums and four minimums

2 Correlation between the ionizing effects in layers F and E is characteristic ($r = 0.91$ in January, $r = 0{,}83$ in October), similar case is in months of equinox ($r = 0.92$ in March, $r = 0.85$ in September) This correlation is weak in December ($r = 0.36$), in February ($r = 0.23$), in Avril ($r = -0.04$) and in June ($r = 0.34$)

3 Variation shows over a 2 month period

4 Further consequences can be determined by an even more sophisticated correlation analysis Interaction between the different layers is doubtless Further development of Solar Physics could give a new perspective for such theories.

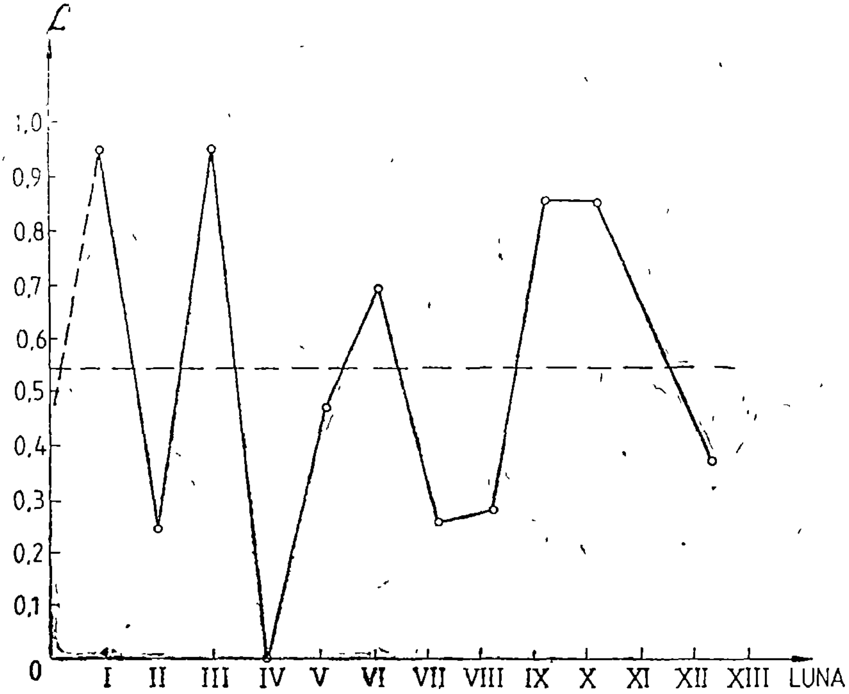

Fig 1 Graphical representation of correlation coefficients variation as function of month.

Note

The relationship between layers E and $F2$, which take place in different heights of the ionosphere, is too complicated to study by a correlation computation based on monthly hour averages The behaviour of layer E is similar to that of the Chapman-layer that is the electron-density related to f_0E_1 varies in accordance with zenith-distance of the Sun

As for layer $F2$, electron-density related to f_0F2 is not governed by this law. The ionization in the two layers is generated by radiations of different wave-length (80—102,6 nm in layer E and 20—91 *nm* in layer F) moreover the recombination processes in the two layers are different, also In layer E quadratic while in layer F linear recombination takes place. Transport of charges is different, as well In layer E transport of charges is negligible, while in layer $F2$ it plays an important role by plasma diffusion.

Fluctuation of the curve shown in Fig. 1. (2 month period) may just be attributed to that in layer E (as it is well known) effect of geomagnetic activity is hardly observed, in layer $F2$ it results in considerable changes

REFERENCES

1. Bencze P, Saiko, J, Szendrői J, *Miről vallanak az ionogramok*, Ionoszféra es magnetoszféra-fizica **XIII** MANT, 155—177 (1986)
2. Bencze P, Major Gy, Mészáros E, *Fizikai meteorologia*, Akadémiai Kiadó, Budapest, 1982
3. Sátori G, Ionoszféra es magnetoszféra fizika **XIII** MANT, 43—53 (1985)
4. Szőcs G, Szőcs H, Lucrările sesiunii Jub de Com Ştiinţ, vol **2**, 124—127 (1988)
5. Szőcs G, Szőcs H, Al III-lea Colocviu Naţ Fiz şi Tehn mat. crist şi amorfe, Rezumatele lucr, Iaşi, 349—350, 1988
6. Szőcs G, Teză de doctorat, Univ Cluj-Napoca, 1989
7. Szőcs, G, Szőcs H, *Progrese în fizică*, Sesiune ICEFIZ, Constanţa, 730—740 1988
8. Ionospheric Data Observatorie Pruhonice and Panska Ves Chechoslovak Akademy of Sciences-Geophysical Institute, 1959—1986
9. Geophysikalische Beobachtungsergenbisse Geophysical Data, H Hertz Inst Deutsche Akad. der Wissenschaften zu Berlin, 1969—1982

STUDIA UNIV BABEŞ-BOLYAI, PHYSICA, XXXV, 2, 1990

EPR INVESTIGATION OF Fe^{3+} IONS IN THE [$95TeO_2 \cdot 5PbO$] GLASSES

M. PETEANU* and I. ARDELEAN*

ABSTRACT. — EPR absorbtion spectra due to Fe^{3+} ions in xFe_2O_3 $(1 - x)$ [$95TeO_2 \cdot 5PbO$] glasses for $0.5 \leqslant x \leqslant 20$ mol % revealed a strong dependence of their structure and the values of the EPR parameters on the glass composition. At low Fe_2O_3 content, resonances due to isolated Fe^{3+} ions in sites of distorted cubic field, prevail in the spectra. As rising concentration, a very marked clusterizing tendency of the impurities was evidenced. For both types of absorptions, the EPR parameters dependence on the Fe_2O_3 content in the studied matrix, was able to give us informations about the Fe^{3+} ions distribution in the matrix, along the proposed concentration range. In the 80—300 K temperature range, our samples behave as paramagnetic ones.

Introduction. The paramagnetic resonance spectra of Fe^{3+} ions in oxidic vitreous matrices were successful in identifying the vicinities in which the crystal field effects result in absorptions having g factor values very different from 2.0023, and also in evidencing the clusterizing tendencies of the paramagnetic ions over a concentration limit [1—5, 10, 11]. The interactions involving them, depend on the strength and type of bindings in the host diamagnetic matrix, and also of the magnetic dilution of impurities, so that the absorption spectra and the EPR parameters dependence on the paramagnetic ions concentration may provide informations about the microstructure of the studied ions vicinity.

Because of their peculiar properties having number of applications, tellurate glasses become over more studied in the last time. By melting tellurium dioxide and transition-metal oxides in suitable proportions one obtains amorphous compounds which are electronic semiconductors, their properties being intensively used in microelectronics. Series of papers concerning the $TeO_2—V_2O_5—Fe_2O_3$ glassy system, reported its electrical properties, connected with the concentration and mobility of the current carriers, and the phase equilibrium diagram [6, 7]. The vitreous state formation in binary tellurate systems containing transition metal oxides has been investigated in detail [8]. The binary $TeO_2—Fe_2O_3$ system was studied from the point of view of its electrical properties [6] as well as structural ones, by means of Mossbauer and I.R. spectroscopy, and positron anihilation [9].

In order to obtain more informations about this system we studied the magnetic properties [12] and the EPR absorption spectra of Fe^{3+} ions in vitreous $95TeO_2 \cdot 5PbO$ matrices.

Experimental. Our investigation concerns the xFe_2O_3 $(1 - x)$ [$95TeO_2 \cdot 5PbO$] system, for x varying in the range of $0.5 \leqslant x \leqslant 20$ *mol* %. Vitreous samples were obtained by melting the oxidic mixtures corresponding to different concentrations in an electrically heated furnace, at about 1000 °C

---

* *University of Cluj, Department of Physics, 3400 Cluj-Napoca, Romania*

After an hour of stabilization at the melting temperature samples were quenched on a stainless steel plate at the room temperature Typical glasses were obtained as both aspect and structure

Electron paramagnetic resonance measurements were performed at both room and liquid nitrogen temperature, by using a JES-3B type spectrometer, in the X frequency band, and a 100 *kc/s* field modulation

Results and discussions. Along the investigated concentration range the magnetic susceptibility follows a Curie-Weiss law, with a negative paramagnetic Curie temperature, θ_p, increasing linearly in absolute value as the Fe$_2$O$_3$ content rises [12] The temperature dependence of the reciprocal magnetic susceptibility over the investigated temperature range is linear, the magnetic transition temperature having a very low value The magnetic ordering, if exists, takes place far below 80 K A linear dependence of the Curie constants on the Fe$_2$O$_3$ content was obtained The values of C, were situated between the two limit values, when only Fe^{3+} or Fe^{2+} ions would be present in the matrix, suggesting the presence of both in our samples

Over the investigated temperature range a paramagnetic behaviour was evidenced The magnetic ordering at lower temperatures has a local character, in agreement with the amorphous structure of our samples

The presence of the Fe^{3+} ions, and their distribution in the vitreous matrix, was evidenced by means of the EPR measurement

The EPR investigation of the xFe$_2$O$_3$ $(1-x)$[95TeO$_2$ 5PbO] system, for $0.5 \leqslant x \leqslant 20$ mol % revealed a strong dependence of the structure of the absorption spectra, and the values of the EPR parameters on the sample composition. For comparing the EPR absorptions intensity, and to follow their evolution on the proposed concentrations range, the same amount of sample, i e 100 *mg*, was tested The structure of the absorption spectra was not affected by the temperature lowering, excepting for the signal intensity increasing, and a better resolution The features of these spectra are evidenced in Fig 1 The Fe^{3+} recorded spectra, mainly consist in absorptions centered at $g_{ef} \sim 4\ 3$ and $g_{ef} \sim 2\ 0$ It is known that the absorption at $g \sim 4.3$ is due to isolated Fe^{3+} ions subjected to crystal field effects, acting as principal interaction in the spin hamiltonian Such an absorption was interpreted in terms of the axially symmetric crystal field, or of the rhombic one, prevailing in the spin hamiltonian [1, 4] It was also pointed out [5] that the $g \sim 4\ 3$ absorption increasing as temperature lowering cannot be assigned to transitions inside the median excited Kramers doublet, as in the case of the rhombic field model [1] Therefore, it seems appropriate to consider the distorted cubic field case, which results in transitions having an isotropic $g = 4.28$ value inside the lowerest Kramers doublet.

In our EPR investigation of the Fe^{3+} ions in xFe$_2$O$_3$ $(1-x)$Na$_2$B$_4$O$_7$ glasses the cubic vicinities of the paramagnetic ion having a tetragonal distortion, were taken into account [10] The specific structure of the borax glasses [15] supported this choice Tellurate glasses being more distorted, the complexes involving the impurity are almost planar [16] The theory of the $g \sim 4.3$ absorptions was detailed for a variety of distorted vicinities [13], options for the most convenient case being available according to the structural peculiarities of the investigated matrix

According to Fig 1 the spectral structure dependence on concentration shows that at low impurities content resonances centered at $g \sim 4.3$ prevail in

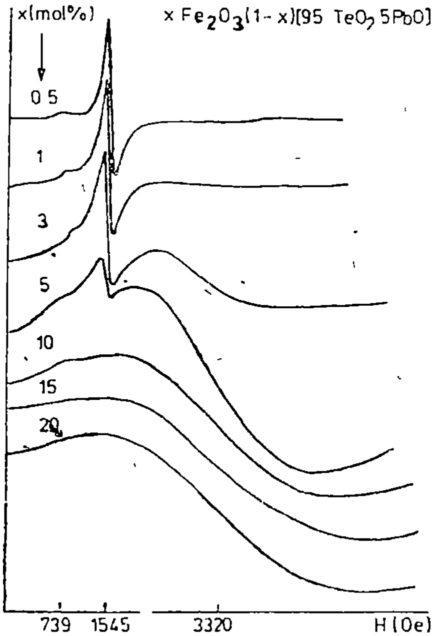

Fig 1 EPR absorption spectra of the Fe^{3+} ions in the xFe$_2$O$_3$ $(1-x)$[95TeO^2 5PbO] glasses, for 0 5 $\leqslant x \leqslant$ 20 *mol* % Spectra were recorded at different degrees of amplification, according to their details

the spectrum. As rising concentration, their intensity suddenly decreases absorptions, becoming favoured at $g \sim 2$ 0 The EPR absorptions evolution along the proposed concentration range is easier to follow by considering the composition dependence of the characteristic EPR parameters, that is the peak-to-peak height I of the absorption line, the linewidth ΔH, and the intensity approximated as $J = I \cdot \Delta H^2$ The concentration dependence of these parameters is plotted in figs 2 and 3 for the absorptions centered at $g \sim 4$ 3 respectively those centered at $g \sim 2$ 0.

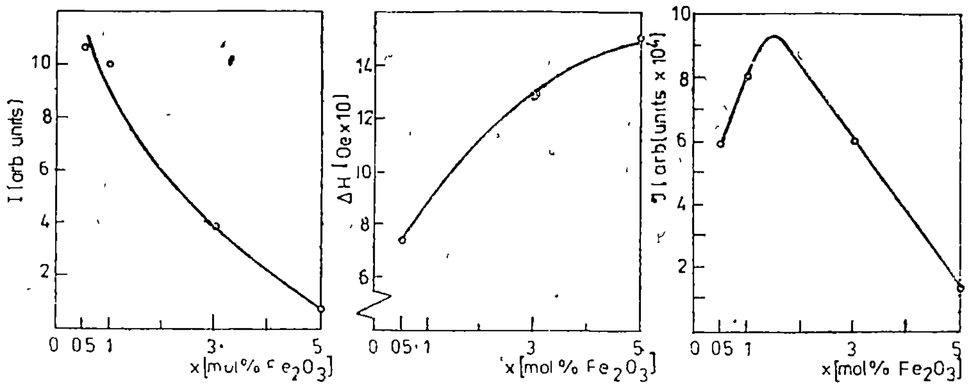

Fig 2 EPR parameters dependence on the Fe$_2$ O$_3$ content, for resonances having $g = 4.3$

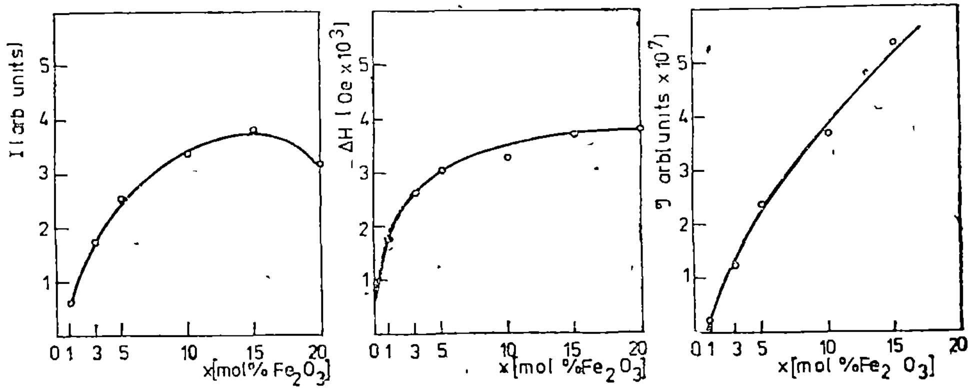

Fig. 3. EPR parameters dependence on the Fe_2O_3 content for the absorptions centered at $g = 2.0$.

In contrast to the $g \sim 4.3$ resonances whose intensity increases on an extremely short concentration range, suddenly decreasing and completely disappearing for $x > 5$ mol % Fe_2O_3, the $g \sim 2.0$ absorptions intensity increases almost linearily till about 15 mol % Fe_2O_3 and diminishes only after. The increasing of the $g \sim 2.0$ absorptions is in prejudice of those centered at $g \sim 4.3$ values. A similar behaviour was detected for the Fe^{3+} ions in borate glasses [10, 11, 14]. However, the $g \sim 2.0$ intensity increasing is much more pronounced and takes place at lower Fe_2O_3 content in tellurate glasses than in the borate ones, providing a striking clusterising tendency of the Fe^{3+} ions. In the composition dependence of the $g \sim 4.3$ absorptions plotted in Fig. 2 the intensity reaches its maximum at $x = 1.5$ mol % Fe_2O_3, whereas in the natrium borate glasses $xFe_2O_3 \cdot (1 - x)Na_2B_4O_7$ this maximum occurs for $x > 4.00$ *mol* % Fe_2O_3 [10], and in the lead borate ones for $x = 8$ mol % Fe_2O_3 as in the case of the $xFe_2O_3 \cdot (1 - x)[PbO \cdot 3B_2O_3]$ system [14], or $x = 7$ mol % Fe_2O_3 in the case of the $xFe_2O_3 \cdot (1 - x)[PbO \cdot B_2O_3]$ glasses [15]. The Fe^{3+} ions vicinity seems to be more ordered in the borate glasses than in the tellurate ones, and more stable as configuration during the process of impurities accumulation along the investigated concentration range.

Having in view the structural origin of the $g \sim 4.3$ resonances, Moon et al. [18] explained their evanescence by the removal of the local symmetry distortions, at the iron ions addition. The fact that the vicinity in tellurate glasses is strongly distorted was already evidenced, and also the fact that the Te ions microvicinity in amorphous compounds is similar to that of the crystalline TeO_2 [16, 19]. During the impurifying process, the Fe^{3+} ions substitute for Te. The symmetry of the neighbours determining the crystal field is low enough for justify the $g \sim 4.3$ absorptions. The microvicinity of the Te ion is a distorted tetrahedron in the form of a roughly planar complex. Subsequent studies [9] showed that the tellurium-oxygen configuration type depends on the modifier content. One supposes that the TeO_4 tetrahedral complex has, in tellurate glasses, an extra-trigonal distortion due to the nonbridging oxygens. The explanation of the $g \sim 4.3$ resonances evanescence by means of the distortions removal seems to be nonrealistic in tellurate glasses [3].

Another possibility of the $g \sim 4.3$ resonances diminishing would be the dipol-dipol broadening of the absorption line by adding iron ions in random positions in the matrix, or, so as [18] demonstrate, the connection of the paramagnetic ions in clusters, growing as the concentration rises. By simulating the effects of interactions with the nearest neighbours and the next-nearest ones, Duff and Canella [20] showed that the isolated ions concentration culminates at values of x much smaller than those predicted by the theory of a random clusterising process. The shift of this maximum to smaller values of x was atributed to exchange interactions extended to a wide range.

In our opinion the $g \sim 4.3$ absoprtion removal during the impurifying process, is primarily due to destroying of the neighbours configuration in the iron ions vicinity. Although randomly distorted these vicinities are in some kind alike to each other, having at the origin the same crystalline structure, and the same ability of the Fe^{3+} ions to order their surrounding. These microagregates also assure the degree of independence of the paramagnetic ions and, their specificity of "isolated" ones. The gradual increasing of the paramagnetic ions density destroys the microstructural ordering in their neighbourhood and their vicinities as characteristic entities become less represented.

The linewidth of the $g \sim 4.3$ resonances increases on the proposed concentration range, but the initial slope corresponding to the dipolar broadening at low paramagnetic ions content, is changed at higher concentration. The linear dependence at low concentration show a random distribution of the Fe^{3+} ions in the vitreous matrix [17]. At higher concentrations the site population deviates from randommess, the ions interacting strong enough to be incorporated in a cluster structure. This explains the ΔH values much lower as those predicted by the initial slope (Fig. 2), due to the superexchange interactions of the nearest neighbours. The increase of the Fe_2O_3 content involves smaller distances between the Fe^{3+} ions and consequently magnetic interactions. These are expected to take place by a superexchange-type mechanism. The strenght of the exchange interactions is not as great as to favour macroscopic magnetic ordering, the samples remaining essentially in paramagnetic state over the studied temperature range.

The composition dependence of the $g \sim 2.0$ absorptions (Fig. 3) show an increasing of both intensity and linewidth along the concentration range, but these parameters do not follow linearily the Fe_2O_3 content. This is due to the fact that during the melting process of the oxidic compounds besides the Fe^{3+} ions, Fe^{2+} enter the vitreous matrix too at a certain step of the composition scale. Fe^{2+} ions are not involved in the EPR absorption, but their interactions with Fe^{3+} influence the characteristics of the absorption spectra. The Fe^{3+}/Fe^{2+} balance depends on the matrix composition, the melting temperature, and ohter specific conditions [22, 23].

Conclusions. The EPR of Fe^{3+} ions in $x\mathrm{Fe_2O_3} \cdot (1 - x)[95\mathrm{TeO_2} \cdot 5\mathrm{PbO}]$ glasses, for $0.5 \leqslant x \leqslant 20$ mol % reveals a strong dependence of the structure of the absorption spectra and the EPR parameters value, on glass composition.

At small impurity ions content, resonances centered at $g_{ef} \sim 4.3$ prevail in the spectrum. These are due to Fe^{3+} isoltated ions in sites of distorted crystal field. Their number increases on an extremely short concentration range, the corresponding sites being occuped at low concentrations.

At higher concentrations the ions interact strong enough to be incorporated in a cluster structure The corresponding EPR absorptions are centered at $g \sim 2\ 0$ Tellurate glasses are characterized by very pronounced tendencies of clusterizing of impurities in their matrix.

In the 80—300 K temperature range, the investigated tellurate glasses are paramagnetic The magnetic ordering is supposed to take place far below 80 K.

REFERENCES

1. T Castner, G. S Newell, W C. Holton, C P. Slichter, J Chem Phys 32, 668 (1960)
2. H H Wickman, M P Klein, D A Shirley, J Chem Phys, 42, 2113 (1965)
3. C R Kurkjian, E A Sigety, Phys Chem Glasses, 9, 73 (1968)
4. D Loveridge, S Parke, Phys Chem Glasses, 12, 19 (1971)
5. I. V Chepeleva, Dokl Acad Nauk SSSR, 202, 1042 (1972)
6. V S Kozhouharov, M P Marinov, Compt. rend Acad bulg Sci, **26** (3), 343 (1973), **28** (4), 505 (1975), **28** (6), 783 (1975)
7. V S Kozhoukarov, M. P. Marinov, J. N. Pavlova, Compt rend Acad bulg. Sci, **30** (1), 73 (1977).
8. V S Kozhouharov, M P Marinov, G Grigorova, J noncryst Solids, **28**, 429 (1978)
9. V S Kozhouharov, M P. Marinov, T Troev, Mat. Res Bull, **14**, 735 (1979)
10. Al Nicula, M. Peteanu, Studia Univ. B—B, Physica, **42** (1976)
11. E Burzo, I Ardelean, Phys. Stat Sol (b) **87**, K 137 (1978)
12. I Ardelean, Gh Ilonca, M Peteanu, I Luca, Studia Univ B—B, Physica 1, 65 (1979).
13. M. Peteanu, Al. Nicula, Studii şi Cercetări de Fizică **33** (1), 29 (981), **34** (1), 15, (1982).
14. E. Burzo, M Chipară, D Ungur, I. Ardelean, Phys Stat Sol (b) 124, K 117 (1984)
15. R Reisfeld, J Res Nat Bur Stand (U 8) **76** (A), 613 (1972)
16. G Sperlich, P. Urban, Phys Stat Sol (b) **61**, 475 (1974)
17. C Kittel, E. Abrahams, Phys Rev **90**, 238 (1953)
18. D W Moon, J M Aitken, R K McCrone, G S Cieloszyk, Phys Chem Glasses **16** (5), 91 (1975)
19. E J Friebele, N C Koon, L K Wilson, D. L Kinser, J Amer Ceram Soc. **57**, 237 (1974)
20. K F Duff, V Canella, *Amorphous magnetism*, p. 207, Plenum Press, New York, 1973.
21. H Laville, J C Berthier, J Mat Sci **15**, 73 (1980)
22. E Burzo, I Ursu, D Ungur, I Ardelean, J Appl Phys, **58** (9), 3628 (1985).
23. I Ardelean, Gh Ilonca, O Cozar, G Mureşan, Studia Univ B—B, Physica 2, 37 (1989)

STUDIA UNIV BABEŞ-BOLYAI, PHYSICA, XXXV, 2, 1990

THE DETERMINATION OF OPTICAL INDICATRIX AXES IN UNIAXIAL NONLINEAR CRYSTALS

GABRIEL MOAGAR-POLADIAN*

ABSTRACT. — A method for optical indicatrix axes determination is presented. Its use is of practical interest for uniaxial nonlinear crystals It is a fast method, which doesnt' need *X*-ray apparatuses

Introduction. The recent development in optical communications systems, optical radar and other branches in which nonlinear media are involved, needs methods for last determination of their optical properties, in particular of their optical axes

Theory. The optical indicatrix is the surface of second degree which describes the value of the refractive index of a crystal as a function of crystalographic direction. Its equation is

$$\frac{x^2}{n_x^2} + \frac{y^2}{n_y^2} + \frac{z^2}{n_z^2} = 1 \qquad (1)$$

where n_x, n_y, n_z are the refractive indexes along the three perpendicular directions X, Y, Z.

In the case of biaxial crystals, the indicatrix has the shape of an ellipsoid with unequal semiaxes In the case of uniaxial crystals, the indicatrix has the shape of a revolution ellipsoid, and for isotropic media the shape of a sphere.

When an electric field is applied to uniaxial or isotropic media, their symmetry is changed, this change being translated (from the point of view of optical properties) in changes of optical indicatrix So, in the case of a uniaxial nonlinear medium, the equation of the indicatrix in the absence and, respectively, in the presence of the applied electric field is

$$\frac{x^2 + y^2}{n_0^2} + \frac{z^2}{n_e^2} = 1, \text{ with } n_x = n_y = n_0,\ n_z = n_e \qquad (2a)$$

$$\frac{x^2}{n_y'^2} + \frac{y^2}{n_x'^2} + 2r_{xyz}E_zXY = 1 \qquad (2b)$$

where r_{xyz} is the (xyz) element of the electrooptic tensor Equation (2b) could be transformed to the canonical form Let the electric field E be applied parallel with the optical axis (Z) of the crystal Then, the transformation to canonical form is realized by turning the initial system of axes (XYZ) around Z-axis, with a certain angle α The new axes are $X'Y'Z$ The turning angle is obtained from the equation (see 1)

$$\operatorname{tg} 2\alpha = \frac{2r_{xyz}E_z}{\dfrac{1}{n_x^2} - \dfrac{1}{n_y^2} + (r_{xxz} - r_{yyz})E_z} \qquad (3)$$

---

* *Institute of Atomic Physics, Laser Devices Department IFTAR—DSL Bucureşti*

and it is seen that the angle depends on the elements r_{xyy} of the electrooptic tensor and on applied field. In the case of uniaxial crystals $n_x = n_y$, so

$$\operatorname{tg} 2\alpha = \frac{2r_{xxz}}{r_{xxz} - r_{yyz}} \tag{4}$$

In the presence of the electric field the uniaxial crystal becomes biaxial

The introduction of the crystal between two polarizers gives an optical transmission for a light beam passing through the system equal to (see 1), (Fig 1):

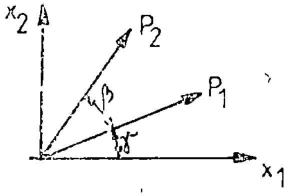

Fig 1 The optical transmission axes

$$T = \cos^2(\gamma - \beta) - \sin^2\gamma \sin 2\beta \sin^2 \frac{\Gamma}{2} \tag{5}$$

where Γ is the retardation induced by the electric field In the case of crossed polarizers, each of them being parallel to one of the old axes X, respectively Y, the optical transimssion becomes

$$T_{\perp} = \sin^2 2\gamma \sin^2 \frac{\Gamma}{2} \tag{6}$$

Applying an alternative electric field, the optical transmission of the system, and thus the transmited light intensity, will be modulated at a frequency which is equal with that of the field. Turning the crystal around its optical axis (Z), the optical transmision will vary with γ as in (5). When the input polarizer P_1 (see figures 1, 2) is parallel with one of the X' or Y' axes, the system doesn't work as an intensity modulator ($\gamma = 0$) and the signal on the osciloscope (which is on the A C input) becomes zero. Knowing α, it is possible to determine the X, Y axes in the absence of the electric field

In this method it is assumed that the optical axis (Z) was determined earlier A method of determining this axis is that of the conoscope (see 2) It is assumed, also, that the values of r_{xyz} coefficients, with which α is calculated, are known.

Experiment. The scheme of the experimental arrangement is shown in the figure 2

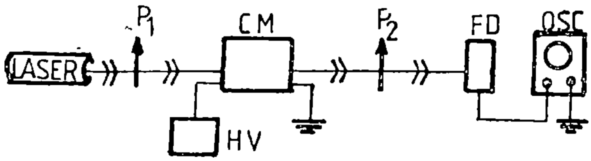

Fig 2 The scheme of the experimental arrangement

It is typical arrangement of an intensity modulator using longitudinal Pockels effect P_1, P_2 are the polarizers (which are crossed), *H V* represents the source of voltage which is applied on the crystal, *CN* means the nonlinear crystal (the optical axis, the applied field and the propagation direction of the light beam are parallel), *LASER* represents the light source it was used (a low power He-Ne laser), *FD* is the photodetector and *OSC* is the osciloscope

An alternative electric field . taken from the electric net through an up-converter voltage transformer, is applied on the crystal. The electrodes on the crystal are obtained by colloidal silver deposition on the lateral facetes of the crystal. After the determination of X, Y axes, the electrodes are eraised.

About the two polarizers, P_1 is mounted on a fix assembling The maximum transmission axis lies in vertical direction. P_2 is mounted on a nobile support and is turned till there is obtained the maximum extinction (in this case the polarizers being crossed) It is preferably that P_1 be a Glenn-Thompson prism, which has a very small closing ratio (measured to 10^{-5}) The *CN* crystal is mounted in a mobile, graded support For the determination of *X, Y* axes was used the next algorithm

— apply the alternative voltage on the electrodes

— observe on the oscilloscope screen if the A.C voltage appreas or not. If it appears, this means that one of the *X* or *Y* axes is not parallel with P_1. In this case, the next steps are

— turn the crystal till on the oscilloscope screen doesn't appear the A C. signal In this case, P_1 is parallel with one of the *X* or *Y* axes (so that axis lies in vertical direction).

— read the angle indicated by the crystal support

— turn the crystal with an angle equal to that given by (3), In this moment the *X* axis (or *Y*) lies in vertical direction Mark on the crystal this position.

The experiments were done using *KDP* and, respectively *KD*P* crystals. These crystals were already cut as in the next figure

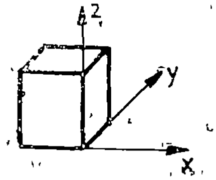

Fig 3 The cut crystal axes

Turning the crystal as described before, the *X, Y* axes were obtained as in figure 3, with a precision of 30′ (given by the reading accuracy). Also, the angle between the position for which no signal appears on the screen was found equal to 90°, in concordance with the theory (the angle between *X′, Y′* axes, respectively, *X, Y,* being 90°).

Request. a) It must be determined with high accuracy the position of maximum transmission axis of the P_1 polarizer

b) it is necessary a fine mechanics (for the support in which the crystal is mounted) of very good quality, for increasing the determination accuracy

c) the use of an amplifier between photodetector and oscilloscope, for making the electonic part more sensitive to very small beam intensities

Conclusions. At the end, some aspects could be underlined:

a) The done experiments put in evidence that the method is appllicable. The method could replace the X-rays apparatuses used for the determination of X an Y axes

b) It is used a minimum number of components and devices Also, the electrodes could be whashed off, so the crystal does not remain with them in the next processing step, that of cutting.

c) It is a fast method

d) The method could reach a very high accuracy, this fact depending, on one hand, on the used mechanics, and on the other hand on the photodetection electronic system.

e) This method could be automatized.

REFERENCES

1. G Nemeş, *Introduction to Nonlinear Optics*, 1972, Ed Academiei RSR (in Romanian).
2. M. Born, E Wolf, *Principles of Optics*, 1962.

STUDIA UNIV. BABEŞ-BOLYAI, PHYSICA, XXXV, 2, 1990

CHARGE TRANSFER REACTIONS IN THE SYSTEMS IMPLYING ISOTOPIC METHANES AT SMALL ENERGIES

P. ARDELEAN*

ABSTRACT. — The charge transfer reactions of H_2^+, CH_4^+, CH_3^+ and N^+ ions with CH_4, CH_3D, CH_2D_2 and CD_4 were studied in a perpendiculary type tandem mass spectrometer. An influence of the kinetic and internal energy of the incident ions on the secondary mass spectra and on the isotope effects was observed. The isotope effects are expressed as $\pi_1(D/H)$, $\Gamma_1(H)$ and $\Gamma_1(D)$ factors. The dependence of the isotope effects on kinetic energy could indicate a conversion of kinetic energy into internal energy. It was also observed a momentum transfer in the charge transfer reactions. The new variable angle tandem mass spectrometer is shortly described.

Introduction. The data obtained from the study of the charge transfer reactions are very useful in understanding of some actuality phenomena in physics and chemistry.

So the data concerning these reactions are useful in the study of high atmosphere [1—4], in the radiation chemistry [5, 6], in astrophysics [7—9], in the study of the flames [10—11], in the gas discharges [12—13], in the problems of chemical kinetics [14—15], in the study of some processes occuring in the fusion plasma [16, 17], and generally in the mass spectrometry.

Experimental. The apparatus was a perpendicular type tandem mass spectrometer, described earlier [18—20]. It consists of a 180° primary mass spectrometer with an inhomogeneous magnetic field, a retarding system, a collision chamber with an accelerating system for the secondary ions, a 90° secondary mass spectrometer with homogeneous magnetic field and an ion counter.

The pressure in the collision chamber was $1.5-2.5 \times 10^{-4}$ torr. The primary ions kinetic energy was in the range 8—160 eV and the intensity of the primary ion currents was in the range $3 \times 10^{-10} - 1.5 \times 10^{-11}$ A. The intensity of the secondary ion currents was in the range $10^{-18} - 10^{-15}$ A.

Results and discussions. The secondary ions which could appear in the charge transfer reactions between a primary ion P^+ and CH_4 are CH_4^+, CH_3^+, CH_2^+, CH^+ and C^+.

For the case of the methane, the secondary ions could appear in a large range of recombination energy of the primary ions [21], not only at the given fixed values [22]. That is because in the polyatomic molecules there are many energy levels and at least one of the sufficiently high recombination energy ($R.E.$) of an ion could be in quasiresonance with one of the appearance potentials ($A.P.$) of the secondary ion, that means: $\Delta\varepsilon = A.P. - R.E. \approx 0$.

The results are given in terms of the relative cross sections (percents of the total charge transfer cross sections) versus the kinetic energy of the primary ions.

There were studied charge transfer processes implying as primary (reactant) ions: H_2^+, CH_4^+, CH_3^+ and N^+ and as neutral molecules CH_4, CH_3D, CH_2D_2 and

---

* *Institute for Isotopic and Molecular Technology, P.O.B. 700, Cluj 5, 3400 Cluj-Napoca, Romania*

CD_4. In all these systems there were taken into account ionic species CX_4^+, CX_3^+ and CX_2^+, C^+ and sometimes CX^+ being neglected from quantitative reasons (X being H or D)

1 *The systems implying H_2^+ and CH_4^+ [23—25] as primary* In these systems the variation of the relative cross sections versus the kinetic energy of the primary ions is relative small That is probably because H_2^+ primarily, but also CH_4^+, have a relative large range of R E, which makes that a contribution of kinetic energy be not so important. In fig. 1 are given the relative cross sections Q_r [24, 29] versus the kinetic energy E_c of the primary ions, obtained for systems $CH_4^+ - CH_3D$. The isotope effects have a more important variation, versus the kinetic energy of the primary ions. This dependence is more important for the systems implying CH_4^+ than that for the systems implying H_2^+ The isotope effects are given in terms of π_i and Γ_i factors [26]

The explanation of such a type of isotope effects could consist in the difference between zero point energy of $C-D$ and $C-H$ bonds and in the different density of the vibrational levels of the two bonds

The decrease of the π_i (D/H) and $\Gamma_i(D)$ and the increase of $\Gamma_i(H)$ factors, all of them indicating a increase of the elimination of H atoms relative to the elimination of D atoms by the dissociative charge transfer, versus the kinetic energy of the primary ions, could indicate a conversion of kinetic energy into internal energy, Table I.

In the case of $\Gamma_1(H)$ and $\Gamma_2(H)$ their values become equal to 1 (dissappearance of the isotope effect)at ~ 20 eV kinetic energy and become smaller at energies under 20 eV (the isotope effect is reversed).

This could indicate a change in the reaction mechanism It was observed the apperance of the CX_5^+ at energies under 20 eV and this could confirm the possibility of complex formation

It was estimated [27] that charge transfer reactions could proceed by a frontal collision complex when the relative velocity of the reactants is $v > 10^6/\mu^{1/2}$ (where $\mu = M_1M_2/(M_1 + M_2)$). For this velocity we have $E < 2{,}2$ eV lab, in our case (M_1, M_2 — the reactants masses)

It results that between 8—20 eV, the charge transfer reactions could take place by frontal collision complex, a polarisation complex being improbable.

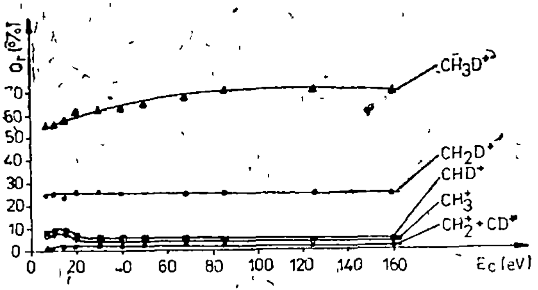

Fig 1 The variation of the relative cross sections for the system $CH_4^+ - CH_3D$

Table I

The isotope effects in the systems $CH_4^+-CD_iH_{4-i}$

Kinetic energy (*eV*)	Γ'(D/H)	$CH_4^+ - CH_2D_2$			$CH_4^+ - CH_3D$		
		Γ_2(H)	Γ_2(D)	π_2(D/H)	Γ_1(H)	Γ_1(D)	π_1(D/H)
8	0,89	0,88	0,98	0,90	1,05	1,18	0,91
10	0,83	0,93	0,88	0,78	1,06	1,16	0,91
15	0,81	1,02	0,75	0,59	1,02	1,12	0,89
20	0,81	1,06	0,76	0,58	1,12	0,95	0,69
30	0,80	1,16	0,78	0,54	1,19	0,93	0,63
40	0,82	1,22	0,77	0,52	1,16	0,82	0,58
50	0,78	1,26	0,75	0,47	1,20	0,73	0,47
68	0,77	1,26	0,74	0,45	1,20	0,62	0,39
85	0,76	1,25	0,73	0,44	1,24	0,59	0,36
125	0,79	1,27	0,67	0,42	1,29	0,55	0,34
160	0,77	1,33	0,66	0,38	1,28	0,58	0,35

2 *The systems implying CH_3^+ and N^+ as primary ions* In these cases [28, 29], the RE of the primary ions are a quite narrow band Probably for this reason the influence of the kinetic energy of the primary ions on the secondary spectra is more evident The relative cross sections for $CH_3^+-CH_2D_2$ are given in fig 2

The variation of the isotope effects versus the kinetic energy of the primary ions could also indicate a conversion of kinetic into internal energy, Table II. At kinetic energies under 20 *eV* it could be observed an important variation of the isotope effects, probably the explanation being the same as for the systems $CH_4^+-CD_iH_{4-i}$

3 *The role played by the excitation of the primary ions in the charge transfer reactions* [*30*]. As it knows the variation of the energy of the ionizing electrons gives a variation in the proportion of the excited states of the primary ions.

It was observed an important influence of the ionizing electrons in the primary mass spectrometer, on the relative cross sections for CX_3^+ ions This could be explained by the decreasing of the energy defect caused by the excitation energy of the primary ions

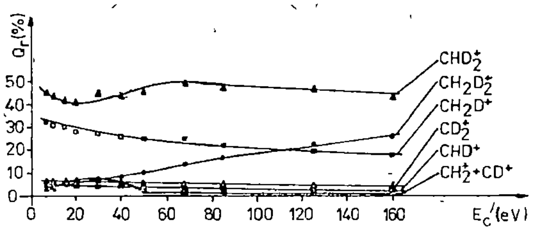

Fig 2 The relative cross sections for the system $CN_3^+-CH_2D_2$

Table II

The isotope effects is the systems $CH_3^+ - CD_iH_{4-i}$

Kinetic energy (eV)	$\Gamma'(D/H)$	$CH_3^+ - CH_2D_2$			$CH_3^+ - CH_3D$		
		$\Gamma_2(H)$	$\Gamma_2(D)$	$\pi_2(D/H)$	$\Gamma_1(H)$	$\Gamma_1(D)$	$\pi_1(D/H)$
8	0,92	0,93	0,72	0,71	0,84	0,68	0,74
10	0,98	0,94	0,70	0,73	0,87	0,67	0,75
15	1,08	0,97	0,66	0,73	0,94	0,65	0,74
20	1,11	1,02	0,64	0,70	0,97	0,61	0,70
30	1,12	1,07	0,60	0,61	1,03	0,48	0,52
40	1,13	1,05	0,58	0,61	1,09	0,45	0,47
50	1,11	1,13	0,60	0,59	1,08	0,45	0,46
68	1,09	1,25	0,57	0,50	1,14	0,43	0,41
85	1,05	1,26	0,58	0,48	1,16	0,43	0,39
125	1,01	1,26	0,57	0,46	1,15	0,45	0,38
160	1,03	1,30	0,53	0,42	1,20	0,42	0,36

At energies of the ionizing electrons greater than $\sim 35\ eV$, the primary ions have enough internal energy and the reaction becomes termoneutral or exotermic, and in this case the dependence by the electrons energy is vanished The relative cross section of CH_3^+ obtained for the system $CH_4^+ - CH_4$ is given in fig 3

It was also observed an important dependence of the isotope effects on the electrons energy.

It seems that an increase of the internal energy of the primary ions is competitive with an increase of the primary ions kinetic energy, Table III

4 *The momentum transfer* [31] The knowledge of the momentum transfer which take place in the charge transfer reactions could give informations concerning the reaction mecanism.

The quasiresonant and resonant reactions $\Delta\varepsilon \approx 0$ take place by "long range interactions" and the momentum transfer is small In the general case, reactions are unsymmetrical These reactions take place, generaly, by "short range interactions", and a momentum transfer could by implied For to observe the momentum

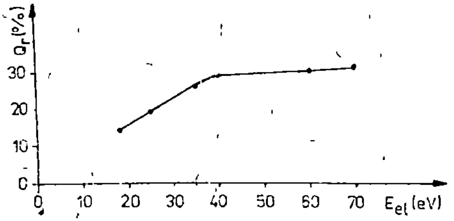

Fig 3 The elimination of H atoms by dissociative charge transfer

Table III

The intramolecular isotope effect ($\pi_2(D/H)$ factor) versus the ionizing electrons energy

Ionizing electron energy (*eV*)	Primary ion kinetic energy (*eV*)						Electronic impact
	8	10	20	30	50	100	
18	1,09	0,97	0,72	0,64	0,59	0,57	0,47
25	1,05	0,80	0,65	0,60	0,54	0,50	0,45
35	0,93	0,80	0,61	0,55	0,49	0,42	0,42
40	0,90	0,78	0,58	0,53	0,47	0,41	0,40
60	0,87	0,75	0,56	0,53	0,46	0,40	0,36
70	0,82	0,75	0,57	0,52	0,45	0,39	0,35
							0,37*

* See ref [26]

transfer the secondary currents were measured versus the repeller tension of the collision chamber

It was observed an important variation of the relative cross sections. The results shows that CX_4^+ ions appear by a mechanism which implies in a higher degree a short range interaction than the appearance of CX_3^+, or, more probably, the kinetic energy is converted into internal energy more efficiently in the appearance of CX_3^+ than for CX_4^+

From the study of the isotope effects it results that for the ions containing more D atoms, which appear by H atoms elimination, the kinetic energy of primary ions is converted in a smaller degree in internal energy than for the secondary ions containing more H atoms which appear by D atoms elimination

For to improve experimental method in these studies, it was constructed a variable angle tandem mass spectrometer The measurements made with this apparatus will allow to obtain more complete data concerning the ion molecule reactions

The variable angle tandem mass spectrometer consists of a 180° primary mass spectrometer with a inhomogeneous magnetic field, a retarding system, a collision chamber with a colimation and focalisation system for the secondary ions, an energy analyser, an secondary mass analyser, and a channeltron multiplier The system of the secondary analysing and detection can rotate around the collision chamber axis, and this makes possible the measurement of the angular distribution of the secondary ions

There are in progress the measurements concerning the $CH_4^+—CH_4$ system, and the intention is to obtain more exact data concerning the reaction mechanism.

REFERENCES

1 W Lindinger, F C Fehsenfeld, A L. Schmeltekopf and E E Ferguson, J Geophys Res, **79**, 4753 (1974)

2 E Graham, R Johnsen and M A Biondi, J Geophys Res, **80**, 2339 (1975)

3 F C Fehsenfeld, C J Howard, W J Harrop and E E Ferguson, J Geophys Res, **80,** 2229 (1975)

4 D J de Bruijn, J Neuteboom, T R Govers and J Los, Phys Rev A **34,** 3847 (1986)

5 P Ausloos, Prog React Kinet, **5,** 193 (1970)

6 S G Lias, in *Interaction between Ions and Molecules*, Ed P Ausloos, Ed Plenum Press, New York and London, 1975, p 541

7 U Wille, *Fund Proc in Atom*, Coll Phys, Ed H Kleinpoppen, Plenum Publ Corp 1985, p 719

8 U Wille, J Phys B At Molec Phys, **20,** 417 (1987)

9 U Wille, Phys Lett A, **125,** 52 (1987)

10 A N Hyhurst and T M Sugden, Proc Roy Soc, A **293,** 36 (1966)

11 H F Calcote and D E Jensen, Adv Chem Ser, **58,** 291 (1966)

12 P E Knewstubb and A W Tickner, J Chem Phys, **36,** 688 (1962)

13 M M Shahin, Adv Chem Ser, **58,** 315 (1966)

14 T M Miller, R E Wetterskog and J F Paulson, J Chem Phys, 80, 4922 (1984)

15 J M van Doren, S E Barlow, C H De Puy, V M Bierbaum, J Phys Chem, **90,** 2772 (1986)

16 A S Schlachter, K H Berkner, R J McDonald and J W Stearns, Nucl Instrum and Meth Phys Res, **B 27,** 573 (1987)

17 B H Brandsden, Nucl Instrum and Meth Phys Res, **B 24/25,** 377 (1987)

18 D Ioanoviciu, V. Mercea, C Cuna and P Ardelean, J of Phys E Sci Instrum, **6,** 129 (1973)

19 P Ardelean, V Mercea, D Ioanoviciu and C Cuna, Rev Roum Phys **19,** 49 (1974)

20 D Ioanoviciu, D Ursu, C Cuna, A Pamula and P Ardelean, St Cerc Fiz, **24,** 1035 (1972)

21 I Szabó, Ark Fys, **35,** 339 (1968)

22 F D Morrison and J. C Traeger, Int J Mass Spectrom Ion Phys, **11,** 289 (1973)

23 P Ardelean, V Mercea and D Ursu, *Report at the Internat Meet on Izotope Effects in Chem and Phys*, Proc june, 1973, Cluj, Romania

24 P Ardelean, V Mercea and A Pamula, Rev Roum Phys, **20,** 231 (1975)

25 P Ardelean, and V. Mercea, Int J Mass Spectrum, Ion Phys, **18,** 201 (1975)

26 L P Hills, M L Vestal and J M Futrell, J. Chem Phys, **54,** 3834 (1971)

27 V L Talrose and G K Karachetsev, Advan Mass Spectrom, **3,** 211 (1966)

28 P Ardelean, V Mercea and D Ursu, Rev Roum Phys, **21,** 141 (1976)

29 P Ardelean and V Mercea, Rev Roum Phys, **21,** 739 (1976)

30 P Ardelean and V Mercea, Int J Mass Spectrom, Ion Phys, **28,** 107 (1978)

31 P Ardelean and V Mercea, Rev Roum Phys, **25,** 767 (1980)

STUDIA UNIV BABEŞ-BOLYAI, PHYSICA, XXXV, 2, 1990

RECENZII

F. Twyman, **Prism and Lens Making**, Adam Hilger, Bristol and New-York, 1989

If the Holy Bible is The Book for all Cristians, I think that Twyman's book is in its way a bible, a reference work, never out of fashion. Two editions, in total 7 printings, have been issued so far — the first edition in 1942 and the last printing in 1989. This shows in the most evident way the continuous actuality of this extraordinary book.

For those who haven't had yet the priviedge to have in their hands Twyman's book, it is of interest to know that Twyman was not only a well-known specialist in the field of optical components making, but he was also the most generous and unbelivebly sincere author, offering to the reader all his treasures, i.e. technological secrets. All basic knowledges on materials for optical components, on grinding materials, on necessary machinery and procedures in making prisms and lenses, testing apparatuses and their use are there, guiding the reader in the difficult, but profitable and wonderful world of optical components' manufacturers.

PETRU ŞTEŢIU

P. T. Moseley and B. C. Tofield, **Solide State Gas Sensors**, Adam Hilger, Bristol and Philadephia, 1987

A modern chemical industry, more generally a modern industry is unthinkable today without appropriate sensors, able to give necessary information of concentration of different types of gases.

The monography edited by Adam Hilger Publishing Company is derived from a symposium, held in Oxford in 1985, on gas sensors and contains, the up-to-that-year results in this field. The book contains ten chapters, each of them being a concentrated overview presented by UK wellknown specialists in this field.

Almost half of this book deals with semiconductor gas sensors (SGS), based on SnO_2, as probably one of the technologically most promissing material. But reported results can be used as a guide line in searching and characterising other interesting materials.

In spite the fact that the book is published in 1987 it is surely of great interest for those who work in the noble field of science and SGS making industry. At the same time it gives to users a general view of limits and possibilities of industrialmade SGS and other gas-sensors.

PETRU ŞTEŢIU

Tiparul executat la Imprimeria „ARDEALUL“ Cluj c-da 184

În cel de al XXXV-lea an (1990) *Studia Universitatis Babeş-Bolyai* apare in următoarele serii :

matematică (trimestrial)
fizică (semestrial)
chimie (semestrial)
geologie (semestrial)
geografie (semestrial)
biologie (semestrial)
filosofie (semestrial)
sociologie-politologie (semestrial)
psihologie-pedagogie (semestrial)
ştiinţe economice (semestrial)
ştiinţe juridice (semestrial)
istorie (semestrial)
filologie (trimestrial)

In the XXXV-th year of its publication (1990) *Studia Universitatis Babeş-Bolyai* is issued in the following series :

mathematics (quarterly)
physics (semesterily)
chemistry (semesterily)
geology (semesterily)
geography (semesterily)
biology (semesterily)
philosophy (semesterily)
sociology-politology (semesterily)
psychology-pedagogy (semesterily)
economic sciences (semesterily)
juridical sciences (semesterily)
history (semesterily)
philology (quarterly)

Dans sa XXXV-e année (1990) *Studia Universitatis Babeş-Bolyai* parait dans les series sui[illegible]es :

mathématiques (trimestriellement)
physique (semestriellement)
chimie (semestriellement)
geologie (semestriellement)
géographie (semestriellement)
biologie (semestriellement)
philosophie (semestriellement)
sociologie-politologie (semestriellement)
psychologie-pedagogie (semestriellement)
sciences economiques (semestriellement)
sciences juridiques (semestriellement)
histoire (semestriellement)
philologie (trimestriellement)

43 904

Abonamentele se fac la oficiile poştale, prin factorii poştali şi prin difuzorii de presă, iar pentru străinătate prin „ROM PRESFILATELIA", sectorul export-import presă, P. O. Box 12--201, telex. 10376 prsfir, Bucureşti, Calea Griviţei nr. 64–66.

Lei 55